MINERALOGY AND ISOTOPIC GEOCHEMISTRY OF STALAGMITES IN NAMJANG CAVE, PANGMAPHA, MAEHONGSON PROVINCE, THAILAND

PANISARA PHUTONG

A THESIS SUBMITTED IN PARTIAL FULFILLMENT
OF THE REQUIREMENTS FOR
THE DEGREE OF MASTER OF SCIENCE
(TECHNOLOGY OF ENVIRONMENTAL MANAGEMENT)
FACULTY OF GRADUATE STUDIES
MAHIDOL UNIVERSITY
2008

Thesis
Entitled

MINERALOGY AND ISOTOPIC GEOCHEMISTRY OF STALAGMITES IN NAMJANG CAVE, PANGMAPHA, MAEHONGSON PROVINCE, THAILAND

……………………………………….
Miss Panisara Phutong,
Candidate

……………………………………….
Assoc. Prof. Nathsuda Pumijumnong,
Ph.D. (Natural Science)
Major-Advisor

……………………………………….
Assoc. Prof. Seriwat Saminpanya,
Ph.D. (Geology)
Co-Advisor

……………………………………….
Prof. Ming Tan,
Ph.D. (Quaternary Geology and Geomorphology)
Co-Advisor

……………………………………….
Lect. Narin Boontanon,
Ph.D. (Biological Sciences)
Co-Advisor

……………………………………….
Prof. Banchong Mahaisavariya,
M.D.
Dean
Faculty of Graduate Studies

……………………………………….
Lect. Kulvadee Kansuntisukmongkol,
Ph.D. (Ecology)
Chair
Master of Science Programme in
Technology of Environmental Management
Faculty of Environment and Resource Studies

Thesis
Entitled

MINERALOGY AND ISOTOPIC GEOCHEMISTRY OF STALAGMITES IN NAMJANG CAVE, PANGMAPHA, MAEHONGSON PROVINCE, THAILAND

was submitted to the Faculty of Graduate Studies, Mahidol University
for the degree of Master of Science
(Technology of Environmental Management)
on
August 22, 2008

……………………………………….
Miss Panisara Phutong,
Candidate

……………………………………….
Lect. Pol Chaodumrong,
Ph.D. (Geology)
Chair

……………………………………….
Assoc. Prof. Nathsuda Pumijumnong,
Ph.D. (Natural Science)
Member

……………………………………….
Assoc. Prof. Seriwat Saminpanya,
Ph.D. (Geology)
Member

……………………………………….
Prof. Ming Tan,
Ph.D. (Quaternary Geology and Geomorphology)
Member

……………………………………….
Lect. Narin Boontanon,
Ph.D. (Biological Sciences)
Member

……………………………………….
Prof. Banchong Mahaisavariya,
M.D.
Dean
Faculty of Graduate Studies
Mahidol University

……………………………………….
Asst. Prof. Sittipong Dilokwanich,
Ph.D. (Human Geography)
Dean
Faculty of Environment and Resource Studies
Mahidol University

ACKNOWLEDGEMENTS

The success of this thesis can be attributed to the extensive support and assistance from my major advisor, Assoc. Prof. Dr. Nathsuda Pumijumnong (the Faculty of Environment and Resource Studies, Mahidol University) who lights up the idea in this thesis with encouragement and patience. I am indept with my co-advisor, Assoc. Prof. Dr. Seriwat Saminpanya of the Faculty of Science, Srinakharinwirot University for his kindness in educating the basic of geology to me and he helped on everything related to the thesis as well as checking the English of the manuscript. I would like to thank Prof. Dr. Ming Tan of the Institute of Geology and Geophysics, Chinese Academy of Science for his comment to improve this thesis and Dr. Narin Boontanon of the Faculty of Environment and Resource Studies, Mahidol University for teaching me the basic isotope. I am ever so grateful to Dr. Binggui Cai (the Institute of Geology and Geophysics, Chinese Academy of Science) for his helps in all steps of this thesis including literature review, method and suggestions with his patience and encouragement.g

I am equally pleased to acknowledge the valuable kindness and suggestion received from the external examiner, Dr Pol Chaodumrong of the Department of Mineral Resources, Ministry of Natural Resources and Environment.

I wish to thank Mr. Payungsuk Saitong for help on thin section preparation, Mr. Satit Sanam and Mr Sermsuk Radreng for their appreciatively helps in laboratory.

I am very grateful to P' Ton, Ae and Namphueng for their helps on sample collection. Furthermore, I would like to convey my thanks to local people in the study area for their taking care and helps during the sampling expedition in Mae Hong Son. My special thanks to all my friends especially White, P' Mam, P' Toon, Nut, Oui, Kuk and P' Korn for their encouragement and friendship.

This research was financial supported by the National Research Council of Thailand and the Center for Toxicology, Environmental Health and Management of Toxic Chemicals under Science & Technology Postgraduate Education and Research Development Office (PERDO) of the Ministry of Education.

The National Metal and Materials Technology Center, Thailand (MTEC), the Tree Ring and climate change laboratory, Faculty of Environment and Resource studies, Mahidol University, the Faculty of Science, Srinakharinwirot University, the Department of Mineral Resources, Ministry of Natural Resources and Environment, the Environmental Isotope Lab of the Institute of Geology and Geophysics, Chinese Academy of Science, the Department of Geology and Geophysics, University of Minnesota, USA and the Radiogenic Isotope Laboratory University of Queensland, Australia for their laboratory supporting and kindness.

Finally, I deeply appreciate that my mother and father who give me a lot of loves and financial supports. Oat, my love one, he encourages and cares for me. Without these people, I would not succeed in thesis and obtain my master’s degree.

Panisara Phutong

MINERALOGY AND ISOTOPIC GEOCHEMISTRY OF STALAGMITES IN NAMJANG CAVE, PANGMAPHA, MAEHONGSON PROVINCE, THAILAND

PANISARA PHUTONG 4837305 ENTM/M

M.Sc. (TECHNOLOGY OF ENVIRONMENTAL MANAGEMENT)

THESIS ADVISORS: NATHSUDA PUMIJUMNONG, Ph.D. (NATURAL SCIENCE); SERIWAT SAMINPANYA, Ph.D. (GEOLOGY); MING TAN, Ph.D. (QUATERNARY GEOLOGY AND GEOMORPHOLOGY); NARIN BOONTANON, Ph.D (BIOLOGICAL SCIENCES)

ABSTRACT

This study examined the mineral species and morphology of two stalagmites from Namjang cave, Pang Ma Pha, Mae Hong Son, Thailand. Under the microscope, the stalagmite column shows brown to dark brown layers separated from each other by a dark brown layer. Observation by SEM, under low magnification (100x) shows that each layer contains many fibrous crystals forming fan-like polycrystalline. But under high magnification (2,000x), individual grain of aragonite (confirmed by XRD) shows tabular (10x40x5 µm) or bladed (10x40x1 µm) habits whereas the parent rock is biosparite limestone of Permian.

Thorium-230 ages, $\delta^{18}O$ and $\delta^{13}C$ of a stalagmite have characterized the climatic oscillations in low-latitude during the last 1,701 years. Fluctuation in the $\delta^{13}C$ affecting C_3/C_4 ratios whereas abrupt changes in $\delta^{18}O$ values result from changes in tropical precipitation. Excess rainfall years (more than 189 mm during wet season) occurred 1701 and 491 years BP (before 2006). These results were obtained by paleoclimatic reconstruction for the stalagmite NJ1 and they agree well with the results from dendroclimatology at the same province. Moreover, the values of $\delta^{18}O$, $\delta^{13}C$ and rainfall from reconstruction plotted against the time series can be used for anticipation roughly of the trend of those three parameters in the future.

KEY WORDS: STALAGMITE/ MINERAL SPECIES/ MORPHOLOGY/ LOW-LATITUDE/ PALEOCLIMATIC RECONSTRUCTION

128 pp.

แร่วิทยาและธรณีเคมีไอโซโทปของหินงอกในถ้ำน้ำจาง ปางมะผ้า จังหวัดแม่ฮ่องสอน ประเทศไทย (MINERALOGY AND ISOTOPIC GEOCHEMISTRY OF STALAGMITES IN NAMJANG CAVE, PANGMAPHA, MAEHONGSON PROVINCE, THAILAND)

ปาณิสรา ภูทอง 4837305 ENTM/M

วท.ม. (เทคโนโลยีการบริหารสิ่งแวดล้อม)

คณะกรรมการควบคุมวิทยานิพนธ์: นาฏสุดา ภูมิจำนงค์, Ph.D. (Natural Science); เสรีวัฒน์ สมินทร์ปัญญา , Ph.D. (Geology); Ming Tan, Ph.D. (Quaternary Geology and Geomorphology); นรินทร์ บุญตานนท์, Ph.D. (Biological Sciences)

บทคัดย่อ

จากการศึกษาเปรียบเทียบหินงอกสองแท่ง (NJ1 และ NJ2) ในถ้ำน้ำจาง อำเภอปางมะผ้า จังหวัดแม่ฮ่องสอน พบว่าทั้งสองตัวอย่างมีชนิดของแร่และลักษณะทางโครงสร้างที่เหมือนกัน โดยการศึกษาภายใต้กล้องจุลทรรศน์แสดงถึงชั้นของหินงอกที่มีสีน้ำตาลและแต่ละชั้นถูกแบ่งโดยชั้นสีน้ำตาลเข้ม จากการถ่ายภาพด้วยเทคนิค SEM ด้วยกำลังขยายต่ำ (100x) พบว่าในแต่ละชั้นของหินงอกประกอบด้วยกลุ่มผลึกรูปเส้นใยจำนวนมากรวมกลุ่มกันเป็นรูปร่างคล้ายพัด แต่ภายใต้กำลังขยายที่สูงขึ้น (2,000x) พบว่ากลุ่มผลึกเหล่านั้นประกอบไปด้วยผลึกเดี่ยวของแร่ Aragonite ซึ่งมีลักษณะผลึกเป็นแผ่นหนา (Tabular) ขนาด 10x40x5 ไมโครเมตร และแผ่นคล้ายใบมีด (Blade) ขนาด 10x40x1 ไมโครเมตร โดยชนิดของแร่นั้นใช้เทคนิค XRD ในการศึกษา นอกจากนี้ยังพบว่าหินปูนต้นกำเนิดของหินงอกเป็นชนิด Biosparite ในยุคเพอร์เมียน

จากการศึกษาอายุของหินงอก NJ1 โดยใช้เทคนิค ^{230}Th ในการหาอายุ รวมถึงได้มีการวิเคราะห์ค่าออกซิเจน-18 และคาร์บอน-13 ของหินงอก ซึ่งข้อมูลเหล่านี้สามารถบ่งบอกถึงความผันแปรของภูมิอากาศในเขตละติจูดต่ำในช่วง 1,701 ปีที่ผ่านมา โดยความผันแปรของคาร์บอน-13 เป็นผลเนื่องมาจากการเปลี่ยนแปลงของชนิดพืช (C_3 หรือ C_4) ส่วนการเปลี่ยนแปลงของ ออกซิเจน-18 เป็นผลเนื่องมาจากการเปลี่ยนแปลงของปริมาณน้ำฝนในเขตร้อน ซึ่งฝนมีปริมาณมาก (ปริมาณมากกว่าค่าเฉลี่ยของปริมาณน้ำฝนในช่วงหน้าฝน ซึ่งมีค่าเท่ากับ 189 มิลลิเมตร) ใน 1701 และ 491 ก่อนปี 2006 และได้มีการนำข้อมูลปริมาณน้ำฝนที่ได้จากหินงอกไปเปรียบเทียบกับปริมาณน้ำฝนที่ได้จากวงปีไม้ในจังหวัดแม่ฮ่องสอน พบว่าข้อมูลของทั้งสองแหล่งมีความสอดคล้องกัน นอกจากนี้ค่าออกซิเจน-18, คาร์บอน-13 และค่าปริมาณน้ำฝนที่ได้จากการผันกลับของ ออกซิเจน-18 เมื่อนำมาหาความสัมพันธ์กับช่วงเวลา นำไปสู่การทราบถึงแนวโน้มของทั้งสามค่าเหล่านี้ในอนาคตได้

128 หน้า

CONTENTS

Page

ACKNOWLEDGEMENTS iii
ABSTRACT IN ENLISH iv
ABSTRACT IN THAI v
LIST OF TABLES ix
LIST OF FIGURES x
LIST OF GLOSSARIES AND ABBREVIATIONS xv

CHAPTER

I INTRODUCTION

- 1.1 Objectives 2
- 1.2 Hypothesis 3
- 1.3 Conceptual framework 3
- 1.4 Scope of the study 4
- 1.5 Time table 4
- 1.6 Expected outcomes 4

II LITERATURE REVIEW

- 2.1 Geomorphology 5
  - 2.1.1 Karst topography 5
  - 2.1.2 Carbonate deposition 6
  - 2.1.3 Cave 13
  - 2.1.4 Speleothems deposition 16
- 2.2 Isotopes 20
  - 2.2.1 Environmental isotopes 20
  - 2.2.2 Speleothems isotopes 22

CONTENTS (Continued)

Page

CHAPTER

III METHODOLOGY
3.1 Study area 36
3.2 Sample selection 40
3.3 Sample collection 40
3.4 Sample preparation 40
3.5 Morphology and mineral species of stalagmites 41
3.6 Stable isotope and dating technique 45
3.7 Counting of annual growth layer 49
3.8 Stalagmite reconstruction 50
3.9 Petrography, mineral species and chemical composition of parent rock 50
3.10 Data interpretation 51

IV RESULTS AND DISCUSSION
4.1 Parent rock 53
  4.1.1 Petrography and mineral species 53
4.2 Stalagmites 58
  4.2.1 Morphology and mineral species 58
  4.2.2 Mineral species for comparison 69
  4.2.3 The $\delta^{18}O$ and $\delta^{13}C$ variations of stalagmite NJ1 71
  4.2.4 Stalagmite chronology 74
  4.2.5 Past variations in $\delta^{18}O$ and $\delta^{13}C$ 76
  4.2.6 Rainfall reconstruction 82

V CONCLUSIONS AND RECOMMENDATIONS
5.1 Conclusions 93
5.2 Recommendations 96

CONTENTS (Continued)

Page

REFERENCES 97

APPENDIX

A Methodology of CaO convert to $CaCO_3$ 106

B The result from counting the layers of growth of stalagmite NJ1 by Tree-ring width measurements (TSAP. version 3.2) 106

C Uranium and thorium isotopic compositions and ^{230}Th ages 107

D The values of $\delta^{18}O$, $\delta^{13}C$ and data interpretation from stalagmite NJ1 108

E Statistical treatment of GNIP data at Bangkok (Copyright IAEA) 114

F Rainfall at Mae Hong Son and Pang Ma Pha station 124

G Rainfall reconstruction from stalagmite is compared with that of Teak tree-ring 127

BIOGRAPHY 128

LIST OF TABLES

Table **Page**

2-1 Properties of limestone minerals 8

2-2 The principal component of limestone 9

2-3 Properties of dolomite mineral 12

4-1 Chemical composition of the parent rock for the stalagmites in Namjang cave 57

4-2 The aragonite species in another locations 68

4-3 Samples identification the ages and equipments used for ^{230}Th dating 74

4-4 Growth rate of the layers in stalagmite NJ1 75

4-5 Characteristics of stalagmites of the present study (Namjang cave) and other locations which are affected by the Indian and Pacific monsoon climates 79

4-6 The dark brown layer with $\delta\ ^{18}$O and $\delta\ ^{13}$C of stalagmite NJ1 81

4-7 R values of correlation between the rainfall data of different pairs of site 87

LIST OF FIGURES

Figure		Page
2-1	Conceptual model of the karst system with its physiology of water flow and CO_2 transport and release	6
2-2	A bulk compositional classification of carbonate rock	7
2-3	Crystal systems of calcite (a) and aragonite (b)	8
2-4	Classification of limestone, reproduced with permission from Fork	10
2-5	Stability Diagram for $CaCO_3$ determined fields of calcite and aragonite	11
2-6	Varieties of caves	16
2-7	Speleothems deposition such as, flowstones (a), stalagmites (b), stalactites, and soda straws (c,d)	17
2-8	Ranges for $\delta^{13}C$ value in selected natural compounds. Especially noteworthy in the spreading of $\delta^{13}C$ seen in different plant groups are resulting on soil CO_2	22
2-9	Factors determining the $\delta^{13}C_c$ composition of speleothems calcite (assuming equilibrium deposition)	23
2-10	The range of $\delta^{18}O$ in various crustal rock and water type	26
2-11	Conversion chart for $\delta^{18}O$ between VSMOW and VPDB with fractionation factors for 25°C	27
2-12	Factors determining the $\delta^{18}O_c$ composition of speleothems calcite (assuming equilibrium deposition)	29
2-13	The ^{238}U decay series, with principal decay pathway decay mechanism and half-life of radionuclides	30
2-14	The ^{235}U decay series, with principal decay pathway decay mechanism and half-life of radionuclides	31
2-15	Graphical illustration of the $^{230}Th:^{234}U:^{238}U$ dating method the principal method used for carbonate speleothems today	33

LIST OF FIGURES (Continued)

Figure **Page**

3-1 Map of Pang Ma Pha district of Mae Hong Son province, Thailand 37
3-2 The map of Namjang cave (Top view) 38
3-3 The profiles of Namjang cave and location of sampling stalagmite NJ1 and stalagmite NJ2 39
3-4 The cave entrance (a) and the flora above the cave (b) 40
3-5 A polarizing microscope equipped with photography unit 43
3-6 The scanning electron microscope (JEOL model: JSM 6301F) (a) and Schematic diagram of a scanning electron microscope (b) 44
3-7 Automated X-ray diffraction (D8 Advance) (a), sample holder (b) 45
3-8 Graph paper lay on top of the cut surface of stalagmite NJ1 for drilling 46
3-9 MAT-253 mass spectrometer linked to a Gas Bench-II (Thermo-Finnigan) machine 47
3-10 Three points were drilled for ^{230}Th dating 48
3-11 VG Sector 54E TIMS (a) and ThermoElemental PQ ExCell quadrupole ICP-MS (b) 48
3-12 The equipment for tree ring width measurements (TSAP version 3.2) 49
3-13 X-ray fluorescence (Axios Advance) 51
4-1 The texture of parent rock (PM_NJ1) from Namjang cave 53
4-2 The texture of parent rock (PM_NJ2) from Namjang cave 54
4-3 The XRD results for stalagmite, PM_NJ1, shows the peak positions similar to those of calcite reference, 72-1650 55
4-4 The XRD results for stalagmite PM_NJ2, shows the peak positions similar to those of calcite reference, 72-1650 56
4-5 The layer of stalagmite NJ1_1 (a) and the morphology of mineral species (b, c, d) 58
4-6 The layer of stalagmite NJ1_2 (a, b) and the morphology of mineral species (c, d) 59

LIST OF FIGURES (Continued)

Figure **Page**

4-7 The layer of stalagmite NJ1_3 (a, b) and the morphology of mineral species (c, d) 60

4-8 The XRD results for stalagmite NJ1_1, shows the peak positions similar to those of aragonite reference, 76-0606 61

4-9 The XRD results for stalagmite NJ1_2, shows the peak positions similar to those of aragonite reference, 76-0606 61

4-10 The XRD results for stalagmite NJ1_2, shows some peak positions similar to those of aragonite reference, 76-0606 62

4-11 The XRD results for stalagmite NJ1_3, shows some peak positions similar to those of calcite reference, 03-0596 62

4-12 The layer of stalagmite NJ2_1 (a, b) and the morphology of mineral species (c, d) 63

4-13 The layer of stalagmite NJ2_2 (a, b) and the morphology of mineral species (c, d) 64

4-14 The layer of stalagmite NJ2_3 (a, b) and the morphology of mineral species (c, d) 65

4-15 The XRD results for stalagmite NJ2_1, shows the peak positions similar to those of aragonite reference, 76-0606 66

4-16 The XRD results for stalagmite NJ2_2, shows the peak positions similar to those of aragonite reference, 76-0606 66

4-17 The XRD results for stalagmite NJ2_3, shows the peak positions similar to those of aragonite reference, 76-0606 67

4-18 Under the SEM, the morphology of stalagmite from Namjang cave (a and b), compared to stalagmite from Tinuey cave (c and d) 69

4-19 The XRD result for the stalagmite from Namjang cave and stalagmite from Tinuey cave 70

4-20 $\delta^{18}O$,$\delta^{13}C$ and distance for measurements along the growth direction from top towards bottom of the stalagmite NJ1 71

LIST OF FIGURES (Continued)

Figure **Page**

4-21 $\delta^{18}O$ and $\delta^{13}C$ plot showing the composition of carbonates from a variety of environments 72

4-22 The $\delta^{18}O$ and $\delta^{13}C$ composition of marine carbonates and secondary "terrestrial" carbonates 73

4-23 $\delta^{13}C$ and $\delta^{18}O$ vs Age for measurements along the growth direction (top towards bottom) of the stalagmite NJ1 77

4-24 The layers of stalagmite NJ1 with dark brown color and white color 80

4-25 Plot of 170 coordinates for $\delta^{18}O$ and $\delta^{13}C$ of the stalagmite NJ1 measured along the growth axis 82

4-26 Negative correlation between monthly $\delta^{18}O$ (independent variable) and monthly precipitation (dependent variable) at Bangkok during year 1968 and 2004 84

4-27 The correlation of mean monthly rainfall between Bangkok and Mae Hong Son during the year 1968 and 2004 85

4-28 The correlation of mean monthly rainfall between Bangkok and Pang Ma Pha during the years 1986 and 2004 86

4-29 The correlation of mean monthly rainfall between Mae Hong Son and Pang Ma Pha during the year 1986 and 2005 86

4-30 Comparison plot of $\delta^{18}O$ in stalagmite NJ1 (relative to PDB) and amount of rainfall base on the same period, dash line shows the mean monthly rainfall in wet period during 1911-2002 year AD 88

4-31 Rainfall is reconstructed by Teak tree-ring (mean monthly from March to May) (upper line) compared to stalagmite NJ1 reconstruction (during wet period) (lower line), as during year 1714-1913 89

LIST OF FIGURES (Continued)

Figure **Page**

4-32 The δ^{18}O observed in Namjang cave from 305 to 1990 AD. The red line is the 6 th-order polynomial fit 90

4-33 The δ^{13}C observed in Namjang cave from 305 to 1990 AD. The red line is the 6 th-order polynomial fit 91

4-34 The rainfall observed in Namjang cave from 305 to 1990 AD. The red line is the 6 th-order polynomial fit 92

LIST OF GLOSSARIES AND ABBREVIATIONS

δ: *the delta notation*, a relative measure of the difference, typically ratios of molar concentrations of stable isotopes between a substance and an agreed-upon standard material

$\delta^{13}C$: notation used to express the value of the carbon isotope ratio ($^{13}C/^{12}C$) in a sample relative to that in a standard. Thus $\delta^{13}C = [(^{13}C/^{12}C_s) / (^{13}C/^{12}C_{std})-1]x1000$, where s is the sample (unknown) and std is a standard that has been calibrated relative to the **PDB** *(Pee Dee Bellemnite)*, usually expected as **VPDB** *(Vienna Pee Dee Bellemnite).*

δD: also known as δ^2H. Notation used to express the value of the hydrogen isotope ratio ($^2H/^1H$) in a sample relative to that in standard. Thus $\delta^2H = [(^2H/^1H_s) / (^2H/^1H_{std})-1]x1000$, where s is the sample (unknown) and std is a standard that has been calibrated relative to the **VSMOW** *(Vienna Standard Mean Ocean Water).*

$\delta^{18}O$: notation used to express the value of the oxygen isotope ratio ($^{18}O/^{16}O$) in a sample relative to that in a standard. Thus $\delta^{18}O = [(^{18}O/^{16}O_s) / (^{18}O/^{16}O_{std})-1]x1000$, where s is the sample (unknown) and std is a standard that has been calibrated relative to the PDB, usually expected as VPDB or VSMOW.

Activity: In this study is referred to radioactivity, which is expressed as the number of disintegrations observed in unit time that derived by the equations of $A=c\lambda N$, where A is the observed counting rate, λN is the actual rate of decay and c is the detection coefficient.

AD: *Anno Domini***,** used to indicate that a time division falls within the Christian era.

BP: *Before Present***,** generally base on 1950 year, this study is the year before 2006 which samples collected.

C_3 plants: *Calvin cycle***,** the C_3 pathway operates in about 85% of plant species and dominates in most terrestrial ecosystem. Most C_3 plants have $\delta^{13}C$ values that range from -24 to -30‰ with an average value of about -27‰. These differences are preserved as distinctive ranges in secondary carbonates, typically -14% to -6% for carbonates deposited in equilibrium with CO_2 respired from C_3 plants.

C_4 plants: *Hatch-Slack cycle*, C_4 species represent less than 5% of floral species, but dominate in hot open systems such as tropical and temperate grasslands, common agriculture. C_4 plants have $\delta^{13}C$ values that range from -10 to -16‰, mean value of about -12.5‰, however in secondary carbonates, typically -6% to +2% for carbonates deposited in equilibrium with CO_2 respired from C_4 plants.

CAM: *Crassulacean acid metabolism cycle*, is favoured by about 10% of plants and dominates in desert ecosystem with plant species such as cacti. They have the ability to switch from C_3 photosynthesis during the day to the C_4 pathway for fixing CO_2 during the night. Their isotopic composition can span the full range of both C_3 and C_4 plants, but usually is intermediate.

Dendroclimatology: the study of climate and environmental change through analysis of trees and annual growth layers in wood.

Disequilibrium: commonly known as 'vital' effects in the case of biogenic carbonates, include a variety of rate effects and micro-environment induced changes that cause the mineral to have an isotope composition that is different from predicted purely by thermodynamics.

DIC: *Dissolved Inorganic Carbon*

DOC: *Dissolved Organic Carbon*

Fractionation factor: ratio of two isotopes in one chemical compound divided by the same ratio in another compound (α). If X and Y are two chemical compounds then the fractionation factor $\alpha_{x-y} = R_x/R_y$, where R mean the ratio of elememt.

GNIP: *Global Network of Isotopes in Precipitation*, the corporate between the IAEA *(International Atomic Energy Agency)* and the WMO *(World Meteorological Organization)*.

High latitude: that part of the Earth's surface near either pole, that part within either the arctic or the antarctic circle. This study is above 66°33'33"N and 63°33'33"S of latitude.

ICP-MS: *Inductively Coupled Plasma- Mass Spectroscopy*

Isotope fractionation: process that result in a change in the isotope ratio of a compound.

Isotopically depleted: a substance that is depleted in the heavy (usually less abundant) stable isotope over a light (usually more abundant) isotope of the same element is said to be isotopically depleted. In the context of carbon isotopes for example an isotopically depleted substance is relatively enriched in ^{12}C and therefore has a relatively low $\delta^{13}C$ value.

Isotopically enriched: a substance that is enriched in the heavy (usually less abundant) stable isotope over a light (usually more abundant) isotope of the same element is said to be isotopically enriched. In the context of carbon isotopes for example an isotopically enriched substance is relatively depleted in ^{12}C and therefore has a relatively high $\delta^{13}C$ value.

Kinetic fractionation: non-equilibrium fractionation, found for example in diffusion-controlled evaporation, or biologically controlled process.

Low latitude: that part of the Earth's surface which is near the equator. This study is below 33°33'33"N and 33°33'33"S of latitude.

Mid latitude: There are between 33°33'33"N- 66°33'33"N and 33°33'33"S- 63°33' 33"S of latitude.

pCO$_2$: *partial pressure of carbon dioxide***,** a measurement of the concentration of CO_2 in the atmosphere and water. The unit is atm.

Per mill ***(‰)*****:** literally parts per thousand, the conventional unit for expressing isotope delta (δ) value.

ppm.: *part per million*

SEM: *Scanning Electron Microscope or Microscopy.*

Soil pCO$_2$: *the partial pressure of CO_2 in soil gas.*

Speleothems: secondary carbonate accumulations such as stalagmites, stalactites and flowstones deposited in cave by degassing of cave drip water that is supersaturated with respect to calcium carbonate.

TIMS: *Thermal Ionization Mass Spectrometry*

Travertine: calcium carbonate deposited by hot or cold water, including speleothems and accumulations at spring.

XRD: *X-ray Diffraction, Diffractometer or Diffractometry*

XRF: *X-ray Fluorescence*

CHAPTER I

INTRODUCTION

Climate is the statistical expression of daily weather events. Many natural systems are dependent on climate and an evidence of such systems in the past still exists. It may be possible to derive paleoclimatic information from them [1]. Fluctuations of climate have crucial impacts on the livelihood of people and natural system. Many studies have focused on paleoclimatic data which provide the basis for testing hypotheses about the cause of climatic change. Only when the causes of past climatic fluctuations are understood will be possible to fully anticipate or forecast climatic variations in the future [2]. All paleoclimatic researches, therefore, must build on studies of climate dependency in natural phenomena today [1] such as dendroclimatology, pollen analysis, ice cores, speleothems etc. Especially, speleothems are the effective proxies in paleoclimate studies for several reasons, including 1) they contain trace element and isotopic tracers that have been used to infer changes in paleotemperature, paleovegetation and paleoprecipitation, 2) they may be continuously deposited over thousands of years and have thin growth bands that can be precisely dated using U-series dating methods, 3) growth rates of these bands may provide proxies for environmental parameters such as aquifer recharge rates, and 4) speleothems form in a wide variety of locations where other high-resolution climate records may be absent [3].

The speleothems are mineral formations occurring in limestone caves, most commonly as stalagmites and stalactites, or slab-like deposits known as flowstones. They are composed primarily of calcium carbonate, precipitation from ground water that has percolated through the adjacent carbonate host rock [1]. The potential of speleothems as paleoclimatic recorders was first explored more than thirty–five years ago [4] and increased markedly during the past decade. Most studies utilize stalagmites rather than stalactites or flowstones because their simple geometry, relatively rapid growth rates and tendency to precipitate close to isotope equilibrium with the cave drip waters facilitates paleoclimatic reconstruction [5]. In the other climatic zone has been educated extensively about speleothems such as China that they present $\delta^{18}O$ records from two stalagmites from Wanxiang Cave, to assess the potential of speleothems from this region as paleomonsoon archives and link may exist between the Asian monsoon and climate in the Eastern Mediterranean region [6]. In addition, a high-resolution, 116,000-year carbon stable isotope record from a stalagmite in southern Brazil (temperate zone) - the speleothems provides evidence of paleoenvironmental change in southern Brazil during the last glacial period (It began about 110,000 years ago and ended between 10,000 and 15,000 BP) [7] etc. In the tropical zone, rainfall reconstruction from speleothems in India agrees well with the earlier observations using other proxies such as high rainfall during ~1666 AD by stalagmites from Akalagavi cave agrees with the tree ring width index around this period [8].

Thailand, the data of paleoclimatic have been obtained from tree ring or dendroclimatology and pollen etc. Although, Thailand has a potential for example at Pang Ma Pha, Mae Hong Son province, karst topography that has many caves but the paleoclimatic studies of the isotopic signal imprinted in precipitation of the region by using stalagmites still remain largely unexplored, mainly due to poor data of the long-term sensitivity of isotopic composition of rainfall in the area. Whereas, the link between isotope signature of precipitation and climate at mid latitudes and high latitudes is in general well understood, this is much less the case for the tropics or low latitude [9]. Thus, this research is an essential investigation for the mineralogy and isotopic geochemistry which is contributed to the extensive paleoclimatic researches in this region in the future.

1.1 Objectives

1) To investigate the morphology and mineral species of stalagmites

2) To investigate the petrography, mineral species and chemical composition of parent rock.

3) To investigate the $\delta^{13}C$, $\delta^{18}O$ and age of stalagmite.

4) To reconstruct the paleoclimate of the study area in terms of paleoprecipitation and paleovegetation.

1.2 Hypothesis

1) The precipitation and vegetation may affect the stalagmite.
2) The stalagmite has one annual growth layer to one year.

1.3 Conceptual framework

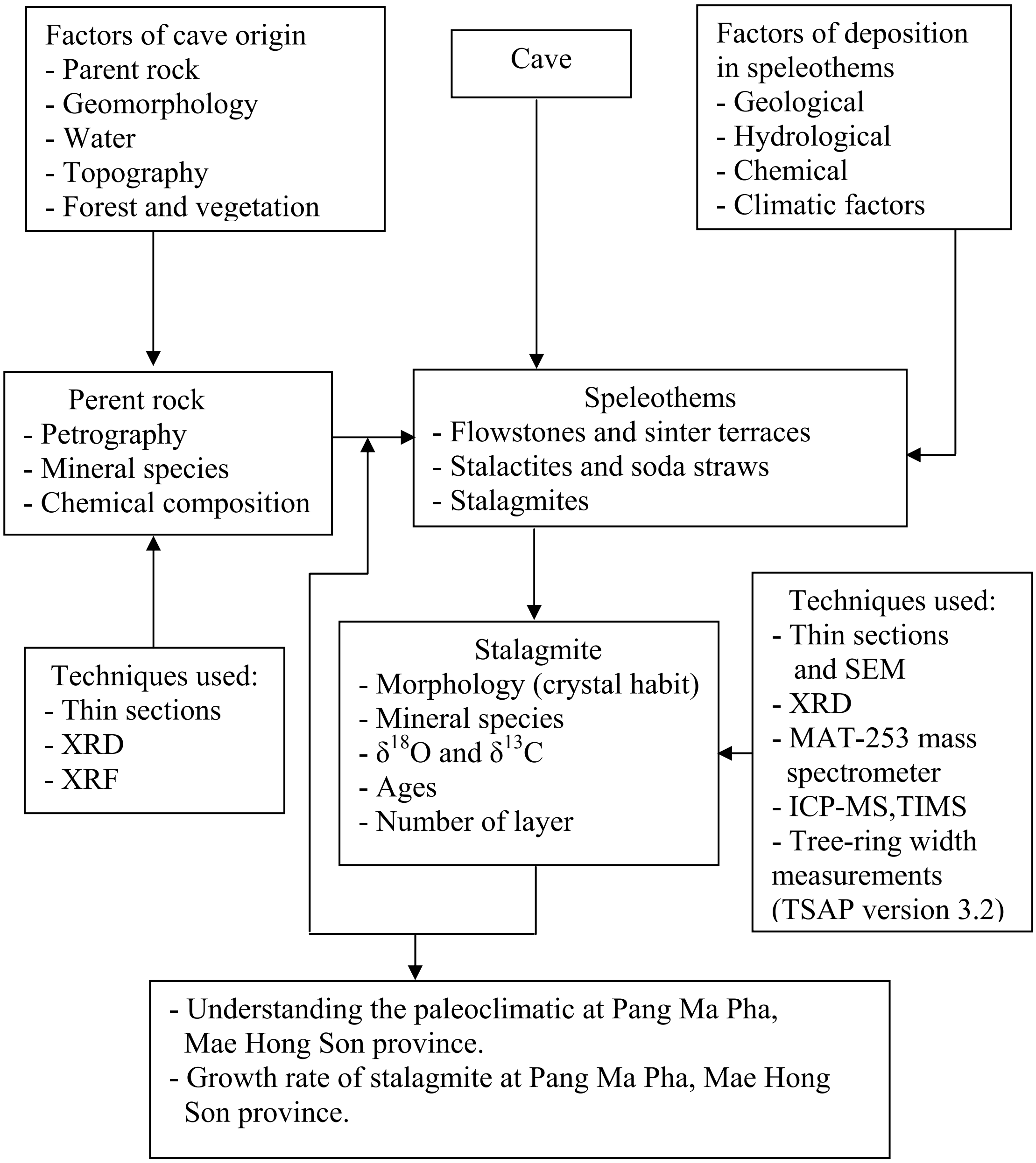

1.4 Scope of the study

The stalagmite, there are 2 samples from Namjang caves at Pang Ma Pha, Mae Hong Son province, Thailand.

1.5 Time table

Procedure	2007												2008							
	Jan	Feb	Mar	Apr	May	Jun	Jul	Aug	Sep	Oct	Nov	Dec	Jan	Feb	Mar	Apr	May	Jun	Jul	Aug
Literature review	←	─	─	─	─	─	─	→												
Proposal presentation									↔											
Field survey										←	→									
Experiments											←	→								
Data analysis													↔							
Conclusion and writing up the thesis														←	─	→				
Defending thesis																	↔			
Thesis publication																		←	─	→

1.6 Expected outcomes

1) The data from this investigation could provide understanding the effect of rainfall and vegetation on the study area.

2) Results of this study could provide a high-resolution record of paleaoclimate in tropical zone, in particular Thailand.

CHAPTER II
LITERATURE REVIEW

2.1 Geomorphology

2.1.1 Karst topography

The term karst describes a distinctive topography that indicates dissolution (also called chemical solution) of underlying soluble rocks by surface water or ground water (Figure 2-1). Although commonly associated with carbonate rocks (limestone and dolomite) other highly soluble rocks such as evaporates can be sculpted into karst terrain [10]. Researches on karst terrains have focused mainly on surface geomorphology, the geometry of cave systems, the hydrology and hydrogeochemistry of major springs, the dating of cave development and the major phases of speleothems formation [11]. Pioneering work in karst topography of Hendy and Wilson in 1968 was published in a leading journal and the same is true of much recent work [12].

1) Epikarst

The epikarst represents the vertical extension of the soil, and as such can act as a reservoir for the accumulation of organic matter. The decomposition of organic matter within this layer produces carbon dioxide (CO_2) which is the main agent of carbonate rock solution, and of karst processes, when dissolved in groundwater. The epikarst is the key site for carbonate rock solution. Karst depressions (dolines) are initiated by drainage of epikarst storage via vertical conduits.

Finally, epikarst is an essential interface between the biosphere and the karst itself. Karst develops and evolves as a result of the epikarst, which distributes the infiltrated water and the rock solvent (CO_2 + water) in such a way that a characteristic landscape is created at the surface (closed depressions, karren) as well as at depth; the conduit network and caves [13].

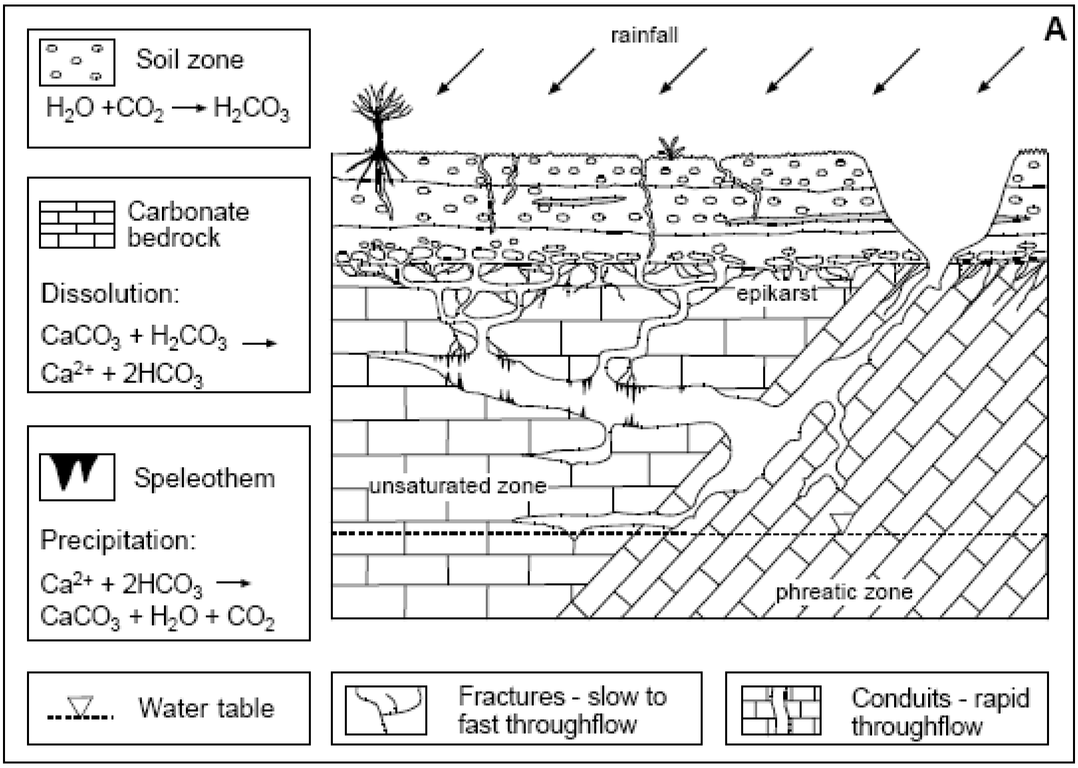

Figure 2-1 Conceptual model of the karst system with its physiology of water flow and CO_2 transport and release [14]

2.1.2 Carbonate deposition

Biological and biochemical process are dominant in the formation of carbonate sediments, although inorganic precipitation of $CaCO_3$ from seawater also takes place [15]. Limestones and dolomites make up about 20 per cent of the sedimentary rocks. Today, calcareous ooze covers nearly half the ocean bottom, but it is apparently rare on the continents. Most limestones have been formed in shallow water, as is shown by their fossils. Among modern shallow water sediments find many limestones, but not to the abundant dolomites (Figure 2-2) [16].

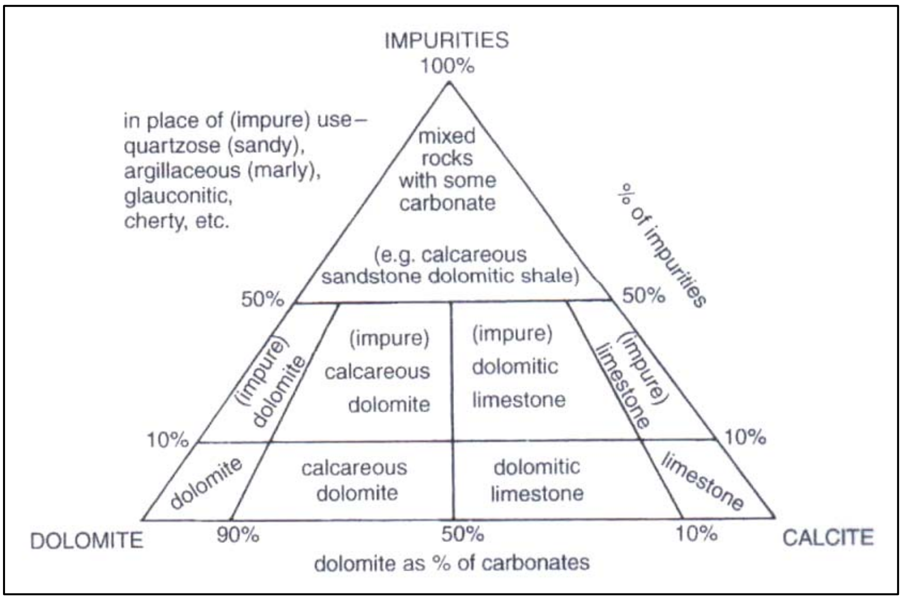

Figure 2-2 A bulk compositional classification of carbonate rock [17]

1) Limestone

Limestone is a sedimentary rock composed largely of the mineral calcite. It often contains variable amounts of silica in the form of chert or flint, as well as varying amounts of clay, silt and sand as disseminations, nodules, or layers within the rock. Limestones occur throughout the world in every geological period from the Cambrian onwards and reflect the changing fortunes, through evolution and extinction, of invertebrates with carbonate skeletons. In the Precambrian, carbonates are also abundant, but they are commonly dolomite and many contain stromatolites, produced largely by microbes, especially the cyanobacteria (blue-green algae) [15]. The primary source of limestone is most commonly marine organisms. These organisms secreting shells are deposited on ocean floors as pelagic ooze or alternatively are conglomerated in a coral reef. Secondary limestone may also be deposited by supersaturated meteoric waters (groundwater that precipitates the material in caves). This produces speleothems such as stalagmites and stalactites. The most important limestone minerals are calcite and aragonite (Table 2-1 and Figure 2-3) [18] which precipitated by marine animals for shell and skeleton building, expelled as faeces or precipitated in the tissues of algal plants. Cementation and recrystallization during diagenesis add inorganic calcite spar that is relatively coarse. These principle components of limestone are summarized in Table 2-2 and classification of limestone in Figure 2-4 [17].

Table 2-1 Properties of limestone minerals [17]

Mineral	Chemical composition	Specific gravity	Hardness	Description
Calcite	$CaCO_3$	2.71	3	Trigonal system; rhombohedral. Habit: massive, scalennohedral. Twinning is rare > 2000 varieties of crystals reported. Colourless or wide rang of colours. Effervesces vigorously in cold, dilute acids
Aragonite	$CaCO_3$	2.95	3.5-4	Orthorhombic system; dipyramidal. Habit: acicular, prismatic or tabular. Frequent twinning. Metastable polymorph of calcite. Colourless, white or yellow. Effervesces in dilute acids.

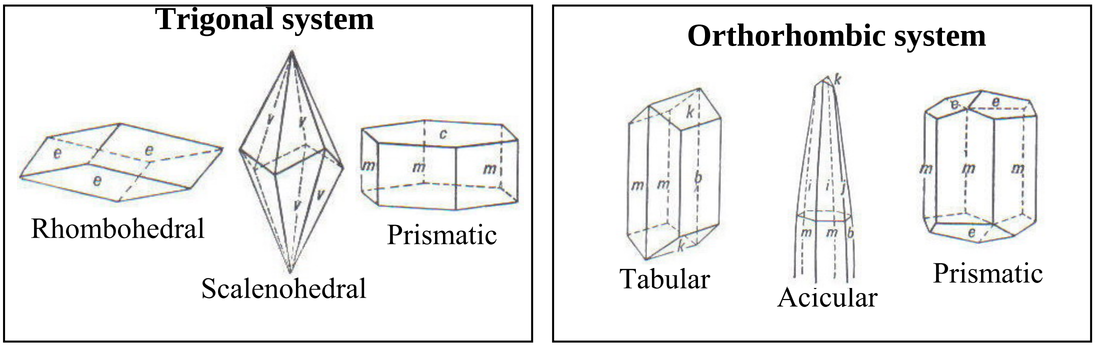

(a) (b)

Figure 2-3 Crystal systems of calcite (a) and aragonite (b)

Table 2-2 The principal component of limestone [17]

Textural type	Deacription	Origin
Micrite	0.5-5 µm diameter lime mud and silt particles. The largest component by volume in a majority of limestone	Clay and silt sized original marine grains
peloids	Faecal pellets, micro-ooliths, 30-100 µm diameter. By volume, the most important larger particles	Ooze
Oolith	Sand-sized spherical accretions	Sand-sized or larger original marine grains, skeletons and growths
Lump or grapestone	Clumped periods, ooliths	
Oncolites	Algal accretionary grains up to 8 cm diameter	
Skeletal	Corals, vertebrates, shell fauna, etc. Algal stems and other flora in situ or transported. Fragments of all genera	
Intraclasts	Eroded fragments of partly lithified local carbonate sediment e.g. beach rock	
Lithoclasts	Consolidated limestone and other fragments; often allogenic	
Framework	Constructed reefs etc., mounds, bioherms, biostromes	
Vadose silt	Carbonate weathering silt	Formed during vadose exposure
Pisoliths	Large ooliths or concretions e.g. nodular caliche, cave pearls	
Sparite	Medium to large calcite crystals as cementing infill; drusy, blocky, fibrous, or rim cement >20 µm diameter	Diagenetic cement
Microspar	5-20 µm grains replacing micrite	

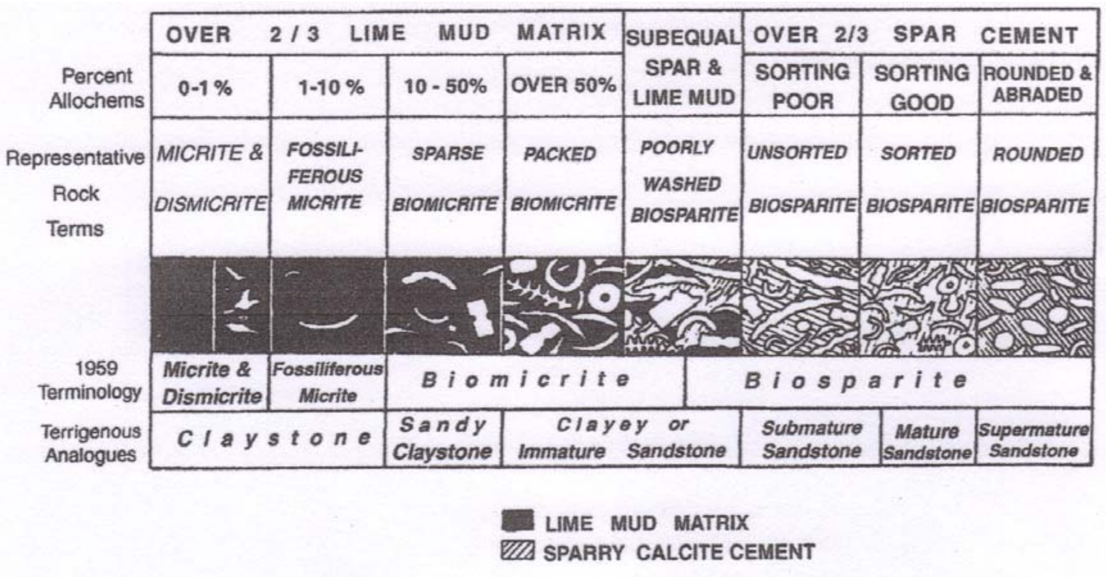

	OVER 2/3 LIME MUD MATRIX				SUBEQUAL SPAR & LIME MUD	OVER 2/3 SPAR CEMENT		
Percent Allochems	0-1 %	1-10 %	10 - 50%	OVER 50%		SORTING POOR	SORTING GOOD	ROUNDED & ABRADED
Representative Rock Terms	*MICRITE & DISMICRITE*	*FOSSILI-FEROUS MICRITE*	*SPARSE BIOMICRITE*	*PACKED BIOMICRITE*	*POORLY WASHED BIOSPARITE*	*UNSORTED BIOSPARITE*	*SORTED BIOSPARITE*	*ROUNDED BIOSPARITE*
1959 Terminology	*Micrite & Dismicrite*	*Fossiliferous Micrite*	*Biomicrite*			*Biosparite*		
Terrigenous Analogues	*Claystone*		*Sandy Claystone*	*Clayey or Immature Sandstone*		*Submature Sandstone*	*Mature Sandstone*	*Supermature Sandstone*

■ LIME MUD MATRIX
▨ SPARRY CALCITE CEMENT

Figure 2-4 Classification of limestone, reproduced with permission from Fork [17]

The carbonate mineral calcite is a calcium carbonate corresponding to the formula $CaCO_3$ and is one of the most widely distributed minerals on the Earth's surface. It is a common constituent of sedimentary rocks, limestone in particular. It also occurs in caverns as stalactites and stalagmites. Calcite is often the primary constituent of the shells of marine organisms. It is the thermodynamically stable form of calcium carbonate under temperature, pressure, and CO_2 partial pressure found in caves [18].

Aragonite is a mineral which has the same composition (formula is $CaCO_3$) but different crystal structure as calcite. Aragonite naturally occurs in almost all mollusk shells. It is less stable than calcite under atmospheric conditions and much less common. Aragonite normally has a very low Mg content (less than 5000 ppm.) but it may contain up to 10000 ppm. (1%) strontium, substituting for calcium [15]. It is precipitated in a narrow range of physicochemical conditions presented by low temperature, near-surface deposits. Experiments have shown that carbonated water containing calcium more often deposits aragonite when the water is warm and calcite when the water is cold. Aragonite is deposited by hot springs; found associated with beds of gypsum and deposits of iron ore where it may occur in forms resembling coral [19].

Stability diagram for $CaCO_3$ at low temperatures and pressures shows that calcite is the expected polymorph in caves at atmospheric pressure. For a given pressure, as temperature is increased, aragonite will generally convert to calcite. Similarly, for a given temperature, as pressure is increased, calcite will convert to aragonite (Figure 2-5).

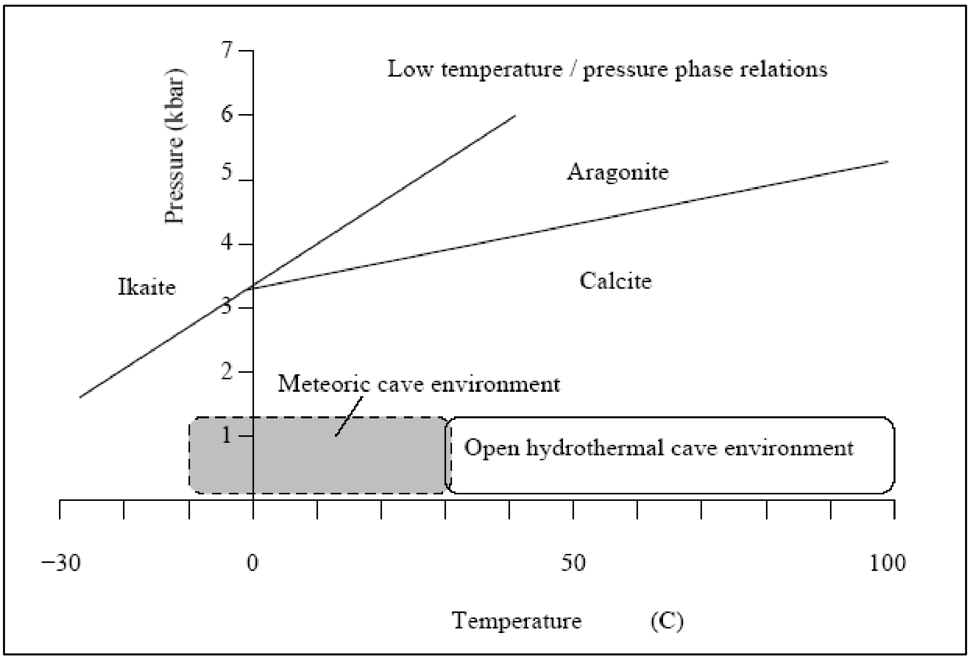

Figure 2-5 Stability Diagram for $CaCO_3$ determined fields of calcite and aragonite, (Ikaite is $CaCO_3 \cdot 6H_2O$ which forms as a pseudomorphs after calcite) [20]

For either aragonite or calcite to deposit, there needs to be a source of bicarbonate ion, HCO^{-}_3 in solution, a means of allowing carbon dioxide to outgas or be otherwise removed from the reaction, and the solution needs to be supersaturated with respect to calcium carbonate. In the cave environment, these conditions usually lead to the deposition of calcite, as that is the most stable polymorph of calcium carbonate for those environmental conditions. However, aragonite forms persist in caves because there are various factors which is substances inhibited the crystallization of calcite and thereby allowed the precipitation of aragonite i.e. magnesium, strontium, pH, supersaturation and rate of precipitation, temperature, pressure, speleothems surfaces and carbon dioxide content [21].

2) Dolomite

Dolomite is described both the mineral and the rock [17]. It is a carbonate of both calcium and magnesium and offers one of the greatest geological puzzles. Dolomite as a rock mass is generally though to be secondary in origin [19]. The content of magnesium carbonate increased irregularly with depth. It was inferred that part of the calcium in the calcite shells had been replaced by magnesium ions from the sea water. Very few organisms secrete shells with an appreciable content of magnesium carbonate, and in the few that do, the ratio of magnesium carbonate to calcium carbonate falls far short of that in dolomite. No inorganic dolomite being deposited in the present seas [16]. Yet dolomite, though extremely rare among the Tertiary rocks, is both widespread and abundant in rocks of the long interval from middle Precambrian through the Mesozoic.

The mineral dolomite (Table 2-3 and Figure 2-3a) corresponding to the formula $CaMg(CO_3)_2$, occurs also as a hydrothermal vein mineral, chiefly in the lead and zinc veins that traverse limestone, associated with fluorite, calcite, barite, and siderite [22].

Table 2-3 Properties of dolomite mineral [17]

Mineral	Chemical composition	Specific gravity	Hardness	Description
Dolomite	$CaMg(CO_3)_2$	2.85	3.5-4	Hexagonal system; rhombohedral. Habit: rhombohedron, massive, sugary (saccharoidal) or powdery. Colourless, white or brown, usually pink tinted. Effervesces slightly in dilute acid.

2.1.3 Cave

Caves are a product of karstification whereby relatively soluble rocks such as limestone are dissolved by downward percolating meteoric waters that have interacted with a soil zone containing elevated levels of CO_2 [1].

Temperatures of caves remain essentially constant throughout the year in poorly ventilated caves (typically $\pm 1^{o}C$), reflecting the high thermal inertia of host rocks. As a consequence, seasonal temperature variations are usually averaged out, and cave air temperatures are similar to the mean annual air temperature of the region above the cave. Cave air is characterized by high relative humidity (typically 95 to 100%) that minimizes evaporation of cave drip water. Aside from areas close to cave entrances where lower humidity and air currents permit evaporation, secondary calcite deposition typically occurs by degassing of CO_2 from carbonate-saturated drip waters, and not by evaporation of water [23]. Mineral deposits take on the form of stalactites, stalagmites, flowstone, and other forms known collectively as speleothems. Because these deposits are nourished by water seeping down from the surface, changes in the climate and vegetation on the surface leave their signatures in the growth bands of the speleothems. The deposits of caves have become an important source of paleoclimatic information [24]. The shape of cave passages influences the distribution of speleothems; the rate of ventilation of caves in relation to the rate of input of fluids is also a critical control on speleothems growth [25]. Dramatic changes in pCO_2 and $\delta^{13}C$ or water and cave air in response to seasonal changes in ventilation have been demonstrated by detailed monitoring at the Austrian Obir cave [26].

1) The factors of cave origin

(1.1) Parent rock

Generally, caves are productive rock that can be dissolved in water as follow as the rocks which have componential carbonate and sulfate; for example, limestone ($CaCO_3$), dolomite ($CaMg(CO_3)_2$), gypsum ($CaSO_4.2H_2O$) etc. Because water is weakly acid when it has a reaction with minerals then it can cause the minerals to dissolve [27].

(1.2) Geomorphology

Most limestone originated from calcium carbonate sediments in the sea which have a million years in occurrence and become to a rock in finally. When the Earth's crust has movement, limestone uplift above the sea level and become to the ground and the mountain. While the Earth's crust moves, structure was changed. In such case, there will be a curve bend within a rock, fracture, and fault in that cracked rocks which contain a lot of void spaces. The fracture or void space is the important factor for creating the caves because of the water flowing through a fracture can make a wider void space [27].

(1.3) Water

Water is an important factor of caves. In the water cycle, when the water in the ocean, the sea, and the river receive the heat from sunlight, it evaporates, and assembles to be the cloud which condenses to be the precipitation and finally falls to the Earth's surface. The precipitation becomes weakly acidic because it reacts chemically with carbon dioxide that occurs naturally in the atmosphere and the soil. This acid is named carbonic acid as equation (I). Rainwater seeps downward through the soil and fractures in the rock responding to the force of gravity. Carbonic acid is fractured as equation (II). The carbonic acid in the ground water dissolves the bedrock along the surfaces of joints, fractures, and bedding planes then it breakdowns to calcium-bicarbonate as equation (III), Calcium-bicarbonate which readily dissolves in water and eventually forming cave passages and caverns [27].

$$2(H_2O) + 2(CO_2) \longleftrightarrow 2(H_2CO_3) \quad \text{Carbonic Acid} \quad \text{(I)}$$

Carbonic acid is fractured as equation (II)

$$2(H_2CO_3) \longleftrightarrow 2(H^+) + 2(HCO_3)^- \quad \text{Bicarbonate Ions (II)}$$

Limestone was dissolved and become to calcium-bicarbonate.

$$2(H^+) + 2(HCO_3)^- + CaCO_3 \longleftrightarrow H_2O + CO_2 + Ca_2^+ + 2(HCO_3)^- \quad \text{(III)}$$

(1.4) Topography

Generally, water flows through from high to low elevations. The rate of stream flow at high landscape (that has slope) rather than plain landscape. The high rates of turbulent flow of stream have a rich power of erosion and rapid solution of rock. In the study area, there are high mountains which have steep slope [27].

(1.5) Forest and vegetation

The forests that cover the surface are important because the fertile forest can absorb a rain and transfer the water into soil. If the surface does not have a tree, the rain will cause the rapid runoff by flowing from the mountain to the river. In contrast, the surface which has a tree can slow down the runoff because water is absorbed and gradually flowing by the root and becomes aquifer flow through bedrock, and creating speleothems in caves [27].

2) Types of caves

In terms of geologic setting, caves have been formed by many processes. Figure 2-6 shows a variety of caves that have different processes for the cave development. Most caves in Thailand are the solution caves that have a common process of cave formation in karstification. Most solution caves are formed in limestone or dolomite. These would be called limestone caves or dolomite caves [28] which dissolved by groundwater in contemporary drainage basins for example Namjang cave of this study at Pang Ma Pha, Mae Hong Son province, Thailand.

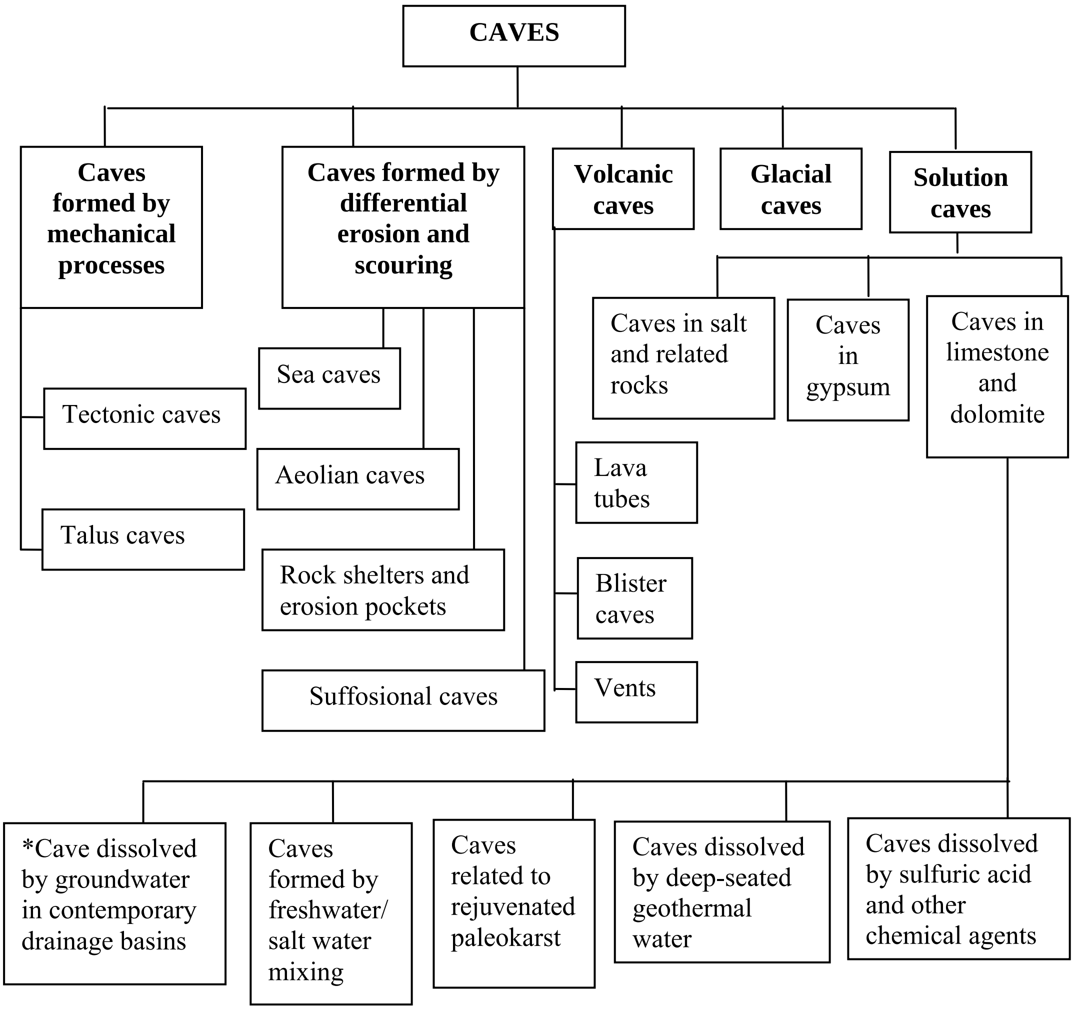

Figure 2-6 Varieties of caves (* Type of cave at the study area) [28]

2.1.4 Speleothems deposition

A word, speleothems is from the Greek for "cave deposit". The deposition of speleothems is dependent on geological, hydrological, chemical, and climatic factors. A change in any one of these factors could cause water percolation to terminate the growth of speleothems at a particular drip site. However, cessation of speleothems growth over a large geographical area is more likely to be due to a climatic factor than anything else, so dating periods of speleothems growth can provide useful paleoclimatic information [1]. Precipitation of calcite from supersaturated H_2O-CO_2-$CaCO_3$ solutions sculpts fascinating cave decorations of stalagmites, stalactites, and other speleothems and also creates flowstones (Figure 2-7).

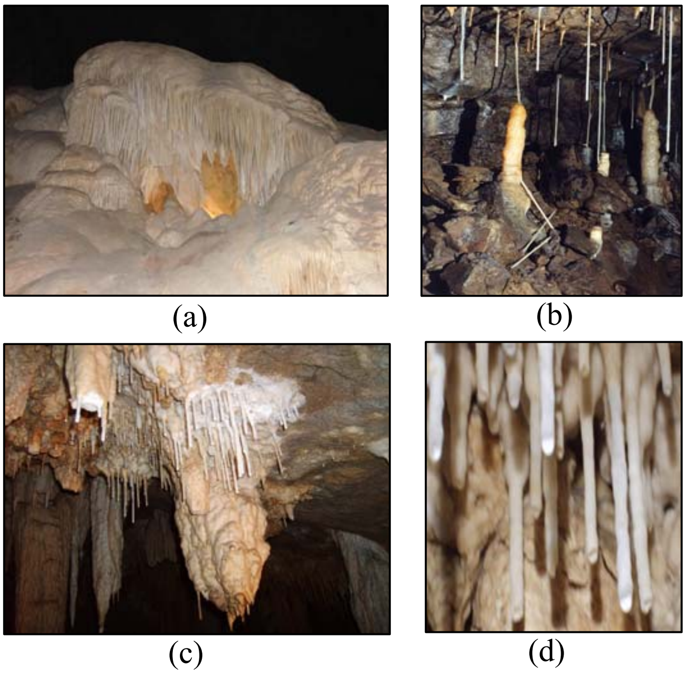
(a) (b) (c) (d)

Figure 2-7 Speleothems deposition such as, flowstones (a), stalagmites (b), stalactites,and soda straws (c,d)

Rainwater seeping through vegetated soils on its way down to the limestone bedrock can absorb large amounts of carbon dioxide, which is present in the soil in much higher concentrations than in the atmosphere. When this water moves down, it dissolves limestone in the soil and in the fissures of the bedrock and saturation with respect to calcite. If such a solution enters a cave, degassing of CO_2 creates a supersaturated solution from which calcite is deposited. This causes the growth of calcite speleothems in their various shapes [24]. An important starting point for modern geochemical studies of the carbonate system in cave waters is that of Holland [29], who related water chemistry to host rock chemistry and cave processes and confirmed that CO_2 degassing, rather than evaporation, was the key process stimulating speleothems formation. Bögli [30] correctly emphasized the key control of organically derived CO_2 in soils in driving more carbonate dissolution and stimulating more speleothems formation in tropical climates. Earlier literature suggested that the seasonal pattern in pCO_2 that is commonly found in karst soils is transmitted to the cave environment, leading to seasonal changes in water hardness and growth rate of speleothems. However, the data exhibit a large scatter and local controls can also be important in determining soil $p\mathrm{CO}_2$.

1) Flowstones

Flowstones are widespread coverings of cave floor and walls that accrete roughly parallel to the host surface and may occur tens or hundreds of metres downstream of the water source. They have in common a tendency to display undulations in surface morphology and the lamina structure is dominantly parallel and continuous, but in detail there are many sub-types reflecting local slopes, water supply and other factors. Laminae arise primarily because of variations in impurity content and they may also fluoresce under ultraviolet excitation. An advantage for paleoenvironmental study is that flowstones can be cored with relatively little damage to the cave environment, and they can grow over tens to thousands of year. Conversely, there are issues of representative of a small core, and dating can be compromised by impurities. Flowstones often form under intermittent or weakly supersaturated thin flows of water and so typically accrete slowly (10-100 μm/year).

2) Stalactites and soda straws

Stalactites are centimeters to meters in scale and they hang from the ceiling and grow toward the floor. Some workers have cut solid stalactites to derive sections for successful paleoclimatic work, but others have avoided them because of concerns over lamina geometry [31], or perhaps for fear of insufficient control on lateral changes in composition on their surface [32]. However, Baldini [33] representation to the relative volume of stalactites versus their underlying stalagmites, and found a correlation with drip rate that can be explained by the incomplete degassing of fast drips from stalactites.

The most common variety of stalactites is the tubular soda straw, consisting of thin, translucent, tubular layers of crystals surrounding a central canal. Soda straws are speleothems generated by sole axial feeding. They are hollow, with a diameter minimized by the surface tension of the water drop at their tip. They have a wall only 0.1-0.4 mm thick, and so accrete primarily downwards with preferentially orientated crystals [34]. Soda straws drip relatively slowly, although the relationship to drip rates on solid stalactites have not been systematically investigated [31]. Soda straws commonly display a lateral banding whose regularity and spacing suggests an annual origin. A particularly neat way of confirming the annual origin of bands was found by Huang [35] who found equally-spaced internal impurity layers, homologous with layers in stalagmites from the same cave and the bands are known to be annual in origin. Although soda straws can be used to derive short, and unusually high-resolution proxy environmental records, but they are difficult to handle and analyze [36].

3) Stalagmites

Stalagmites are convex cave deposits that grow from the floor upward and are commonly fed by water dripping from an overhead stalactites. Stalagmites do not show a central canal. Calcite and aragonite stalagmites commonly form through carbonate deposition from a thin film of supersaturated fluid. Successive stalagmite layers are formed by composite crystals consisting of crystallites, which can be considered as the smallest unit of which composite crystals are built. The stacking pattern of these crystallites yields different fabrics [37]. Folk [38] represented that columnar fabric consists of crystals with a length to width ratio ≤ 6:1, with usually straight crystal boundaries. Where the length to width ratio is ≥ 6:1 the fabric is called fibrous. Likewise, Tan [39] described annual type of stalagmite as; the annual layer, sub annual or supra annual layers and missing annual layers should not be commonplace which called “hiatus”. Stalagmite crystal morphology is related to parent water flow and chemistry, in terms of drip rate and chemistry, capillary or gravitational supply of ions to growth sites, rate of CO_2 outgassing, and the variability of these factors [31]. Columnar and fibrous fabric may show visible alternation of brown and white laminae, which is caused by seasonal variations in drip-water flow and chemistry. The development of layering in columnar calcite has been studied through scanning electron microscopy observation of seasonal precipitates in an alpine cave. Crystallites show relatively large sizes (up to 150 μm wide) and rugged crystal surface morphology in the season when water supersaturation with respect to calcium carbonate is higher [37].

Changes in physical and chemical characteristics of stalagmites are used to extract information on past climate and environment evolution at very high resolution, because stalagmites can be dated precisely with the uranium series method and the counting of annual growth laminae, they contain trace element and isotopic tracers that have been used to infer changes in paleotemperature, paleovegetation and paleoprecipitation [3], and they are particularly important in those areas where speleothems are the only archives of paleodata that cover long time spans, such as arid or high mountain regions.

In China, Beijing cave, annually laminated stalagmites should be expected in caves which have an overlying climate that has a strong seasonality, similar climate zones to where trees grow with distinct annual rings. Although numerous tree ring climate records, which are frequently limited in preserving multi-centennial trends that contrasts continuous laminated stalagmite chronologies (up to several thousand years). However, laminated stalagmites and tree rings should therefore to some degree provide complementary climate information [39]. Moreover, oxygen isotope records of five stalagmites from Hulu Cave near Nanjing bear a remarkable resemblance to oxygen isotope records from Greenland ice cores, suggesting that East Asian Monsoon intensity changed in concern with Greenland temperature between 11,000 and 75,000 years before the present (yr. B.P.) [40].

In India, rainfall reconstruction from speleothems agrees well with the earlier observations using other proxies such as before ~1200 yr BP arid phase is indicated by the GUP (stalagmite in Gupteswar cave) agrees with observed by the sediment cores in the western Arabian sea. In addition, high rainfall during ~1666 AD by AKG (stalagmite in Akalagavi cave) agrees with the tree-ring width index around this period [8].

2.2 Isotopes

2.2.1 Environmental isotopes

Everything in the universe is made of atoms, which are in turn made out of protons, neutrons, and electrons. The heavier protons and neutrons sit in the middle (the nucleus) of the atom with the much lighter electrons orbiting around them. Protons have a positive charge, electrons have a negative charge, and neutrons have no charge. Atoms have an atomic number, which is the number of protons. They also have an atomic mass which is the sum of their protons and neutrons. Sometimes two different atoms may have the same number of protons, but different numbers of neutrons. In this case, the atoms are of the same element, but they have different masses. These two atoms are called *isotopes* [1]. Hence, isotopes or the same element are slightly different in mass and energy which cause differences in physical and chemical properties. These differences are generally greatest for element of low atomic number. In a molecule with two isotopes, the isotope of lighter mass possesses weaker bonds and is more reactive than the heavier isotope. A change in the ratio of the two isotopes during a reaction or process is called a *fractionation* [15].

The environmental isotopes are a subset of the isotopes; both stable isotope which do not spontaneously disintegrate by any known mode of decay and unstable isotopes or radioactive nuclides have a certain probability of decay. Environmental isotopes now routinely contribute to such investigations, complementing geochemistry and physical hydrogeology. The stable isotopic composition of water, for instance, is modified by meteoric processes, and so the recharge waters in a particular environment will have a characteristic isotopic signature. This signature then serves as a natural tracer for the provenance of groundwater. On the other hand, radioisotopes decay, providing us with a measure of circulation time. Environmental isotopes provide, however, much more than indications of groundwater provenance and age. Looking at isotopes in water, solutes and solids tells us about groundwater quality, geochemical evolution, recharge processes, rock-water interaction, and the origin of salinity and contaminant processes [41].

The most used environmental isotopes are: deuterium, tritium, carbon-13, carbon-14 nitrogen-15, oxygen-18, silicon-29, chlorine-36, uranium 234 etc. [42]. However, for investigation of speleothems, stable isotopes of carbon-13 and oxygen-18 and radioactive uranium-disequilibrium dating are used.

2.2.2 Speleothems isotopes

1) Carbon isotopes

In fact, carbon provides the basis for terrestrial life and is omnipresent in the universe and on Earth (Figure 2-8). Chemically, carbon has an atomic weight of 12.011, an atomic number of 6 and a melting point of 3550°C. Two stable isotopes include ^{12}C and ^{13}C with abundances of 98.89% and 1.11% respectively and the radionuclides include ^{11}C and ^{14}C. The latter are either produced artificially through several reactions as, for instance, ^{11}C or naturally through cosmic radiation.

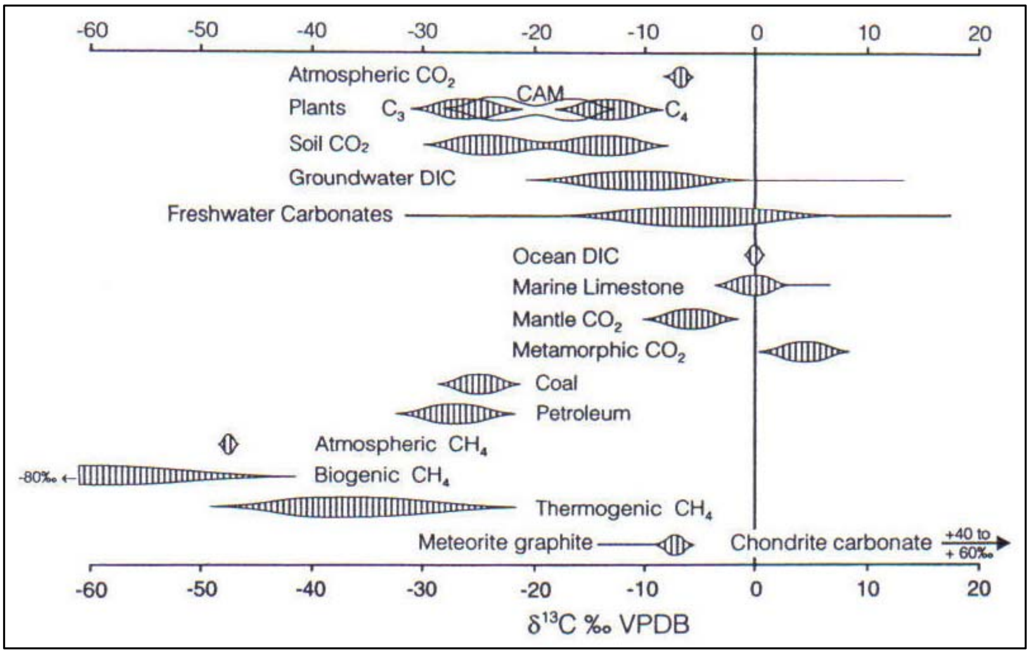

Figure 2-8 Ranges for $\delta^{13}C$ value in selected natural compounds. Especially noteworthy in the spreading of $\delta^{13}C$ seen in different plant groups are resulting on soil CO_2 [41]

The C isotopes are fractionated by incorporation into living systems and/or biochemical processing due to thermodynamic and kinetic effects imposed on the main metabolic pathways. Such biological fractionations are basically retained when organic matter becomes incorporated into sediments. Thus, these effects are introduced into the rock cycle of the geochemical cycle [43].

Carbon-13 in speleothems

The carbon dissolved in drip waters mainly derives from three sources: atmospheric CO_2, soil CO_2 and dissolution of the karstic host rock [31]. The carbon isotopic evolution of speleothems is a complex process that depends upon several factors (Figure 2-9) [32].

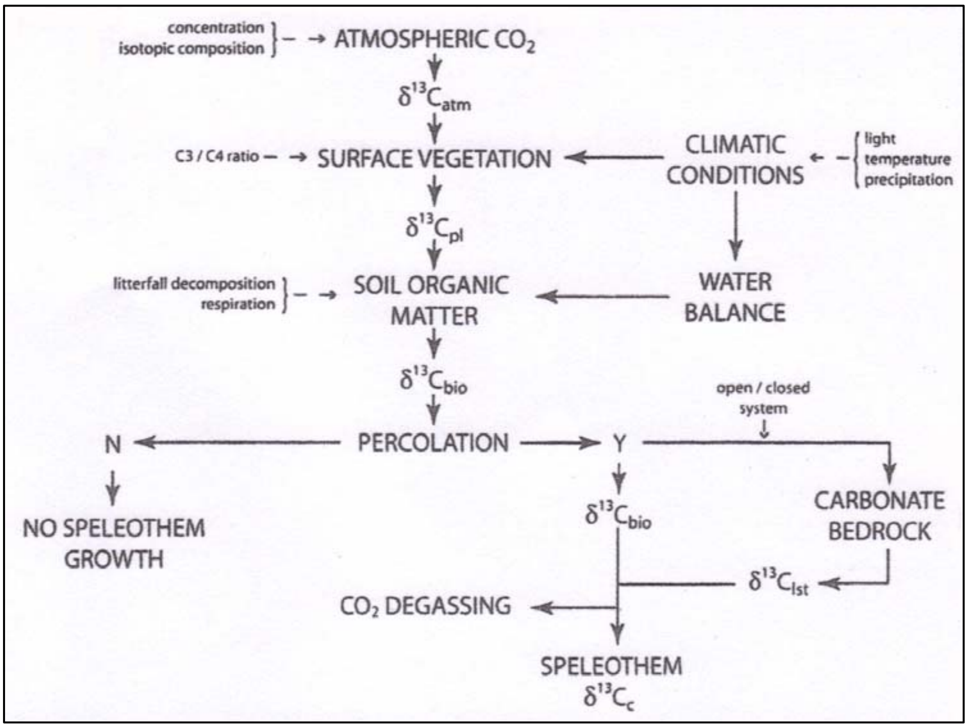

Figure 2-9 Factors determining the $\delta^{13}C_c$ composition of speleothems calcite (assuming equilibrium deposition) [17]

There are four main factors which influence to $\delta^{13}C_c$ as follows;

1) The photosynthetic pathways (i.e. C_3/C_4 pathways)

Plants using the C_4 (Hatch-Slack) cycle of photosynthesis abound in semi-arid environments and synthesize cellulose which has $\delta^{13}C$ lower by about 5‰ (they have $\delta^{13}C$ values between ~ -10 to -16‰, mean value of about -12.5‰) relative to the atmospheric CO_2 (~-7‰), whereas C_3 (Calvin cycle) plants which live in humid environments produce carbon compounds which are depleted by about 19‰ (they have $\delta^{13}C$ between ~ -24 to -30‰, mean value of about -27‰) with respect to the atmospheric CO_2 (~-7‰) [8]. These differences are preserved as distinctive ranges in

$\delta^{13}C$ in secondary carbonates (typically -14% to -6% for carbonates deposited in equilibrium with CO_2 respired from C_3 plants, and -6% to +2% for that from C_4 plants) [44]. As $\delta^{13}C_c$ ($\delta^{13}C$ in calcite) will depend upon CO_2 contributed from both type of plants, any change in their relative proportions caused by climatic change may alter the C_3/ C_4 ratio and hence the relative contribution to the $\delta^{13}C_c$.

2) Biological activity

Carbon dioxide in the soil is derived from two sources: microbial decomposition of the soil organic matter and root respiration of the plants (this has relatively more negative $\delta^{13}C$). Intense respiration process might result in high pCO_2 and depleted $\delta^{13}C$ [8].

3) Bedrock proportion

Limestone dissolution may proceed along two extreme routes:

a) Open-system, continuous equilibration occurs between the seepage water and an infinite reservoir of soil CO_2. This drives a monotonic increase in bicarbonate content as the water progressively acquires more solutes in the unsaturated zone. Under these conditions, the $\delta^{13}C$ of the dissolved species reflects the isotopic composition of the soil CO_2, with no detectable isotopic imprint from the carbonate host-rock.

b) Closed system conditions by contrast, the percolating water becomes isolated from the soil CO_2 reservoir as soon as carbonate dissolution commences, and since CO_2 is consumed in the carbonation reaction $H_2O+CO_2=H_2CO_3$ the extent of limestone dissolution is limited by the finite CO_2 reservoir. Under these conditions the isotopic composition of the carbonate host-rock influences the isotopic (carbon atoms in the solution originate from two sources, the soil CO_2 and dissolved limestone).

In practice most natural systems are likely to be partially open [45].

4) Drip rate in the cave

Higher drip rate results in depleted $\delta^{13}C_c$. As the drip rate is directly proportional to the rainfall in a crude way, this may result in dependence of $\delta^{13}C_c$ on the amount of rainfall [8].

Gentya *et al.* [46] showed that the last glaciations and its climatic events have been clearly recorded in the $\delta^{13}C$ profiles of three stalagmites from caves from Southern France to Northern Tunisia. The three $\delta^{13}C$ records, show great synchroneity and similarity in shape with the Chinese cave $\delta^{18}O$ records and with the marine tropical records, leading to the hypothesis of an in-phase (between 15.5 and 16 ka ± 0.5 ka) postglacial warming in the Northern Hemisphere. Likewise, three modern stalagmites from Brown's Folly Mine, Wiltshire, England, are correlative with a well-documented re-vegetation above the mine. Increased soil pCO_2 resulted in greater amounts of dissolved $CaCO_3$ in the drip waters, which consequently increased annual calcite deposition rates. The absence of deposition prior to 1916 (28 years after the mine was closed) indicates that vegetation had not yet sufficiently developed to allow higher pCO_2 values to form in the soil. Lower $\delta^{13}C$ values through time may reflect the increased input of isotopically light biogenic carbon to the total dissolved inorganic carbon (DIC). $\delta^{18}O$ decreased synchronously with $\delta^{13}C$, reflecting the increased importance of isotopically light winter recharge due to greater biomass induced summer evapotranspiration [47].

2) Oxygen isotopes

With 46.6 mass % and 55.1 atom %, oxygen is the most abundant element in the terrestrial crust. With the atomic number of 8, it has nine isotopes ranging in mass from 13 to 21 of which only the three stable isotopes ^{16}O, ^{17}O and ^{18}O are of geoscientific interest. Oxygen has a valence state of -2 and the three stable isotopes have the following relative abundances: $^{16}O = 99.763\%$; $^{17}O = 0.0375\%$; $^{18}O = 0.1995\%$. Oxygen is necessary for the respiration of nearly all organisms except anaerobic bacteria. Now being practically indispensable to life, its absence in the primeval atmosphere of the Earth was mandatory for the development of the first organic compounds (Figure 2-10) [43].

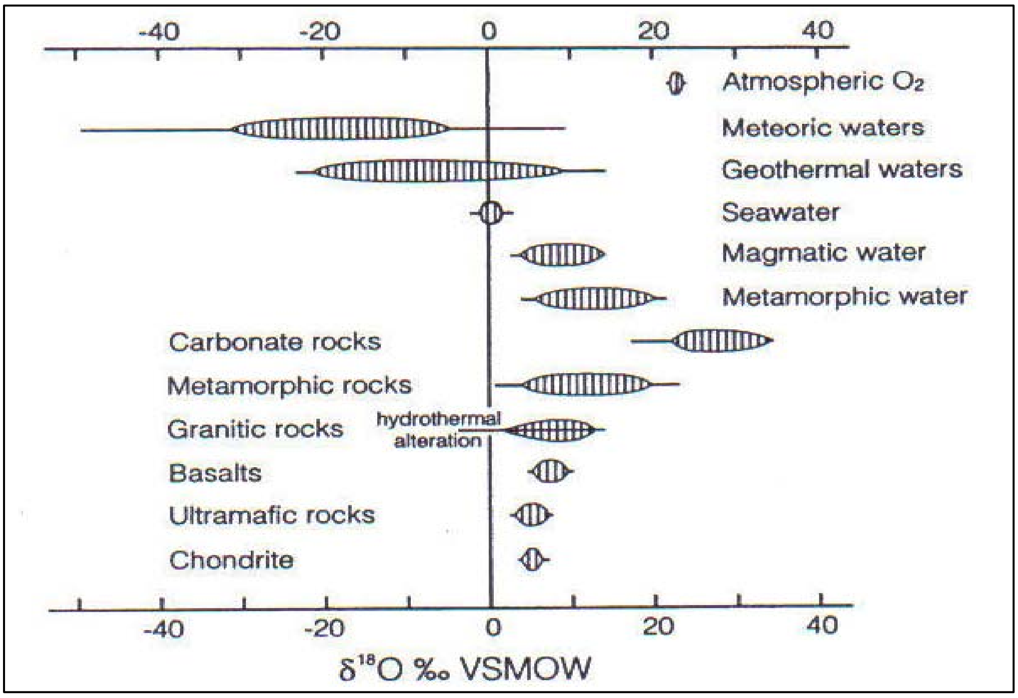

Figure 2-10 The range of δ^{18}O in various crustal rock and water type [41]

Both VPDB and VSMOW are recognized international standards for ^{18}O. While waters are exclusively referenced to VSMOW, carbonates can refer to either. VPDB was originally introduced for paleoclimatic studies. However, the use of carbonate isotopes has gone far beyond this field, and in water-carbonate studies it is common to express δ^{18}O data for carbonate against the VSMOW scale. Conversion is also necessary when deriving information about the δ^{18}O content of the water in which a carbonate has formed. The conversion chart in Figure 2-11 or the equations 2-1 and 2-2.

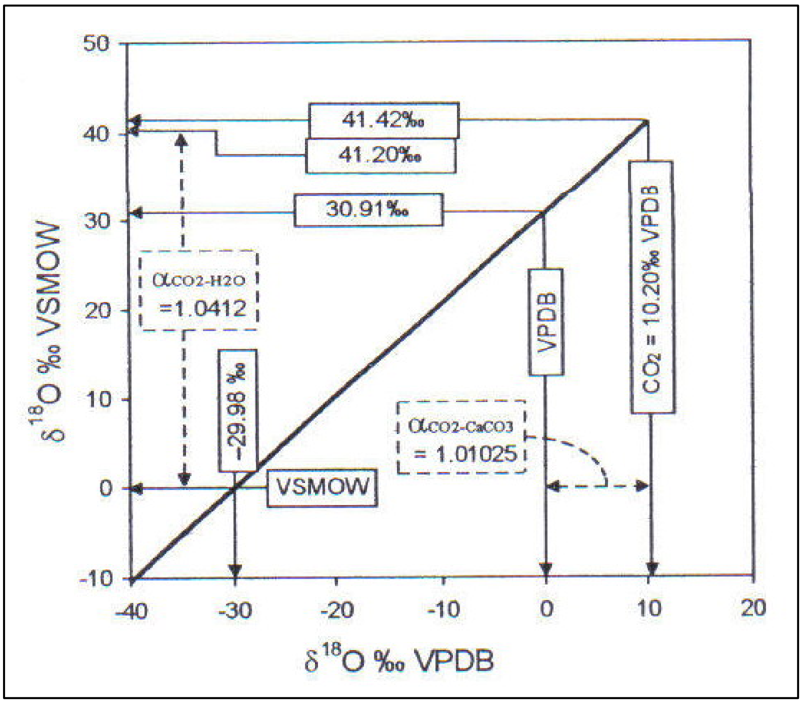

Figure 2-11 Conversion chart for $\delta^{18}O$ between VSMOW and VPDB, with fractionation factors for 25°C [41]

$$\delta^{18}O_{VSMOW} = 1.03091 * \delta^{18}O_{VPDB} + 30.91 \qquad (2\text{-}1)$$

$$\delta^{18}O_{VPDB} = 0.97002 * \delta^{18}O_{VSMOW} - 29.98 \qquad (2\text{-}2)$$

The basis for paleoclimatic interpretation of variations in the stable isotope content of water molecules is that the vapor pressure of $H_2{}^{16}O$ is higher than that of $HD^{16}O$ and $H_2{}^{18}O$ (10% higher than HDO, 1% higher than $H_2{}^{18}O$). The concentrations of deuterium and ^{18}O in meteoric waters exhibit a broad range of variations, both in time and space. Present-day distribution patterns of these isotopes in global precipitation reveal a close linkage with some climatically relevant meteorological parameters, such as surface air temperature, relative humidity of the atmosphere, and amount of precipitation. These empirical relations were used in numerous studies aimed at reconstruction past climates from various environmental archives, such as ice cores, lacustrine deposits, tree cellulose, and others.

In Southeast Asia, there are two monsoon systems operating during summer: the Indian monsoon originating in the Indian Ocean and the Pacific monsoon originating in the western equatorial Pacific. Monsoon rains reveal a distinct isotope signature, δ^2H and $\delta^{18}O$ of rainfall in the northern part of the region (above approximately 35°N of latitude) are mainly controlled by temperature; in the southern and southeastern parts they are dominated by the precipitation [9].

Oxygen-18 in speleothems

In the northern part of the region (above approximately 35°N of latitude), using period of speleothems growth as a rather crude index of paleoclimatic condition, attempts have also been made to use oxygen isotope variations along the speleothems growth axis as an indicator of paleotempertures. When air and water movement in a cave is relatively slow, a thermal equilibrium is established between the bedrock temperature and air temperature in the cave is approximately the same as the mean annual surface temperature outside the cave. During deposition of calcite from seepage (drip) water, as CO_2 is lost, fractionation of oxygen isotopes occurs that is dependent on the temperature of deposition. Thus, in theory oxygen isotopic variations in the speleothems calcite ($\delta^{18}O$) should provide a proxy of surface temperature through time. Unfortunately, the situation is not quite so simple. First, isotopic paleotemperatures are recorded only if the calcite (or aragonite) is deposited in isotopic equilibrium with the drip-water solution. This can be assessed by determining if $\delta^{18}O$ is constant along a growth layer; if values vary for the same depositional interval, it indicates that deposition was affected by evaporation, not just the slow degassing of CO_2; this would alter the simple temperature-dependent fractionation relationship [1].

In tropical regions, speleothems $\delta^{18}O$ and $\delta^{13}C$ are primarily controlled by the amount of rainfall, is a negative correlation. $\delta^{18}O_c$ ($\delta^{18}O$ in calcite) is depleted as amount of rainfall increases and the most intense rainfall correspond to the lowest $\delta^{18}O_c$, an effect is called "amount effect". During $CaCO_3$ precipitation, the stable isotope ratios of oxygen ($^{18}O/^{16}O$) and carbon ($^{13}C/^{12}C$) in the HCO_3^- ions in the dripping water are affected by the cave environment. These ratios are preserved in the $CaCO_3$ laminae and are used to decipher the past cave environment. The isotopic composition of seepage water in caves reflects the average value for the meteoric water falling on the soil above the cave (Figure 2-12).

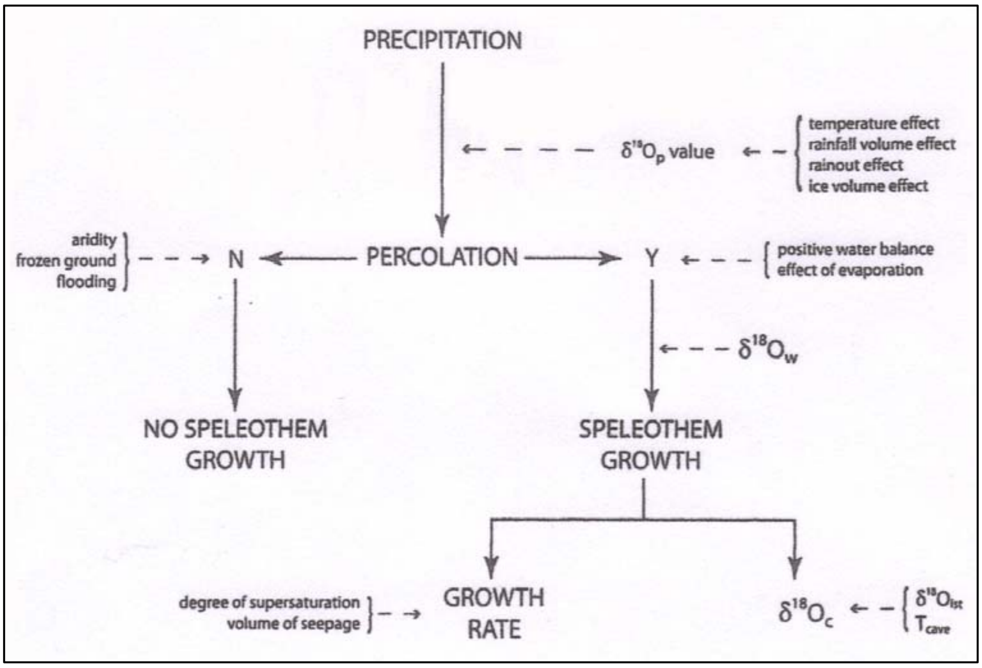

Figure 2-12: Factors determining the $\delta^{18}O_c$ composition of speleothems calcite (assuming equilibrium deposition) [17]

In India speleothems $\delta^{18}O$ is found to be primarily controlled by the $\delta^{18}O$ of the local precipitation. This is observed from the tip $\delta^{18}O$ values of stalagmite AKG (stalagmite in Akalagavi cave). Likewise the $\delta^{18}O$ of stalagmite AKG is depleted and enriched coincide with the excess and deficient rain years observed in the all India rainfall time series [8].

Evaluation of carbon and oxygen isotope ratios together with the speleothems growth history suggest that the carbon isotopic composition of the speleothems is primarily controlled by biogenic CO_2 supply from the soil, which is in turn affected by temperature and secondarily rainfall amount [48].

3) Uranium-thorium

Uranium has two natural parent isotopes, ^{238}U($t_{1/2}$ = 4.47 x 10^9 year) and ^{235}U($t_{1/2}$ = 7.04 x 10^8 years). With such long half-lives they and their daughter isotopes survive as common trace elements in igneous and derived rocks, especially black shales. They decay by emission of α particles (^{4}He nucleii), electrons (β) and photons (γ) to produce stable ^{206}Pb and ^{207}Pb respectively (Figure 2-13 and 2-14). The heavier of the intermediate daughters, ^{234}U($t_{1/2}$ = 2.45 x 10^5 years), ^{230}Th($t_{1/2}$ = 7.54 x 10^4 years), ^{226}Ra($t_{1/2}$ = 1600 years) and ^{231}Pa($t_{1/2}$ = 3.28 x 10^4 years) are also suitable for dating because of their comparatively long half-lives.

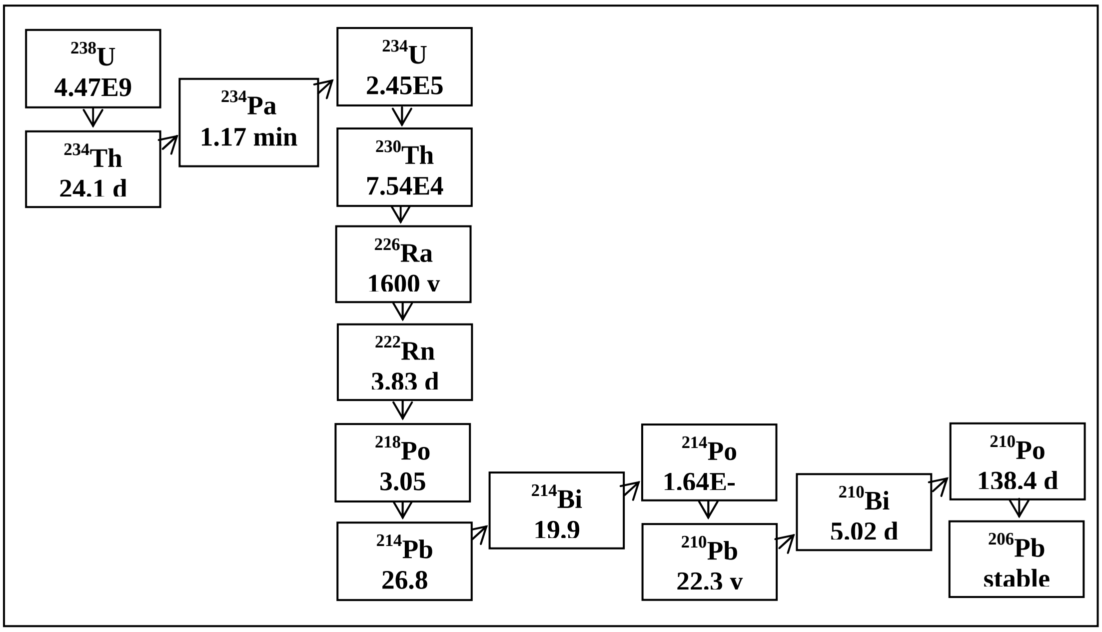

Figure 2-13 The ^{238}U decay series, with principal decay pathway, decay mechanism and half-life of radionuclides (E-10^x, s- second, min-minute, d-day, y-year) [43]

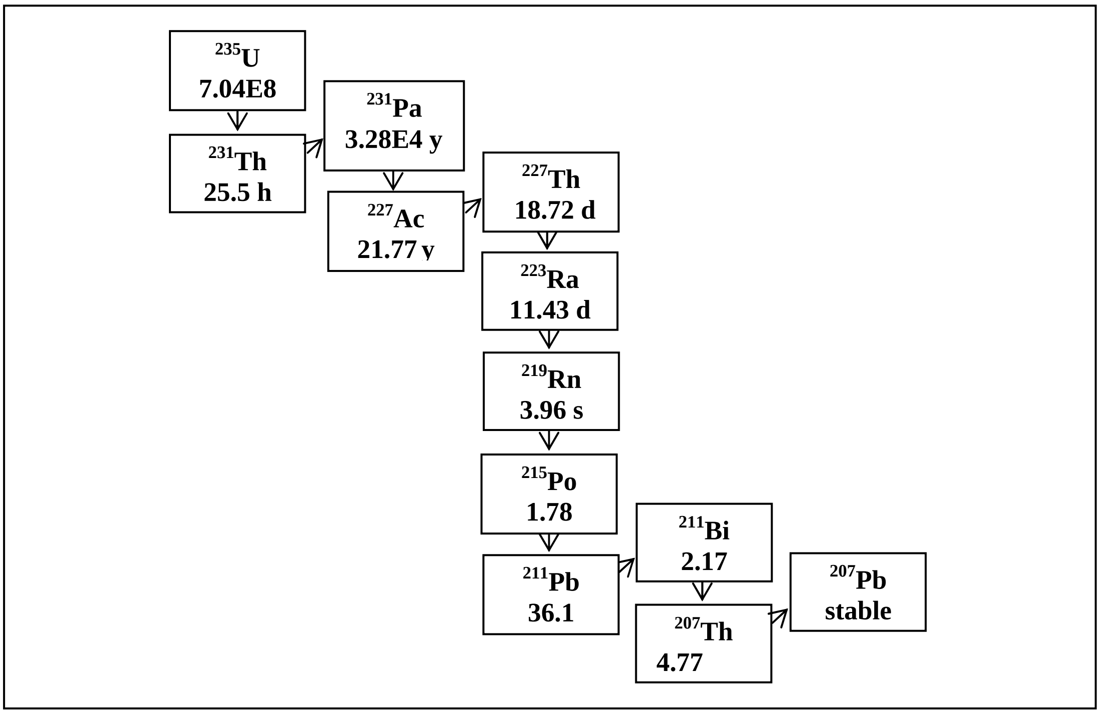

Figure 2-14 The ^{235}U decay series, with principal decay pathway, decay mechanism and half-life of radionuclides (E-10^x, s- second, h-hour, min-minute, d-day, y-year) [43]

Uranium-thorium in speleothems

Disequilibrium in the U species are widely used for dating, for the study of weathering systems and ground-water flow. They are the principal methods of dating speleothems at the present time [17], which can be used between a few hundred years (limited by determination of ^{230}Th) to around 500 ka. The interval dating can be carried out by counting annual layers [31].

Uranium-series disequilibrium dating, also called thorium-230 dating, or uranium-series dating, is a radiometric dating technique. Unlike other commonly used radiometric dating techniques such as rubidium-strontium or uranium-lead dating, the uranium-thorium technique does not measure accumulation of a stable end-member decay product, instead calculating an age from the degree to which equilibrium has been restored between the radioactive isotope thorium-230 and its radioactive parent uranium-234 within a sample [1].

When a rock containing U is weathered, a higher proportion of ^{234}U atoms are mobilized than of ^{238}U or ^{235}U atoms, i.e. there is 'daughter excess'. This is because many of the ^{234}U atoms became loosened in their crystal lattice position when emitting the α particle. All three species are readily oxidized and transported in solution in bicarbonate waters as the complexed ions $UO_2\ (CO_3)_2^{2-}$ and $UO_2(CO_3)_3^{4-}$. They may then be coprecipitated in calcite or aragonite, the latter normally accepting up to ten times more U atoms because of its larger lattice.

The long-lived daughters, ^{231}Pa and ^{230}Th, are essentially insoluble. When detached by weathering these bond to clay or other particles. Therefore, they are not precipitated in the calcite. In an ideal closed system they will accumulate there only as a function of the decay of the parent U species. One gram of calcite with a trace U content of l.0 ppm contains 10^{15} atoms of uranium available for spontaneous decay.

The chief dating method uses the decay of excess ^{234}U to ^{230}Th, with allowance for the parent ^{238}U. Figure 2-15 shows the graph of the dating equation with results from two different stalagmites plotted on it. Most clean speleothems are deposited with an initial ^{234}U:^{238}U activity ratio greater than 1.0 and a ^{230}Th:^{234}U ratio of 0.0. With the passage of time, ratios evolve to the right. Sample 76501 grew between 250 a and 50 a (with one hiatus) with an initial ^{234}U:^{238}U ratio always close to 3.35. The initial ratio in sample 76503 varied between 5.3 and 6.3. The examples are of ά-dated samples: modern mass spectrometric methods have reduced the errors by an order of magnitude.

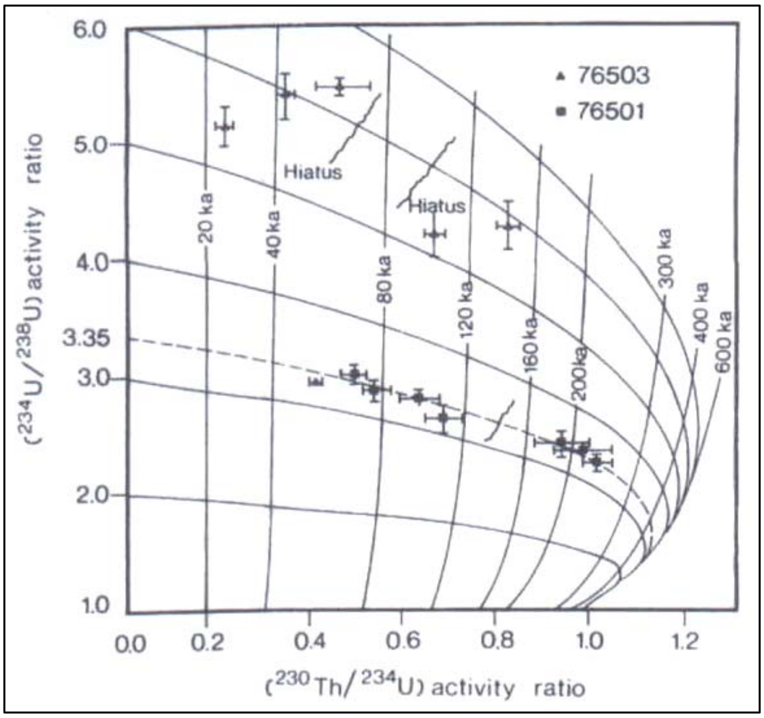

Figure 2-15 Graphical illustration of the ^{230}Th:^{234}U:^{238}U dating method, the principal method used for carbonate speleothems today

Until the late 1980s the abundance of the different isotopes was estimated by counting α disintegrations in a scintillometer. Counting took approximately 1 week before there were sufficient numbers for reliable statistics, and one standard deviation (σ) errors in the age were typically 10%. This has been replaced by direct counting of isotopes by mass spectrometry: for corals first by Edwards in 1986-7, for speleothems first by Li *et al.* in 1989. In thermal ionization mass spectrometry (TIMS) separated extracts of U and Th are burned off of filaments at 1800-2200°C, with manual control required for the Th measurements. Inductively Coupled Plasma- Mass Spectroscopy (ICP-MS) liquid extracts are heated to a plasma at 8000-10,000°C and measured automatically. The two methods give very similar results. Calcite sample sizes need be no more than 0.5-2.0 g and 2σ age errors are reduced to ~1% or better: 2σ = ±40 years for a sample 10 a in age, ±200 years for 50 a, ±15 000 years for 500 a [49]. The current limit of the method is a little over 600 a (Figure 2-15). In situ U series dating by laser-ablation multicollector ICP-MS is currently being investigated with the prospect of dating at a spatial resolution of 100 μm or better, although currently with less precision and accuracy than TIMS methods.

The flow of groundwater through U source rocks or soils that have already been highly leached may lead to deposition of calcite with a deficiency of ^{234}U rather than an excess with respect to ^{238}U. This offers an absolute dating method if the initial deficiency can be determined, and establishes the duration of growth of a deficient calcite where it cannot. Daughter-deficiency is encountered in a few per cent of calcite speleothems.

There are three basic requirements for all U series methods.

1) The calcite or aragonite (or gypsum) speleothems must contain sufficient U. Measured concentrations range ≤ 0.01 ppm. to > 300 ppm. 0.01 ppm. is the current reasonable minimum for ^{230}Th/^{234}U dating. > 80% of assayed calcite speleothems and all aragonite speleothems contain more than this minimum concentration.

2) The system must be closed after coprecipitation of U and calcite. Often this will be violated. Many speleothems are partly or wholly recrystallized. Others are porous so that water flows freely through them and may preferentially leach ^{234}U. This results in too great an age being calculated. For this reason stalactites (with their central feedwater canals) and porous tufa deposits are to be avoided, if possible.

3) The most important requirement is that no ^{230}Th or ^{231}Pa be deposited in the calcite. In fact, most calcite contains a proportion of these species and of ^{232}Th($t_{1/2}$ = 1.39x10^{10} years) bonded to clay or other particulate detritus deposited in the speleothems. They are contaminants. As they increase, reliability of calculated dates deteriorates. In practice, where the ratio, ^{230}Th/^{232}Th, is > 20 it is presumed that radiogenic ^{230}Th completely predominates and that contamination is insignificant; most dating computer programs now correct for it. For highly contaminated deposits (^{230}Th/^{232}Th<5.0) multiple determinations are recommended in order to calculate the isochron, ^{230}Th/^{232}Th versus ^{234}U/^{232}Th. Multiple teachings of samples have also been tried. These approaches often fail. If possible, samples that are visibly dirty should be avoided [17].

U-series dating of speleothems has played a significant part in Quaternary science in recent years. They present high precision Thermal Ionization Mass Spectrometric (TIMS) U-series analyses of speleothems and drip waters from Fogelpole Cave in southern Illinois. Data from all speleothems from the cave show an inverse correlation between $(^{234}U)/(^{238}U)$ and U concentration, following the pattern observed in groundwaters globally. They suggest that $(^{234}U)/(^{238}U)$ in speleothems may record changes in hydrologic flux with time and thus could provide a useful proxy for long term records of paleoprecipitation [50]. In southern Brazil, showed the high-resolution, 116,000-year carbon stable isotope record from a stalagmite, which has been precisely dated using the U-series method [48].

CHAPTER III

METHODOLOGY

3.1 Study area

Pang Ma Pha is a district of Mae Hong Son province, Thailand. It is divided into four sub-districts (Tambons) i.e. Sob Pong, Thum Lod, Na Pu Phom, and Pang Ma Pha. The topography consists of a complex mountain range, which is shown as a majority of limestone and dolomite in the Limestone Resource Map of Thailand [51]. Moreover, this site is a karst topography that contains many caves which have a high potential for paleoclimatic studies on stalagmites. In this study the researcher chooses Namjang cave to study its stalagmites.

Namjang cave

Location: Namjang cave (98º49'55"E, 18º46'3"N, elevation 902 m at the entrance) is located near Namjang village of Tambon Pang Ma Pha (Figure 3-1). It is a non-active cave and has two chambers. The first chamber is long and light through surface which is approximately 6 meters wide and 56 meters long. The second chamber is dark and narrows. There is 5 m of roof thickness (soil layer+bed rock). Stalagmites of Namjang cave (the sample identification used here including NJ1 and NJ2) was actively growing at the time of sampling for NJ1 and not actively growing for NJ2. They were collected in April, 2006. The columnar stalagmite NJ1, 41.7 cm in height and 6.5 cm in diameter, was collected in the first chamber ~18 meters away from the cave entrance. Stalagmite NJ2 of 38.5 cm in height, and 9.5 cm in diameter was collected in the first chamber ~27 meters away from the cave entrance (Figures 3-2, 3-3 and 3-4(a)).

Vegetation: The flora on the hillside above the cave is the mixed-deciduous forest (Figure 3-4(b)).

Geology: The rock types of Namjang cave are limestone and dolomite of Permian period. High purity limestone found in the lower and the upper parts of rock sequence [51].

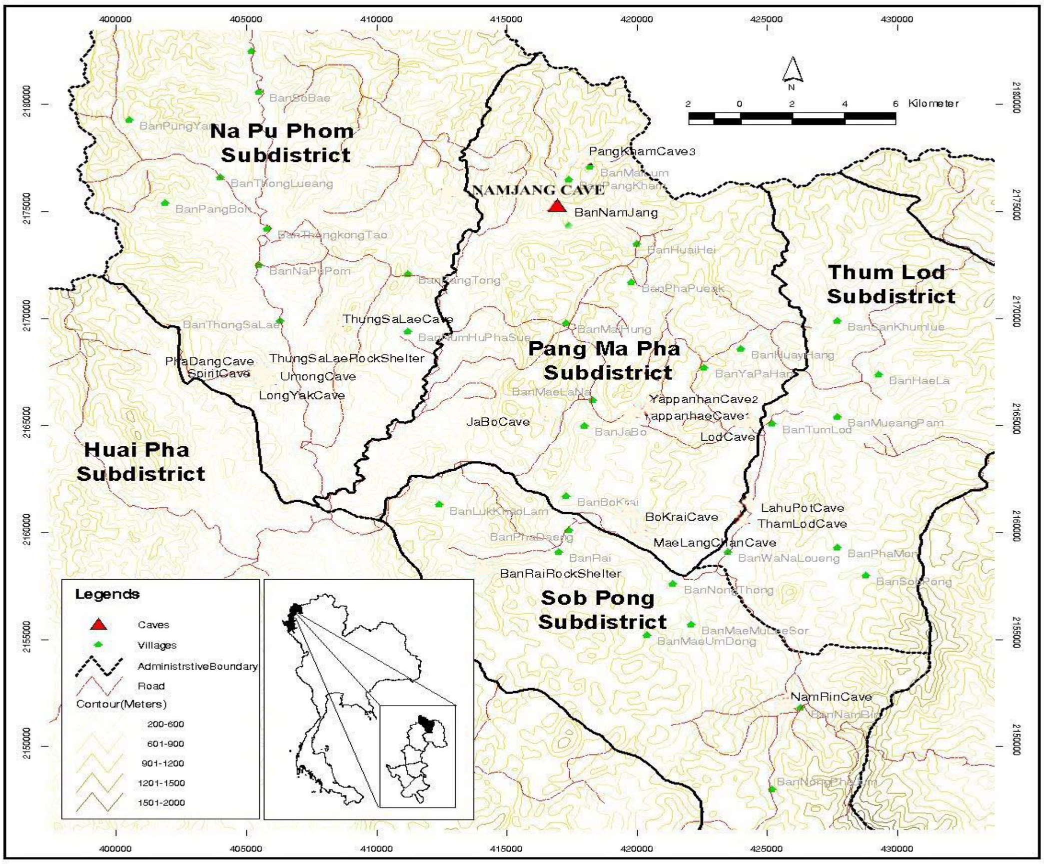

Figure 3-1 Map of Pang Ma Pha district of Mae Hong Son province, Thailand

Meteorology: The recent weather in the area is influenced by the tropical seasonal monsoon, which is generally divided into 3 seasons. Firstly, rainy season (May-October), there is 77 rainy days/year, amount of rainfall is 1095 mm/year with averaged temperature of 28°C. Secondly, winter (November-January), the weather is dry and cold with averaged temperature of 20°C, 4 rainy days/year and 61 mm/year of amount of rainfall. Finally, summer (February-May), the weather is hot and sultry with averaged temperature of 32°C, 6 rainy days/year and amount of rainfall is 81mm/year. Note that the numbers shown here are averaged from the data of 30-year period [52, 53].

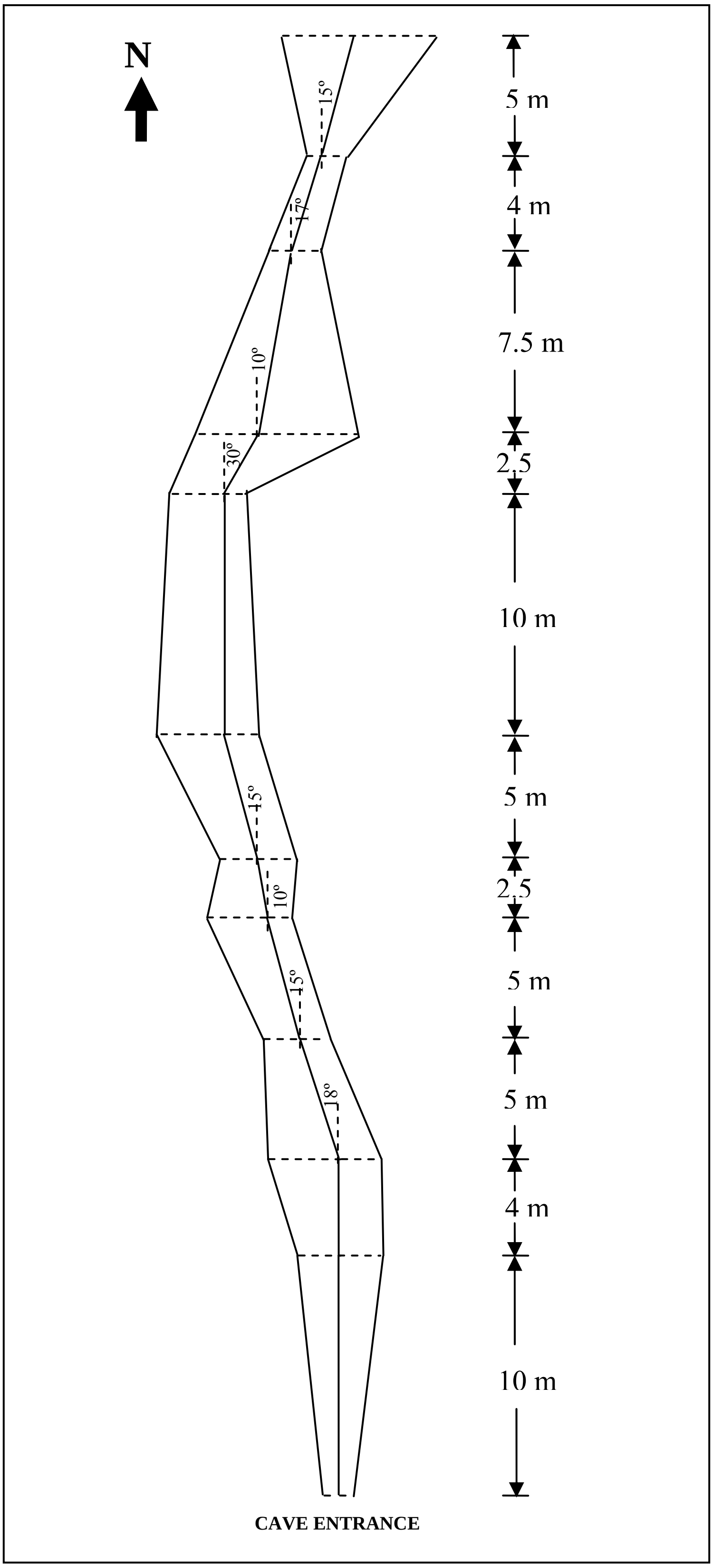

Figure 3-2 The map of Namjang cave (Top view)

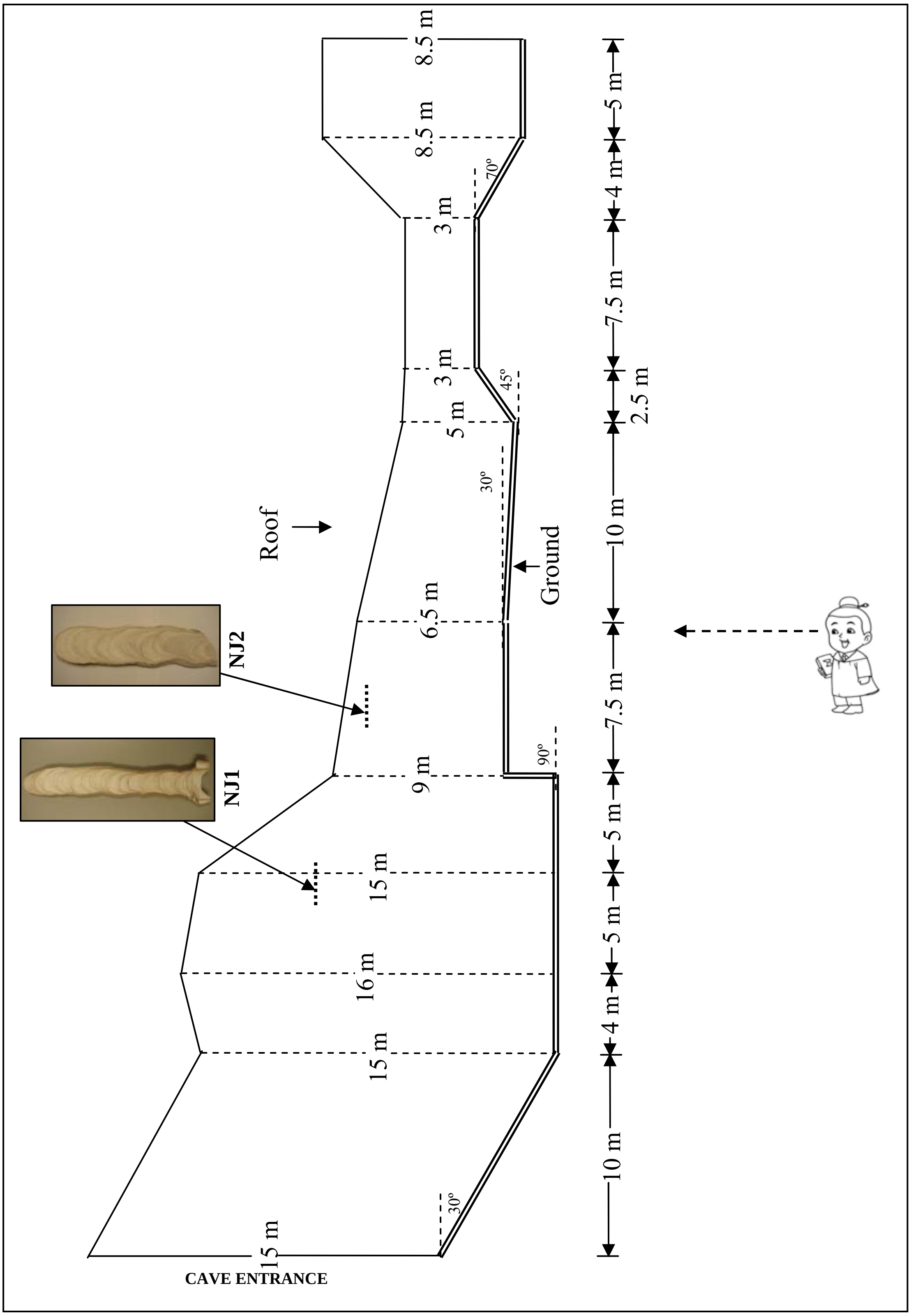

Figure 3-3 The side view of Namjang cave and locations of sampling stalagmite NJ1 and stalagmite NJ2

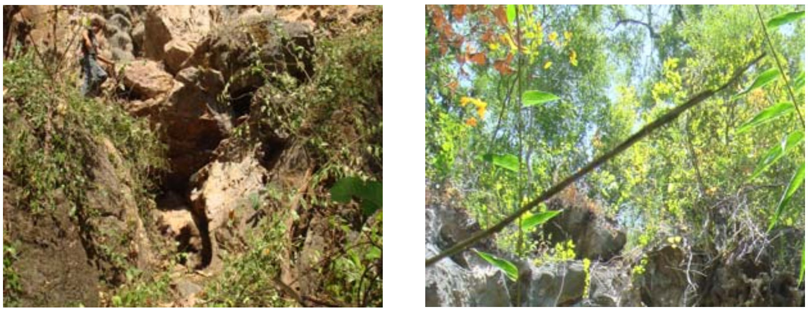

(a) (b)

Figure 3-4 The cave entrance (a) and the flora above the cave (b)

3.2 Sample selection

The most common variety of stalactites include soda straw, which is hollow, with a diameter minimized by the surface tension of the water drop at their tip [34]. Thus, the criteria used are to select only the columnar stalagmites (because stalagmites are naturally not hollow) and possibility chose the actively growing one that likely remained under a steady hydrological state because its topmost layer is known to have formed in that year [54]. Ideally the straight stalagmite is good for the cutting along the growth axis and polished prior to analysis. In addition, this reason suggest to climate reconstruction by annual growth layer as much as possible.

3.3 Sample collection

Two samples of stalagmite in Namjang cave were taken by using a hammer knocking them at the base. Then the sample identifications were labeled as NJ1 and NJ2

3.4 Sample preparation

The samples were washed with tap water by using a brush to clean their surface. After that, they were cut into two halves along the growth axis. The cut surfaces were polished by grinding with a coarse grit (No. 100) followed by fine grit (No. 400) until showing the clear layers. Note that the sample preparation corresponding to particular techniques of analysis will be described separately under those techniques.

3.5 Morphology and mineral species of stalagmites

Morphology for this study is some visual evidence of crystal habit. This is investigated on thin polished sections and fragments of stalagmites. The equipments employed to this information include polarizing microscope and scanning electron microscope (SEM). Mineral species was investigated by the X-ray diffractometer (XRD). Note that each stalagmite is divided into 3 sub-samples (NJ1: NJ1_1, NJ1_2, and NJ1_3; NJ2: NJ2_1, NJ2_2 and NJ2_3) based on different positions along the length of the stalagmite.

3.5.2 Thin section

A rock thin section shows mineral content, abundance and association, grain size, alternation, rock structures and textures, and is a permanent record of a given rock for future reference [55].

Procedures of thin section preparation are as the following chart:

Cutting a rock sample into a block of 0.5x2.5x5

↓

Grinding on one larger side of the block with silicon carbide abrasives No. 100 and No. 200 respectively and followed by No. 600 alumina abrasive in final grinding. Tap water is used to cool down the process, reduce friction and wash the sample.

↓

The dry and clean polished side of the block is cemented on to the glass slide (0.1x2.5x7.5 cm^3 size) by epoxy resin.

↓

Let the epoxy resin set by putting the block sticking on the glass slide in the hot air oven with the temperature of 60°C. Some double clips should be applied to press the block on the glass slide. Leave it overmight for the epoxy resin setting

↓

Cutting the excess part of the block off to leave the very thin section of the rock (~1-2 mm. thick) attached to the glass slide.

↓

Grinding on the open rock surface of thin section by using the silicon carbide abrasive No. 100 and 200 respectively and followed by the alumina powder No. 600.

↓

Labeling the section.

(Modified from Phillips [55])

After that, thin sections were used for observation on morphology (crystal habit), and for measuring the layer thickness of crystallization of stalagmite with a polarizing microscope equipped with photography unit (Figure 3-5). The sample preparation and investigation were performed at the Department of General Science, Faculty of Science, Srinakharinwirot University, Bangkok.

Figure 3-5 A polarizing microscope equipped with photography unit

3.5.2 Scanning electron microscopy (SEM)

The advantages of the SEM as an imaging instrument with a high spatial resolution. It is an invaluable tool in the following branches of geology such as mineralogy. The SEM is very effective for studying crystal morphology on a micro-scale.

Most geological samples, being nonconductors of electricity, require a conductive coating to prevent charging under electron bombardment. Sputter coating is quick and convenient, and is especially suitable for gold and its alloys, as used for SEM work. It lends itself readily to automation, thereby saving time for the user. Since the sputtered atoms arc strongly scattered by gas molecules they travel in all directions, which is advantageous for coating specimens of irregular shape (Figures 3-6) [56]. In this study the fragments of stalagmite samples were coated with gold before investigation under the SEM.

The method of image formation with the scanning electron microscope, giving easily comprehensible, quasi three-dimensional representations of objects examined, at a wide range of magnifications. This leads to a better understanding of the spatial relations of features of micro topography, reveals unsuspected detail and previously undescribed characters [57]. These analyses were performed by the JSM 6301F at the Natural Metal and Materials Technology center (MTEC), Bangkok.

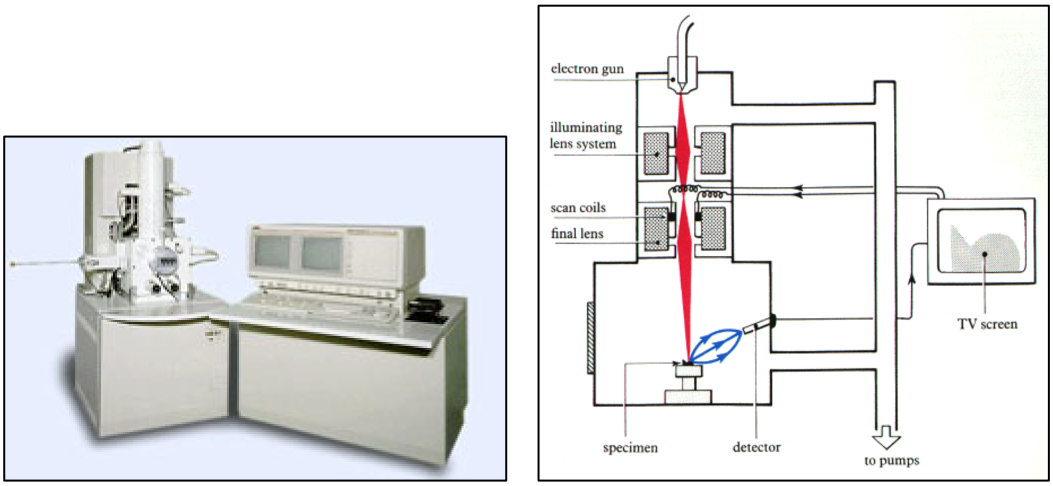

(a) (b)

Figure 3-6 The scanning electron microscope (JEOL model: JSM 6301F) (a) and schematic diagram of a scanning electron microscope (b) [58]

3.5.3 X-ray diffraction (XRD)

X-ray diffraction is a technique reveals information about the characterization and identification of polycrystalline phase [59]. These techniques are fast, easy sample preparation, high-accuracy for d-spacing calculation, and standard are available for many material systems [60]. Likewise, records the information about the "reflections" present as an inked trace on a printed strip chart, or as electronic counts (X-ray counts) that can be stored in a computer.

1) Sample preparation

The samples were crushed by the iron mortar to obtain the very fine grain powder, which is packed in the sample holder (Figure 3-7(b)) for analyses by the XRD to identify the mineral species in stalagmite. If possible, the samples should be crushed down to the particles of about 0.002 mm to 0.005 mm across.

The instrument is so constructed that this slide, when clamped in place, rotates in the path of a collimated X-ray beam while an X-ray detector, mounted on an arm, rotates about it to pick up the diffracted X-ray signals. The automated equipment supplied by one manufacturer is shown in Figure 3-7(a).

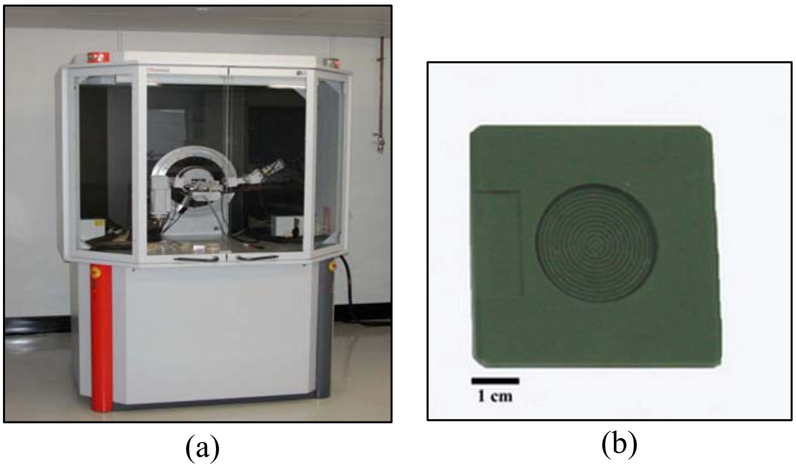
(a) (b)

Figure 3-7 Automated X-ray diffraction (D8 Advance) (a), sample holder (b)

If the specimen has been properly prepared, there will be thousands of tiny crystalline particles on the slide random orientation. As in powder photography, all possible "reflections" from atomic planes take place simultaneously [19].

2) Sample analysis

Today about 50,000 inorganic and 25,000 organic single components, crystalline phases, and diffraction patterns have been collected and stored on magnetic or optical media as standards [59]. The main use of powder diffraction is to identify components in a sample by a search/match procedure. Ideally identifying the intensity lines or peak positions of 2 Theta by comparing the intensities of these lines or peak positions of 2 Theta with those emitted from standards. It is also possible to determine the species of the elements. Samples preparation and investigation were performed by Bruker, D8 Advance XRD at the Department of Physics, Faculty of Science, Srinakharinwirot University, Bangkok.

3.6 Stable isotope and dating technique

Stable isotope and dating technique for this study is investigated only stalagmite NJ1.

3.6.1 Stable isotopes (^{18}O and ^{13}C)

A total of 170 powder samples for oxygen and carbon isotope analyses were taken from the first half of stalagmite NJ1. By the use of a 0.5 mm dental drill with carbide burrs, the cut surface of stalagmite was drilled on the 170 points marked by a graph paper overlaying on the cut surface of the stalagmite. All points with spacing of 1-3 mm were on one line parallel and close to the growth axis of the stalagmite (Figure 3-8). Each powder sample was weighed ~150 µg. Isotopic measurements were done in the Environmental Isotope Lab of the Institute of Geology and Geophysics, Chinese Academy of Science, China.

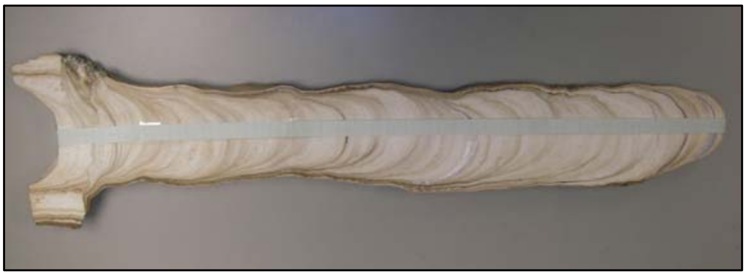

Figure 3-8 Graph paper lay on top of the cut surface of stalagmite NJ1 for drilling

Isotopic measurements using a MAT-253 mass spectrometer linked to a Gas Bench-II **(**Thermo-Finnigan) (Figure 3-9). Each powder sample (~100 µg weigh) was transferred quantitatively to a clean and dried borosilicate exetainer and capped with a rubber septum (Labco Limited, Pierceable Rubber Wad, order code VC302). The exetainers are placed into an aluminum tray kept at 72.0±0.1˚C. The resultant CO_2 is separated from other components using a gas chromatographic column (Poraplot Q with fused silica tubing, 25 m × 0.32 mm) heated to 70˚C. The pressure of Helium carrier gas was set at 0.9 bar. In order to gain better external precision, 3 drops of phosphoric acid (produced by Merck and identifiable through the catalogue number 1.00565.0500) are deposited in each exetainer for subsequent reaction inside.

The precision is 0.1‰. Accuracy and precision was routinely checked by running the carbonate standard NBS-19 after every six sample measurements. All oxygen isotope values are reported in per mil (‰) relative to VPDB [61].

Oxygen and carbon isotopic data are reported in the delta (δ) notation relative to the VPDB standard for carbonate samples [6], where

$$\delta^{18}O = [(^{18}O/^{16}O_{sample}) / (^{18}O/^{16}O_{standard})-1] \times 1000$$
$$\delta^{13}C = [(^{13}C/^{12}C_{sample}) / (^{13}C/^{12}C_{standard})-1] \times 1000 \quad .$$

Figure 3-9 MAT-253 mass spectrometer linked to a Gas Bench-II **(**Thermo-Finnigan) machine

3.6.2 Dating technique (^{230}Th dating)

Typical powder amount ranged from 100 to 300 mg samples were drilled for ^{230}Th dating using a 0.9 mm carbide dental burr following stratigraphic and color layers. The powder is dissolved with nitric acid, a mixed ^{229}Th/^{233}Th/^{236}Th tracer is added, and the sample is dried drown. After the addition of an iron chloride solution, NH_4OH is added drop by drop until the iron precipitates. The sample is then centrifuged to separate the iron from the rest of the solution and the overlying liquid is removed. After loading the sample into columns containing anion resin, HCl is added to elute the thorium and water is added to elute the uranium. With the uranium and thorium separated, each sample is dried down and dilute nitric acid is added for injection in to ICP-MS and TIMS [62].

There are 3 points of sampling including the positions of 8 mm. (NJ1-8), 166 mm. (NJ1-166), and 388 mm. (NJ1-388) apart from the top of the stalagmite (Figure 3-10). The isotopic measurements for samples NJ1-8 and NJ1-166 were analyzed by a VG Sector 54E TIMS (Figure 3-11(a)) in the Radiogenic Isotope Laboratory University of Queensland, Australia. The sample NJ1-388 was analyzed by a ThermoElemental PQ ExCell quadrupole ICP-MS (Figure 3-11(b)) in the Department of Geology and Geophysics, University of Minnesota, USA.

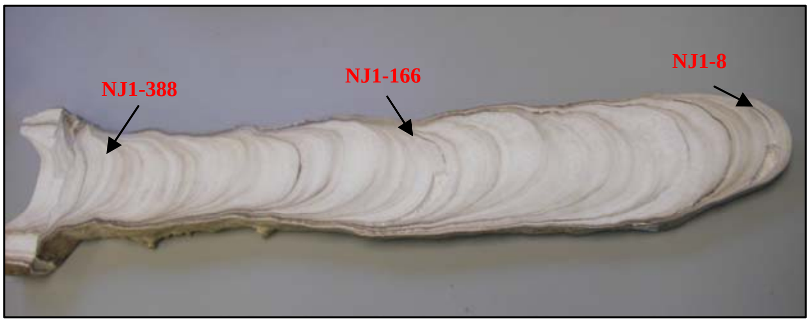

Figure 3-10 Three points were drilled for ^{230}Th dating

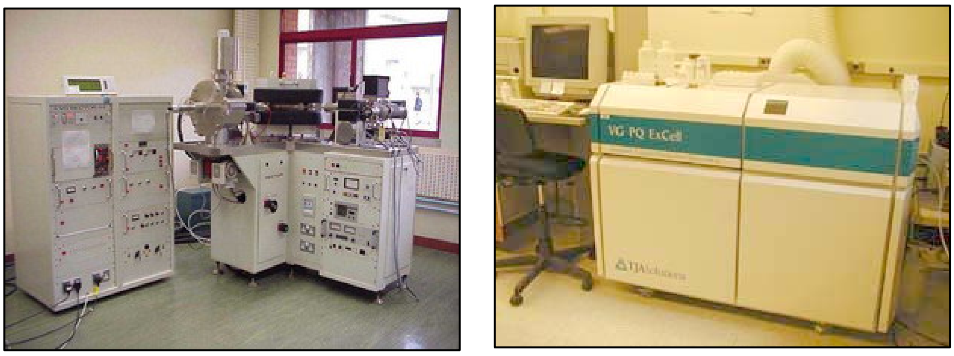

Figure 3-11 VG Sector 54E TIMS (a) and
ThermoElemental PQ ExCell quadrupole ICP-MS (b)

In Inductively Coupled Plasma-Mass Spectrometer ICP-MS liquid extracts are heated to a plasma at 8,000-10,000°C and measured automatically. In thermal Ionization Mass Spectrometry (TIMS) separated extracts of U and Th are burned off of filaments at 1,800-2,200°C, with manual control required for the Th measurements. The two methods give very similar results. Calcite sample sizes need to be no more than 0.5-2.0 g and 2σ age errors are reduced to ~1% or better: 2σ = ±40 years for a sample 10 a in age, ±200 years for 50 a, ±15 000 years for 500 a [49]. The current limit of the method is a little over 600 a [17].

The age is calculated from the ^{238}U-^{234}U-^{230}Th age equation (3-1) if $\delta^{234}U(0)$, $[^{230}Th/^{238}U]_{act}$ and the decay constants are known. Equation (3-2) relates the observed $\delta\,^{234}U(0)$ to the initial state when the system was isolated with $^{230}Th = 0$; where the λ's denote the decay constants and T is the age [62].

$$1-\left[\frac{^{230}Th}{^{238}U}\right]_{act} = e^{-\lambda_{230}T} - \left[\frac{\delta^{234}U(0)}{1000}\right]\left[\frac{\lambda_{230}}{\lambda_{230}-\lambda_{234}}\right] \times \left(1-e^{(\lambda_{230}-\lambda_{234})T}\right) \quad (3\text{-}1)$$

$$\delta^{234}U\,(T) = \delta^{234}U\,(0)\,e^{\lambda_{234}T} \quad (3\text{-}2)$$

Where; $\lambda_{238} = 1.551\times10^{-10}\ y^{-1}$

$\lambda_{234} = 2.835\times10^{6}\ y^{-1}$

$\lambda_{230} = 9.195\times10^{6}\ y^{-1}$

$\delta^{234}U = \{[(^{234}U / ^{238}U) / (^{234}U / ^{238}U)eq] - 1\} \times 10^{3}$

$(^{234}U / ^{238}U)eq = \lambda_{238} / \lambda_{234} = 5.472\times 10^{5}$

3.7 Counting of annual growth layer

One of the half sections was polished and thickness (or width) of each clear layer was measured under a traveling microscope, used for tree-ring width measurements (TSAP version 3.2) (Figure 3-12) at Tree Ring and climate change laboratory, Faculty of Environment and Resource studies, Mahidol University, Thailand.

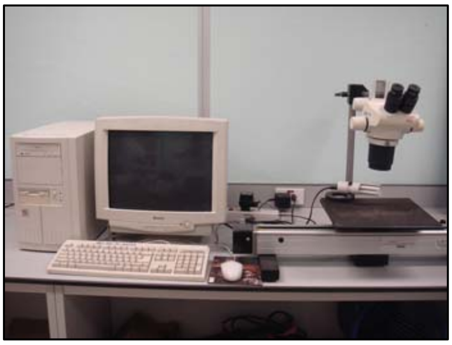

Figure 3-12 The equipment for tree ring width measurements (TSAP version 3.2)

3.8 Stalagmite reconstruction

Polynomial regression statistic was used to analyze the relationship between the data of precipitation and $\delta^{18}O$ of Bangkok station which is available from IAEA. Three pairs of correlation of precipitation data were made (between that of Bangkok station vs Mae Hong Son station, Bangkok station vs Pang Ma Pha station and Mae Hong Son station vs Pang Ma Pha station. This to see whether the correlations are significant or in high R values, then the equation from polynomial regression model in Bangkok site can be applied for paleoprecipitation reconstruction in the study area. Note that the data from Mae Hong Son station are used here because the data available more than Pang Ma Pha does (Mae Hong Son has the data for 37 months, Pang Ma Pha has the data for 19 months only). Pang Ma Pha is a locality where situates in the area of Mae Hong Son province and with the reason of to confirm the reliability of the data.

3.9 Petrography, mineral species and chemical composition of parent rock

Petrography of the parent rock was investigated on the thin section by the use of a polarizing microscope. Mineral species was investigated by the XRD and chemical composition was analyzed by the XRF. Note that the sample preparations for the thin section and the XRD are the same as those of the stalagmites.

3.9.1 X-ray fluorescence (XRF)

Another way to excite characteristic X-rays is to bombard the specimen with X-rays of higher energy, this technique being known as X-ray fluorescence analysis (Figure 3-13). It has been a standard method of elemental analysis in geology for several decades and offers good accuracy for major elements [56].

The analysis sample in this technique is ground to a fine powder and subsequently compressed into a circular pellet, or into a disc with the admixture of a binder. The pellet or disc of sample is irradiated (for a short period of time) with X-rays generated in a high-intensity X-ray tube.

Figure 3-13 X-ray fluorescence (Axios Advance)

Qualitative X-ray fluorescence analysis involves identification of the various spectral lines with the elements responsible for them. Quantitative analysis is more involved because each X-ray intensity must be quantitatively compared with that of a standard (of known composition) of the same elemental makeup. Both peak and background intensities near the peak are counted to permit estimation of peak heights. On-line computers handle quantitative correction programs in extremely short time [19]. The composition of major elements and some trace elements shown in the forms of oxide/elemental contents. These analyses were performed by wdx (wavelength dispersive x-ray) technique with Axios Advance XRF at the Department of Mineral Resources, Ministry of Natural Resources and Environment.

3.10 Data interpretation

The data interpretation is divided into two parts as follow:

3.10.1 Descriptive data

1) The morphology of stalagmite and petrography of parent rock

The descriptive information of morphology of stalagmites, NJ1 and NJ2 in terms of crystal habits and texture is obtained from thin sections and SEM technique. The descriptive petrography of parent rock is also derived from thin section.

3.10.2 Comparative data

1) The mineral species of stalagmite and parent rock

The mineral species of stalagmites, NJ1 and NJ2 as well as of the samples of parent rock (PM_NJ1 and PM_NJ2) are available from the XRD. The identification of mineral species was done by comparing the sample peaks with the reference peaks of known species.

2) The chemical composition of parent rock

The chemical composition of parent rock was analyzed by compare with a standard (of known composition) of the same elemental makeup. Both peak and background intensities near the peak are counted to permit estimation of composition of the parent rock.

3) Stable isotope and dating technique

Stable isotope was analyzed by checking the accuracy and precision of the samples with the carbonate standard NBS-19 after every six samples measurements, using a MAT-253 mass spectrometer linked to a Gas Bench-II (Thermo-Finnigan) [61].

^{230}Th dating was analyzed by investigation for the survival of ^{238}U, ^{234}U, and ^{230}Th which are substituted the equation (3-1) if δ^{234}U(0), [^{230}Th/^{238} U]$_{act}$ and the decay constants are known. Equation (3-2) relates the observed δ ^{234}U(0) to the initial state when the system was isolated with ^{230}Th = 0.

4) Counting of annual growth layer

The relationship between the annual growth layer and the age from ^{230}Th dating of stalagmite NJ1 was analyzed by compare the number of layer counts between known time horizons of stalagmite [39] to find out whether or not one year has one layer.

5) Stalagmite reconstruction

This part, the data have been interpreted according to the results of section 3.8.

CHAPTER IV

RESULTS AND DISCUSSION

4.1 Parent rock

4.1.1 Petrography and mineral species

Parent rock shows gray color with some veins of calcite. According to the Limestone Resources Map of Thailand [51], it is limestone of Permian period. There are 2 samples (PM_NJ1 and PM_NJ2) collected from different positions of the cave entrance. Under the microscope, they contain mainly skeletal composition (Figures 4-1 and 4-2). The calcite species were identified by the XRD (Figures 4-3 and 4-4).

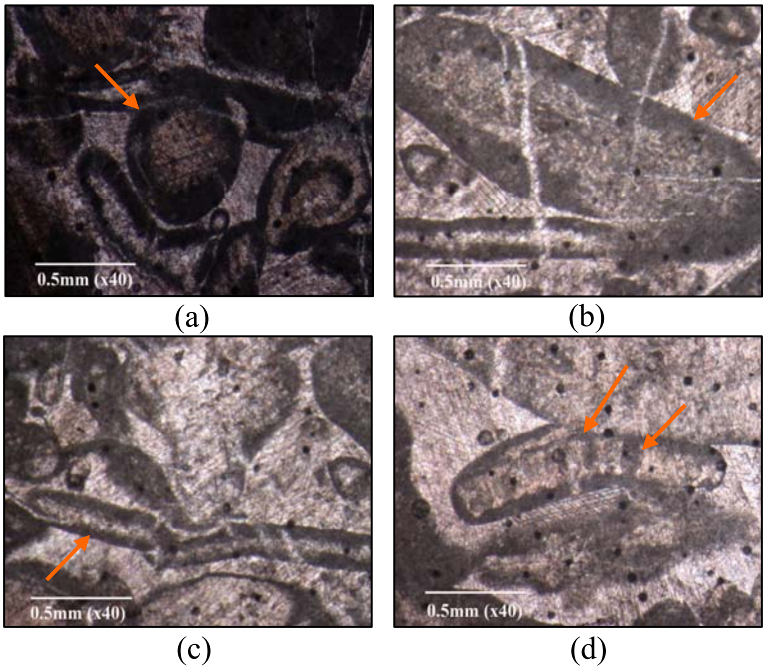

Figure 4-1 The texture of parent rock (PM_NJ1) from Namjang cave

Generally, thin section of PM_NJ1 shows a skeletal grain. The grains exhibit as micritic rim or micrite envelope. The section also contains fossil. Therefore, the rock should be named as skeletal grainstone or biosparite according to Dunham and Folk (cited in Esper *et al*. [63]) respectively. Figure 4-1(a), under crossed polar, presents a line as marked arrow and shows an ooid in the center which is composed of calcite with a concentric structure and a nucleus with a prominent micritic envelope. It is enclosed by bivalve shell (Top and bottom) and ooid (left and right). They are cemented by calcite. Figure 4-2(b), under plane-polarized light, at an arrow the section shows a bend in bivalve fragment within coated grain is replaced by coarse calcite crystals. Figure 4-1(c) shows a bivalve fragment (the elongate grain), now composed of calcite with poor preservation of original concentric structure, and Figure 4-1(d) shows a brachiopod shell and spines with well preserved shell structure coated by micrite and they are cemented by calcite.

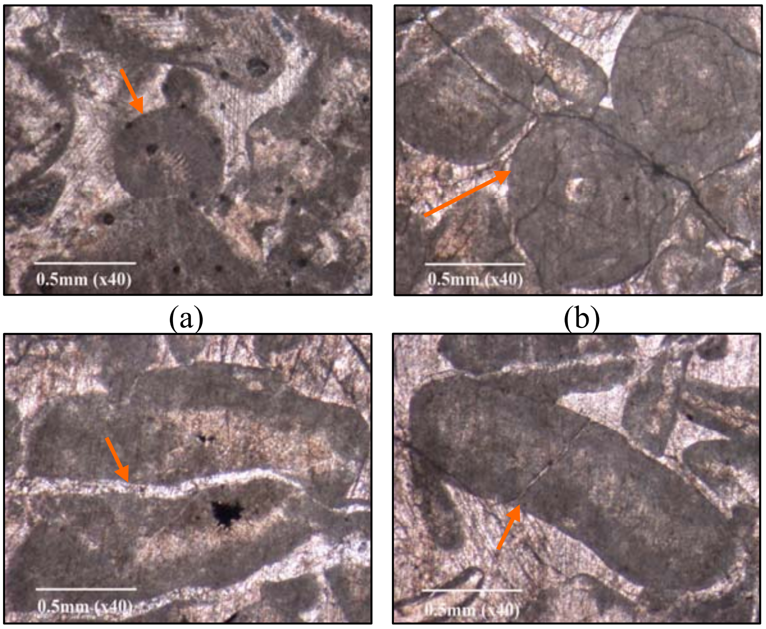

(a) (b)
(c) (d)

Figure 4-2 The texture of parent rock (PM_NJ2) from Namjang cave

Figure 4-2(a), under plane-polarized light, shows a foraminifera with sphere shape (center). This is 0.4-0.5 mm in diameter surrounded by coated skeletal grains with spary calcite cement. Figure 4-2(b), ooids with nucleus show concentric structure and prominent micritic envelope. Figure4-2(c), a mechanical fracture in the bioclast grain was replaced by coarse calcite (arrow). Figure4-2(d), a bivalve shell was composed of calcite with poor preservation of original shape (bivalve has no concentric structure, only ooid does) structure within coated grain is replaced by coarse calcite crystals and micritic enveloped.

The mineral species of the powder samples of PM_NJ1 and PM_NJ2 were known by a search/match procedure. It was identified by compare the intensities of sample lines or peak positions of 2 Theta with those emitted from standards. The sample peaks show the best match to those of the calcite reference 72-1650 which was described by Chessin and Hamilton [64]. Therefore the PM_NJ1 and PM_NJ2 are calcite species (Figure 4-3 and 4-4 respectively).

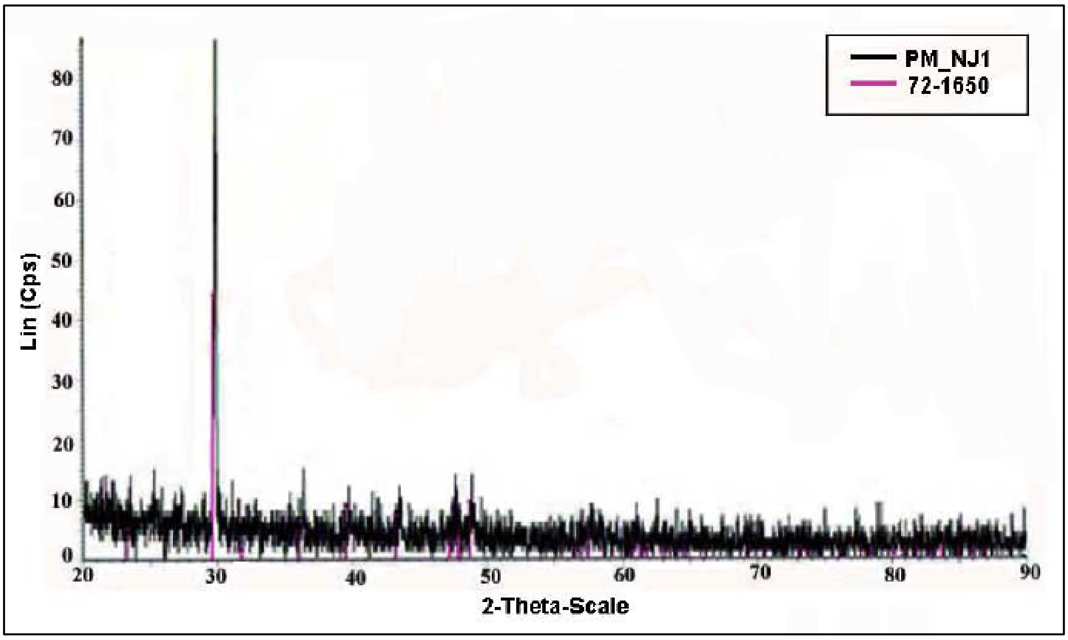

Figure 4-3 The XRD results for stalagmite, PM_NJ1, shows the peak positions similar to those of calcite reference, 72-1650

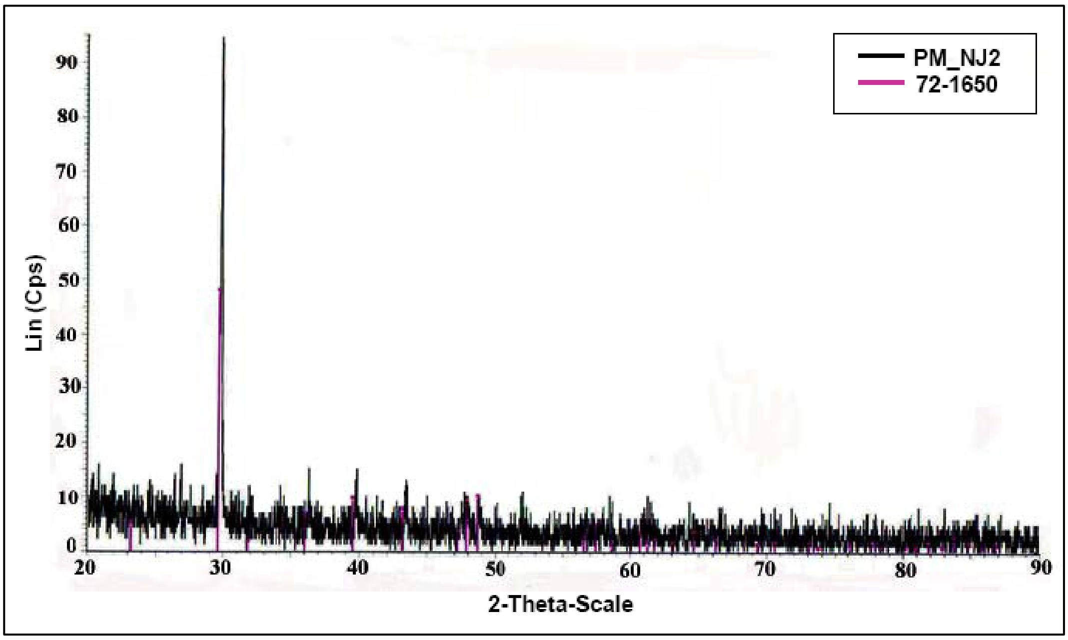

Figure 4-4 The XRD results for stalagmite, PM_NJ2, shows the peak positions similar to those of calcite reference, 72-1650

The mineral species and morphology of parent rock (PM_NJ1 and PM_NJ2) contain calcite species and skeletal grain composition which implied to origin of parent rock and environment factors. The ooid is demonstrated to shallow seawater in tropical areas is supersaturated with respect to $CaCO_3$, so that this, together with water agitation, CO_2 degassing and elevated temperature, might be sufficient to bring about carbonate precipitation on nuclei. Skeletal grain, bivalves have been important contributors to marine carbonate sediments, particularly since the Tertiary following the decline of the brachiopods which are particularly common in Palaeozoic and Mesozoic limestone of the shallow marine origin, and foraminiferas are common in warm, shallow seas, living within and on sediment, and encrusting hard substrates [15]. Moreover, the PM_NJ1 and PM_NJ2 are calcite species. This result indicates that the origin of parent rock from the shallow seawater in tropical. It is limestone in Permian period which confirms the data in the Limestone Resources Map of Thailand [51].

The chemical composition of parent rock (Mixing of PM_NJ1 and PM_NJ2) analyzed by XRF is presented in Table 4-1.

Table 4-1 Chemical composition of the parent rock for the stalagmites in Namjang cave

Element (Oxide)	Concentration (%)
CaO	50.10
MgO	3.93
SiO_2	0.51
Fe_2O_3	0.42
H_2O	0.23
MnO	0.19
Al_2O_3	0.18
K_2O	<0.05
TiO_2	<0.05
P_2O_5	0.01
Na_2O	<0.01
LOI*	44.06

* LOI : loss on ignition

The results in Table 4-1 shows that chemical composition of the parent rock contains the highest CaO among all chemical composition, 50.10% and contains 3.93% MgO, 0.51% SiO_2, 0.42% Fe_2O_3, 0.23% H_2O, 0.19% MnO, 0.18% Al_2O_3, <0.05% K_2O and TiO_2, 0.01% P_2O_5, <0.01% Na_2O and 44.06% LOI. This study contains 3.93% MgO is converted to 17.98% $CaMg(CO_3)_2$ (Appendix A) which is identified as limestone because many natural dolomite have the value of $CaMg(CO_3)_2$ more than 50% (Figure 2-2).

4.2 Stalagmites

4.2.1 Morphology and mineral species

Under the microscope, stalagmite NJ1 shows a brown to dark brown layers separated from each other by a dark brown layer. The observation by the SEM, each layer shows fibrous structure of many groups of fan-like polycrystalline crystals diverging from the bottom to the top. The NJ1 was divided into 3 samples (NJ1_1, NJ1_2, and NJ1_3) based on different position along the length of the stalagmite. Under a high magnification, they contain the many aragonite crystals of tabular and blade habits (Figures 4-5, 4-6 and 4-7 respectively). The aragonite species were analyzed by the XRD (Figures 4-8, 4-9, and 4-10 respectively).

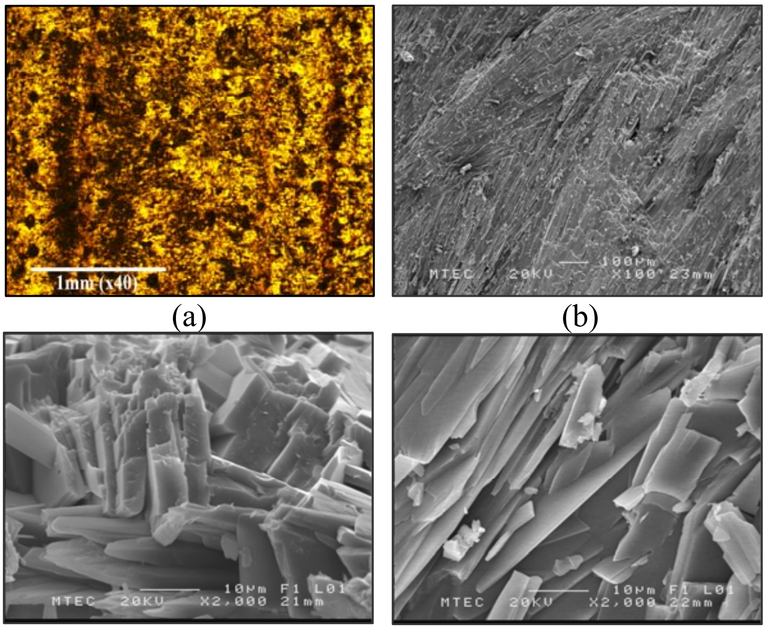

(a) (b)

(c) (d)

Figure 4-5 The layer of stalagmite NJ1_1 (a) and the morphology of mineral species (b, c, d)

Figure 4-5(a) shows the photomicrographs under polarizing microscope (PPL) of the polished section for the stalagmite NJ1_1 (the range between 0 and 5 cm from the top) cut along its lengthwise, the stalagmite column shows a brown to dark brown layers (0.5-1.5 mm. thick) separated from each other by a dark brown layer

(~0.1-0.15 mm. thick). Figure 4-5(b), the fibrous aragonite crystals under the SEM showing the fan-like polycrystalline crystals diverging from the bottom to the top of the stalagmite (lower magnification). Figure 4-5(c), under the higher magnification, the crystals show tabular habit (15x60x5 µm for each crystal), and blade habit with the dimension of approximately 10x70x1 µm for each crystal in Figure 4-5(d).

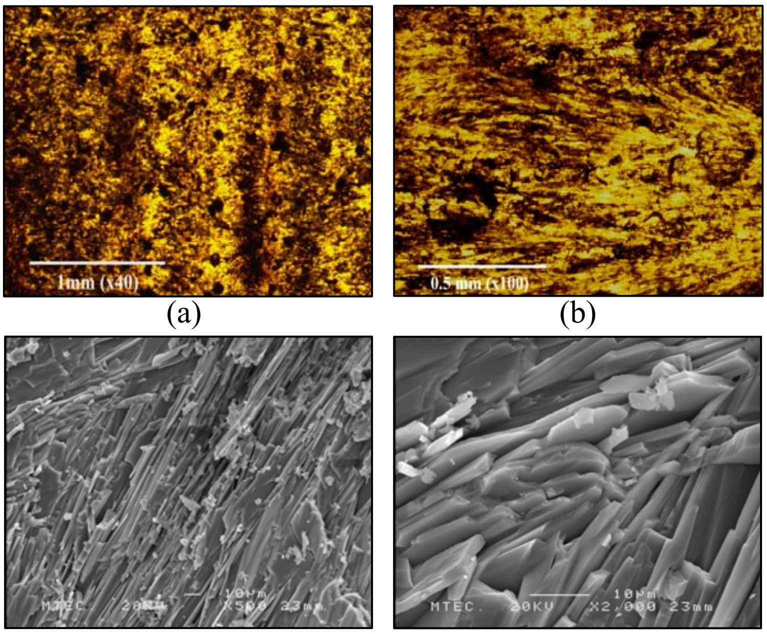

(a) (b)

(c) (d)

Figure 4-6 The layer of stalagmite NJ1_2 (a, b) and the morphology of mineral species (c, d)

Figure 4-6(a) shows the photomicrographs under polarizing microscope (PPL) of the polished section for the stalagmite NJ1_2 (the range between 15 and 20 cm from the top), the stalagmite column shows a brown to dark brown layers (0.6-0.7 mm. thick) separated from each other by a dark brown layer (0.1-0.15 mm. thick) with lower magnification, a higher magnification shows a polycrystalline of acicular or fibrous crystals in Figure 4-6(b). Figure 4-6(c), the aragonite crystals in the stalagmite NJ1_2 under the SEM showing the blade habit (lower magnification), and higher magnification (10x70x2 µm for each crystal) in Figure 4-6(d).

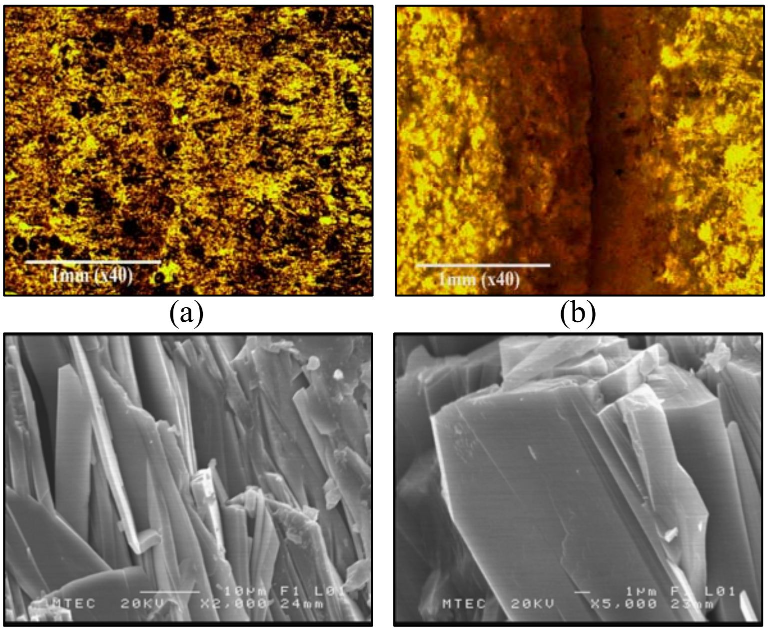

(a) (b)

(c) (d)

Figure 4-7 The layer of stalagmite NJ1_3 (a, b) and the morphology of mineral species (c, d)

Figure 4-7(a) shows the photomicrographs under polarizing microscope (PPL) of the polished section for the stalagmite NJ1_3 (the range between 32 and 37 cm from the top) cut along its lengthwise, laminated deposit composed of fibrous microcrystalline material resemble to the fan, and hiatus which is identification of an erosion (dissolution) layer or through the deposition of detritus or this means that layer formation had stopped in Figure 4-7(b). Figure 4-7(c), the fibrous aragonite crystals under the SEM showing the blade habit (12x60x1.5 µm for each crystal), and tabular habit with the dimension of 10x60x4 µm for each crystal in Figure 4-7(d).

The powder of stalagmite NJ1 (NJ1_1, NJ1_2, and NJ1_3) were identified by XRD with a search/match procedure indicates that the positions of the 2 Theta of the sample match with those of the aragonite reference 76-0606 described by Dickens and Bowen [65] and calcite reference 03-0596 described by Allis-Chalmes Mfg. Co. [66]. Therefore the stalagmite NJ1_1 and NJ1_2 are aragonite (Figures 4-8 and 4-9) whereas stalagmite NJ1_3 contains both aragonite and calcite where the aragonite has the major peaks at 26.3°, 27.3° and 46° matching with those of the aragonite reference

76-0606 and the calcite has the major peaks at 29.5º, 43º and 48.5º matching with those of calcite reference 03-0596 (Figures 4-10 and 4-11) respectively.

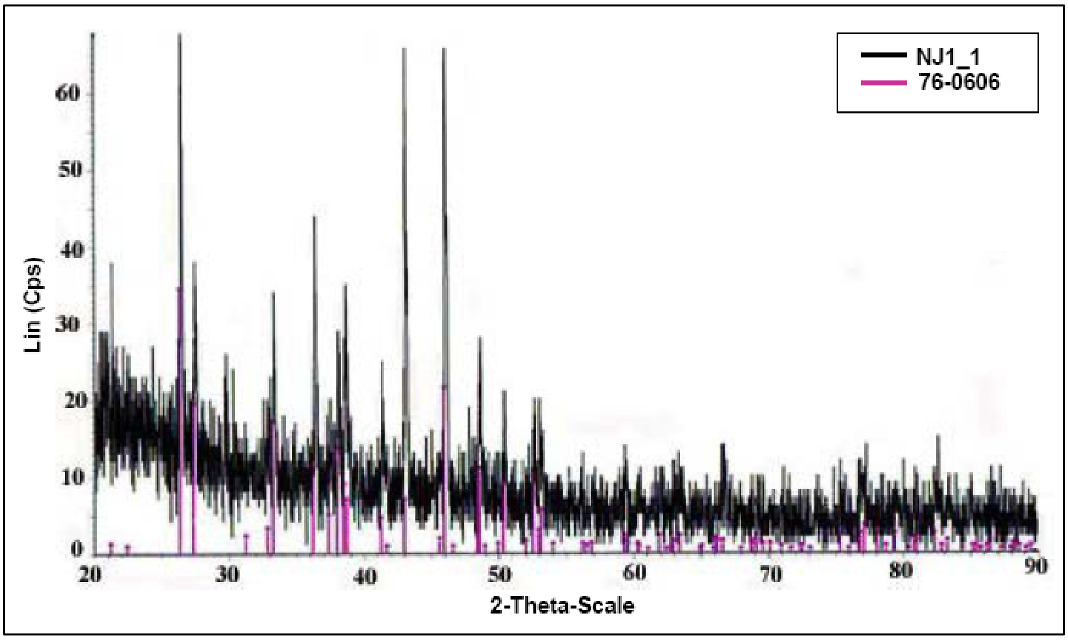

Figure 4-8 The XRD results for stalagmite NJ1_1, shows the peak positions similar to those of aragonite reference, 76-0606

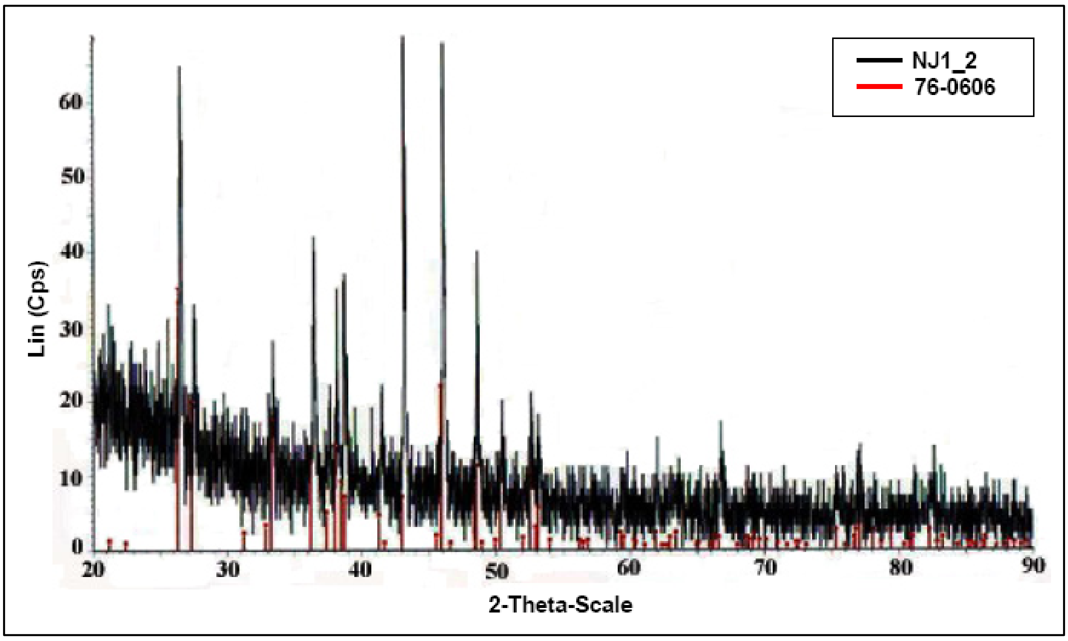

Figure 4-9 The XRD results for stalagmite NJ1_2, shows the peak positions similar to those of aragonite reference, 76-0606

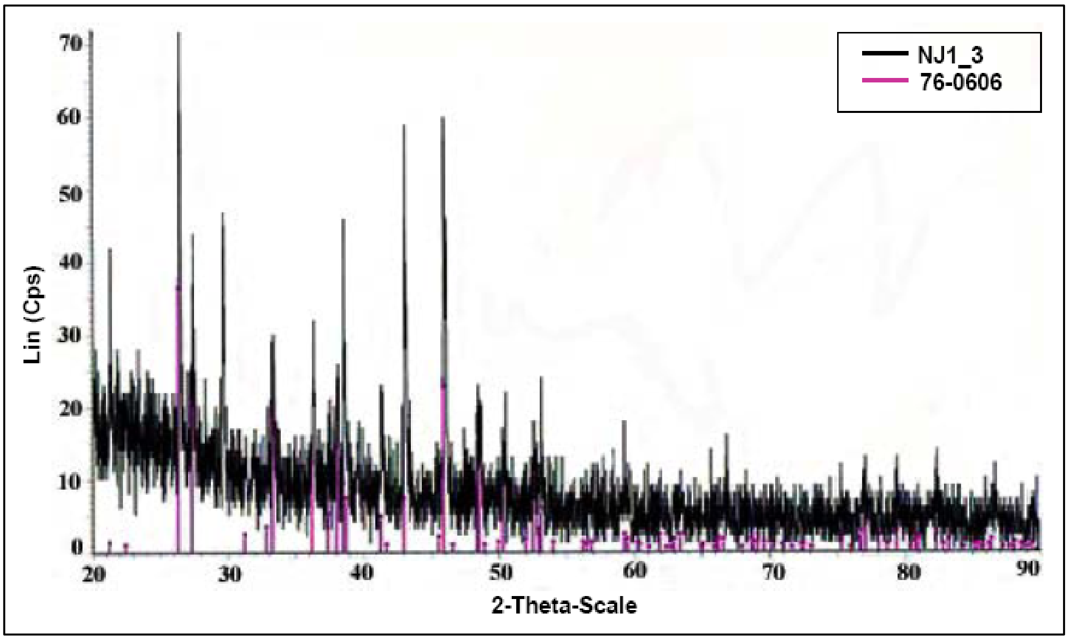

Figure 4-10 The XRD results for stalagmite NJ1_3, shows some peak positions similar to those of aragonite reference, 76-0606

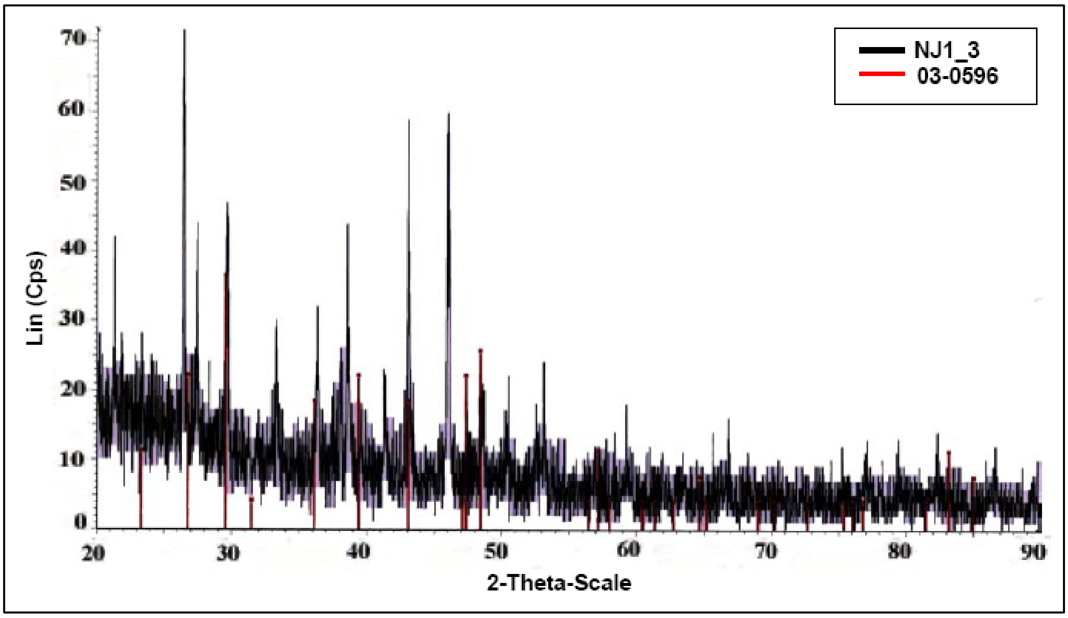

Figure 4-11 The XRD results for stalagmite NJ1_3, shows some peak positions similar to those of calcite reference, 03-0596

Under the microscope, stalagmite NJ2 was divided into 3 samples (NJ2_1, NJ2_2, and NJ2_3) based on different position along the length of the stalagmite. It has two types of layer sequences. One shows a yellow to brown layers separated from each other by a light brown yellow (Figures 4-12(a) and (b)) and another shows a brown to dark brown layers separated from each other by a dark brown layer (Figures 4-13(a) and (b) and 4-14(a) and (b)). The observation by the SEM, it is found that laminated deposit composed of aragonite microcrystalline. The aragonite species were identified by the XRD (Figures 4-15, 4-16, and 4-17 respectively).

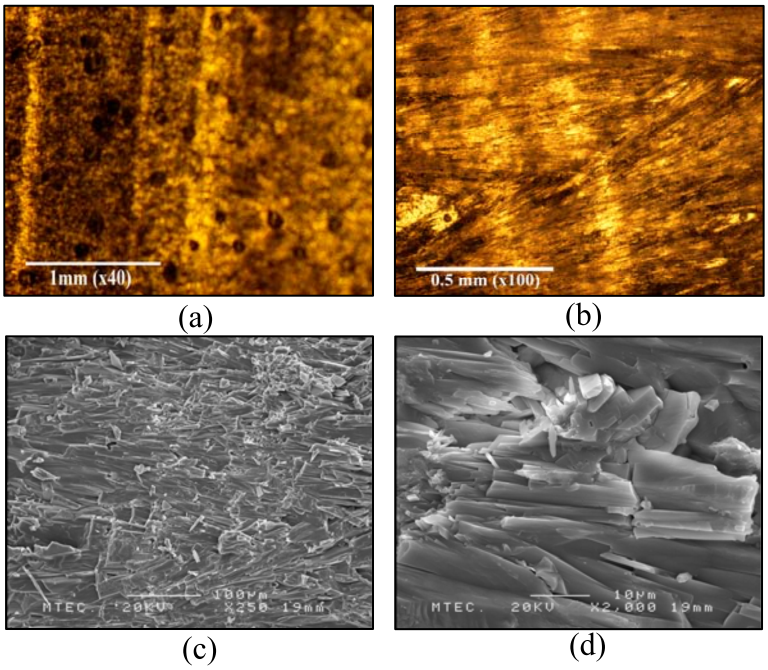

(a) (b)

(c) (d)

Figure 4-12 The layer of stalagmite NJ2_1 (a, b) and the morphology of mineral species (c, d)

Figure 4-12(a) shows the photomicrographs under polarizing microscope (PPL) of the polished section for the stalagmite NJ2_1 (the range between 0 and 5 cm from the top) cut along its lengthwise, the stalagmite column shows a yellow to brown layers (0.5-1 mm. thick) separated from each other by a light yellow layer (0.08-0.15 mm. thick) with lower magnification, under a higher magnification showing fibrous or acicular crystals of aragonite in Figure 4-12(b). Figure 4-12(c), the aragonite crystals in the stalagmite NJ2_1 under the SEM showing the blade habit which assembled to the fan (lower magnification), and higher magnification with the dimension of 10x60x1.5 μm for each crystal in Figure 4-12(d).

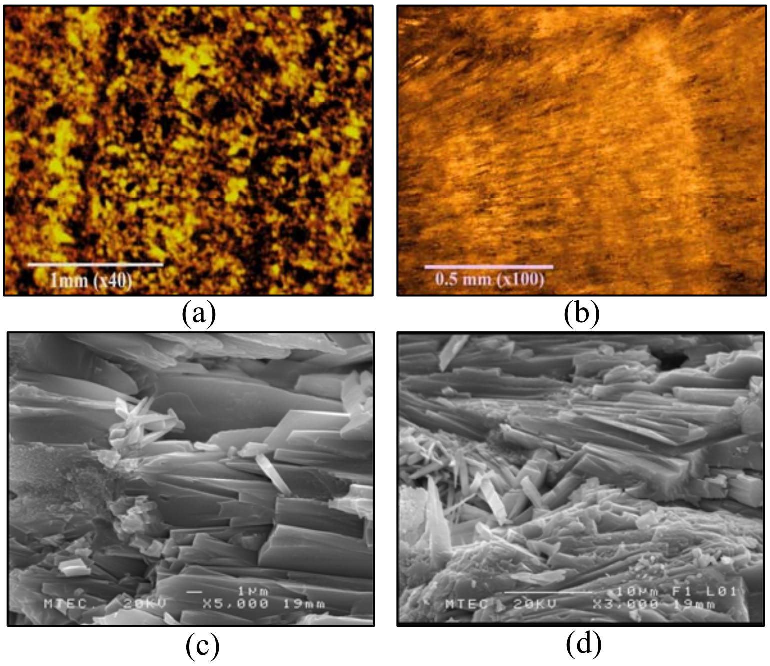

Figure 4-13 The layer of stalagmite NJ2_2 (a, b) and the morphology of mineral species (c, d)

Figure 4-13(a) shows the photomicrographs under polarizing microscope (PPL) of the polished section for the stalagmite NJ2_2 (the range between 13 and 18 cm from the top) cut along its lengthwise, the stalagmite column shows a brown to dark brown layers (0.8-1.2 mm. thick) separated from each other by a dark brown layer (0.08-0.15 mm. thick), under a higher magnification shows a layers having fibrous structure in Figure 4-13(b). Figure 4-13(c), the aragonite crystals in the stalagmite NJ2_2 under the SEM showing the blade habit (8x60x0.5 μm for each crystal), and fibrous structure of the polycrystalline crystals in Figure 4-13(d).

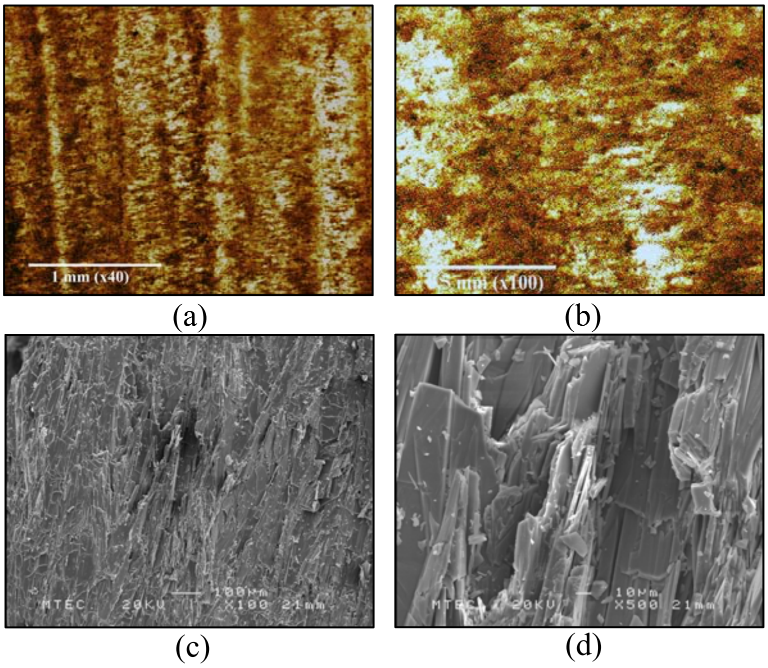

(a) (b)

(c) (d)

Figure 4-14 The layer of stalagmite NJ2_3 (a, b) and the morphology of mineral species (c, d)

Figure 4-14(a) shows the photomicrographs under polarizing microscope (PPL) of the polished section for the stalagmite NJ2_3 (the range between 30 and 35 cm from the top) cut along its lengthwise, there is a brown to dark brown layers separated from each other by a dark brown layer, and a fibrous polycrystalline in Figure 4-14(b). Figure 4-14(c), the aragonite crystals in the stalagmite NJ2_3 under the SEM showing the fan-like polycrystalline crystals of fibrous structure (lower magnification), and a higher magnification with the dimension of 12x65x1.5 μm for each crystal in Figure 4-14(d).

The powder of stalagmite NJ2 (NJ2_1, NJ2_2, and NJ2_3) were identified by XRD with a search/match procedure indicates that the positions of the 2 Theta of the sample match with those of the aragonite reference 76-0606 described by Dickens and Bowen [65]. Therefore the stalagmite NJ2_1, NJ2_2, and NJ2_3 are aragonite (Figures 4-15 to 4-17).

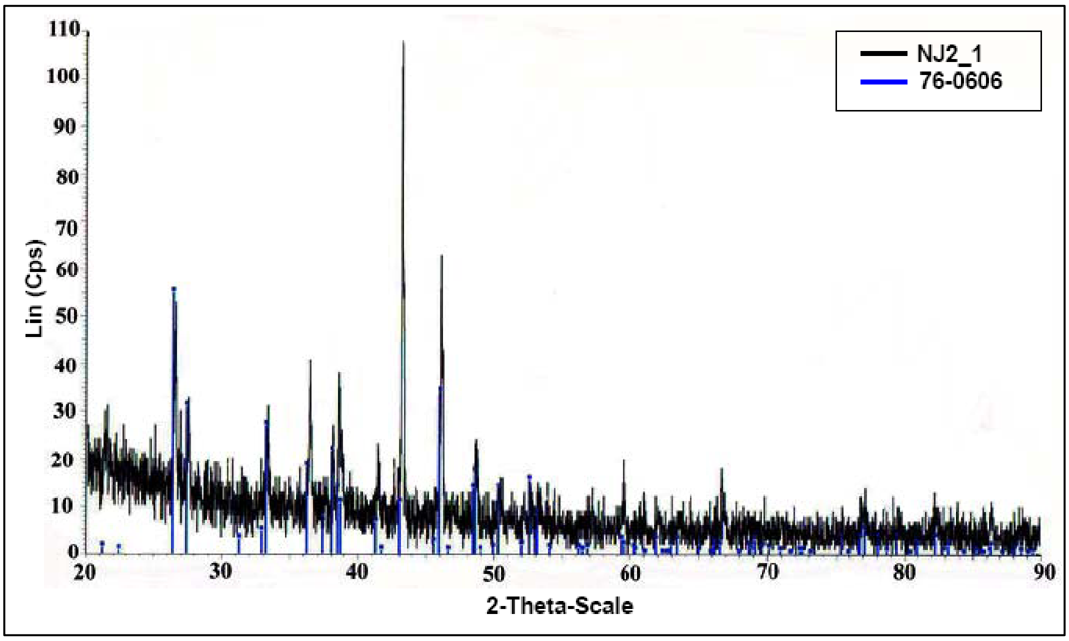

Figure 4-15 The XRD results for stalagmite NJ2_1, shows the peak positions similar to those of aragonite reference, 76-0606

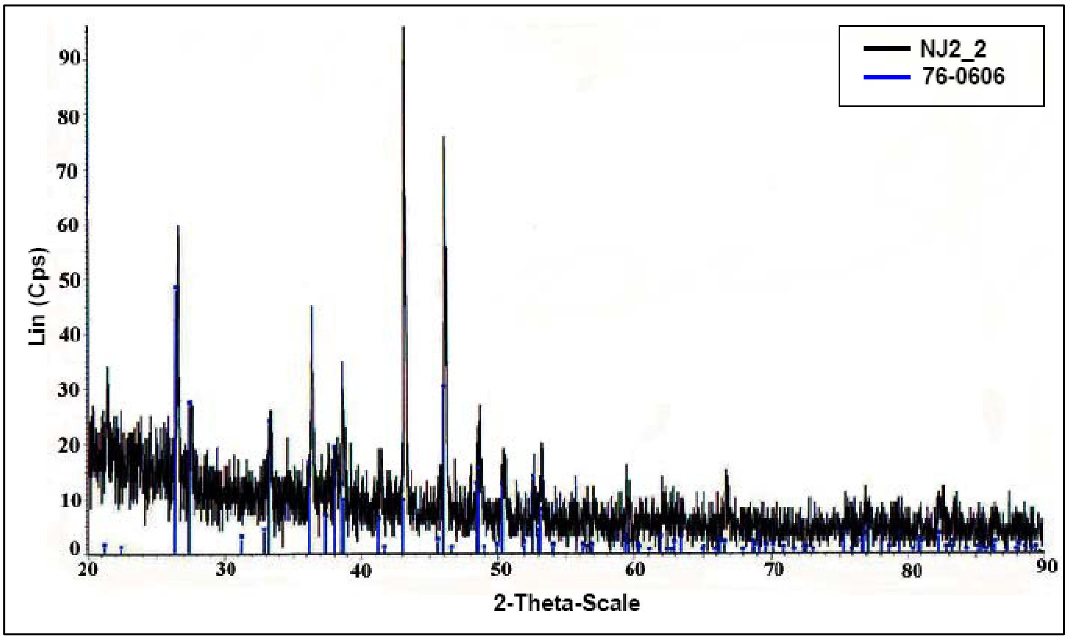

Figure 4-16 The XRD results for stalagmite NJ2_2, shows the peak positions similar to those of aragonite reference, 76-0606

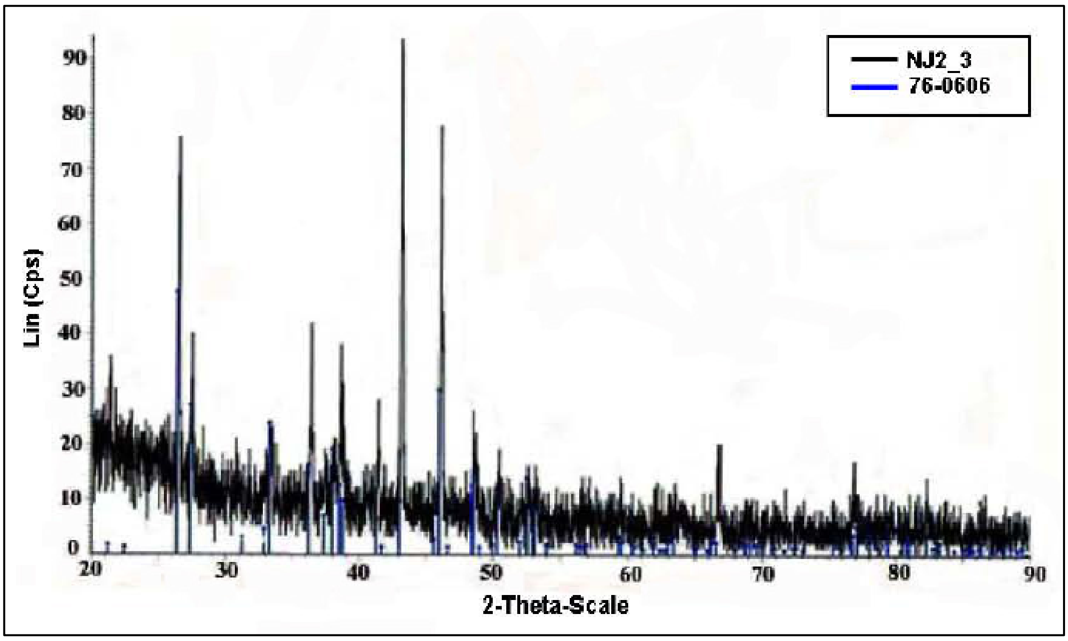

Figure 4-17 The XRD results for stalagmite NJ2_3, shows the peak positions similar to those of aragonite reference, 76-0606

The deposition of mineral species can be used for interpretation to the chemical and physical environment at the location [67]. Tan *et al.* [39] suggested that different stalagmites within one cave can show a different climate response due to difference in their hydrological connection to the surface. Dykoski *et al.* [62] represented the oxygen isotope result in two stalagmites (D3 and D4) from Dongge cave is highly unlikely that the combination of conditions experienced by each set of drips was identical in each case. Therefore, kinetic fractionation and water-rock interactions are not likely to have had a large effect on D4 $\delta^{18}O$. However, the mineral species and morphology in both stalagmites NJ1 and NJ2 are aragonite. This could be because two stalagmites were collected from the same cave within less than 10 m distance and hence changes in cave environment or isotopic composition in the precipitation above the caves should have affected both the stalagmite in a similar way. Temperature in Namjang cave is 22.5 °C, drip rate is 13.95 s / drip, and humidity approximate 70% whereas there are two cave entrances which increase the evaporation. The parent rock is limestone. It should be suggested that aragonite species was caused by evaporation negligible drip rate, temperature and parent rock factors. This study is consistent with Siegel and Reams [68] who suggested that aragonite precipitation is enhanced by high rates of evaporation likewise Rowling [67] illustrated that temperature, CO_2, pressure, presence of clay and strontium are factors not associated with aragonite deposition in aragonite cave of New South Wales. On the other hand, aragonite speleothems in Clamouse cave (France) were being precipitated only where there was dolomitic bedrock, and even then only when the drip rate was very low. This suggested that the role of magnesium is to inhibit the growth of calcite, either by crystal poisoning or by "difficulties in rapid dehydration of the Mg^{2+} ion" [69]. Moreover, Niggeman *et al.* [70] examined coralloids deposited in windy areas of several caves in Germany and Austria. They found that more aragonite was deposited in the areas where the bedrock contained dolomite, either primary dolomite or from hydrothermal alteration of bedrock and McDermott [71] suggested aragonite occurs occasionally, particularly in association with high-Mg calcite or dolomite host-rocks, and/or associated with relatively dry periods when long water–rock contact times facilitate relatively more dolomite dissolution in partially dolomitised limestone hostrocks. These disagree with the result of this study. It could be possibly explained that conditions can vary from cave to cave and between locations. Within a given cave, difference factors can affect the deposition or origin of mineral species. The comparative of aragonite species with location is shows in Table 4-2.

Table 4-2 The aragonite species in stalagmites of many locations

Location or Researcher	**Evaporation rate**	**Parent rock**	**Mineral in stalagmite**
Namjang cave, Thailand	high	limestone	aragonite
Clamouse cave, France [69]		dolomite	aragonite
Several caves in Germany and Austria [70]		dolomite	aragonite
McDermott [71]		dolomite	aragonite
Siegel and Reams [68]	high		aragonite
Hill and Forti [21]	high		aragonite

4.2.2 Mineral species for comparison

The morphology under the SEM of mineral species of the study area was compared to those of the area outside. That is between aragonite species of stalagmite from Namjang cave, Mae Hong Son province and calcite species of stalagmite from Tinuey cave in the Thung Yai Naresuan Wildlife Sanctuary, Kanchanaburi province (Figure 4-18). Note that the mineral species of both localities were identified by the XRD (Figure 4-19).

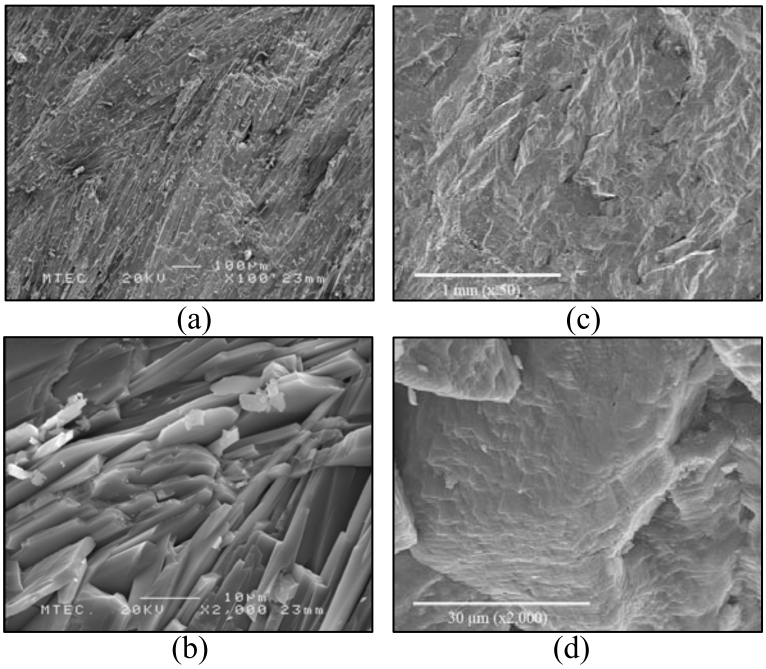

(a) (c)

(b) (d)

Figure 4-18 Under the SEM, the morphology of stalagmite from Namjang cave (a and b), compared to stalagmite from Tinuey cave (c and d)

Figure 4-18 shows the morphology under the SEM between two mineral species. Figure 4-18(a), the fibrous aragonite crystals show the fan-like polycrystalline crystals diverging from the bottom to the top of the stalagmite from Namjang cave, Mae Hong Son province (lower magnification). Figure 4-18(b), under the higher magnification, the aragonite crystals shows the blade habit. Figure 4-18(c) the crystals of the stalagmite from Tinuey cave in the Thung Yai Naresuan Wildlife Sanctuary, Kanchanaburi province shows massive appearance. Figure 4-18(d), calcite crystal shows the layer of rhombohedral cleavage (higher magnification).

With a search/match procedure of the XRD technique, it is found that the peaks of the stalagmite from Tinuey cave shows the best match to those of the calcite reference 72-1650 described by Chessin and Hamilton [64]. Whereas the peaks of stalagmite from Namjang cave shows the best match to those of the aragonite reference 76-0606 described by Dickens and Bowen [65].

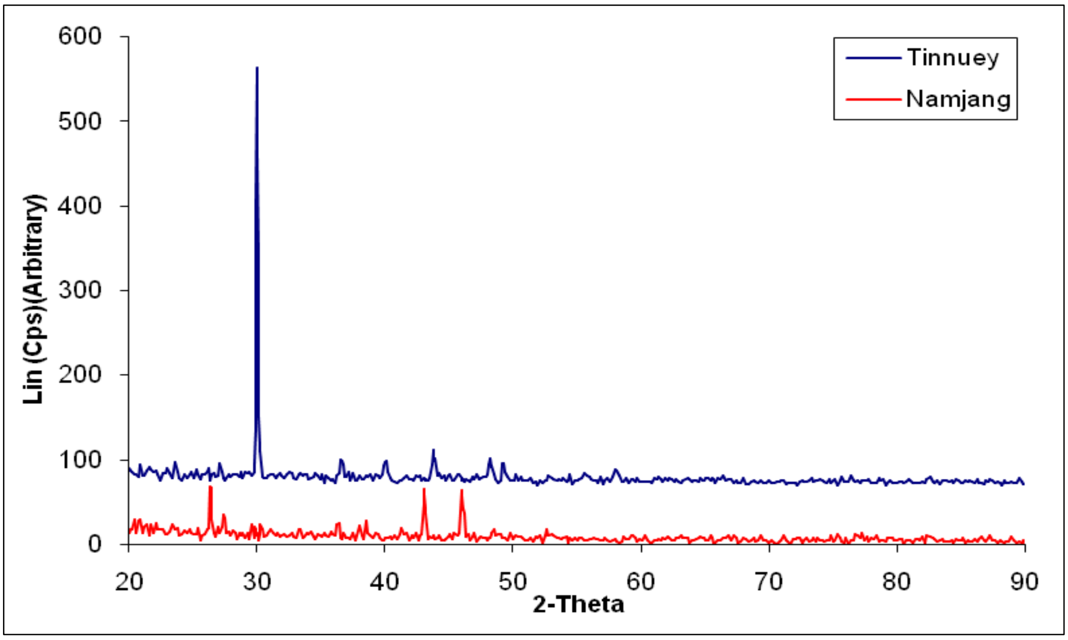

Figure 4-19 The XRD results for the stalagmite from Namjang cave (aragonite) and stalagmite from Tinuey cave (calcite)

4.2.3 The δ^{18}O and δ^{13}C variations of stalagmite NJ1

Stable isotope measurement of 170 subsamples taken from the stalagmite NJ1, the values of δ^{18}O range from -6.95 to -3.75‰ (mean value is -5.22‰) and of δ^{13}C range form -7.69 to -3.08‰ (mean value is -5.42‰) with approximately by 3‰ variations in δ^{18}O and 4‰ in δ^{13}C (this detail shows in Appendix D). The values of both isotopes agree well with each other (Figure 4-20). This suggested that the geochemical or environmental factors affect both δ^{18}O and δ^{13}C values in a similar way.

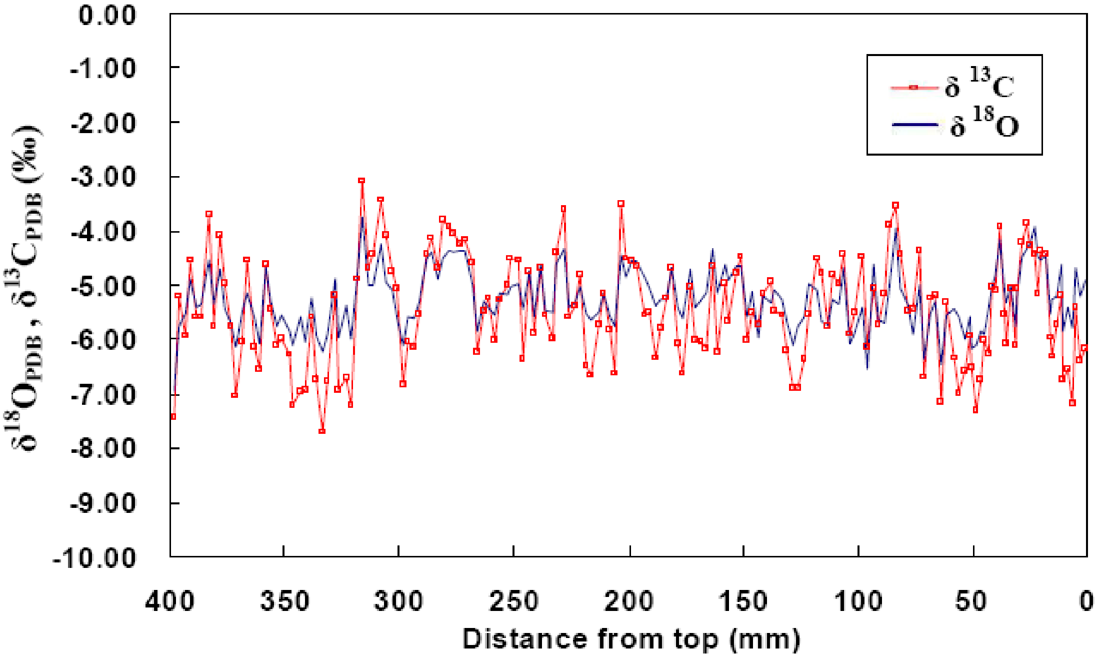

Figure 4-20 δ^{18}O, δ^{13}C and distance for measurements along the growth direction from bottom towards top of the stalagmite NJ1

The isotopic composition is a reflection of the geochemical conditions during precipitation, and can be used to interpret their origin [41]. Figure 4-21 and 4-22 shows the compositions of terrestrial and meteoritic carbonates plotted on a δ^{18}O-δ^{13}C diagram. Compositions are plotted relative to the PDB standard.

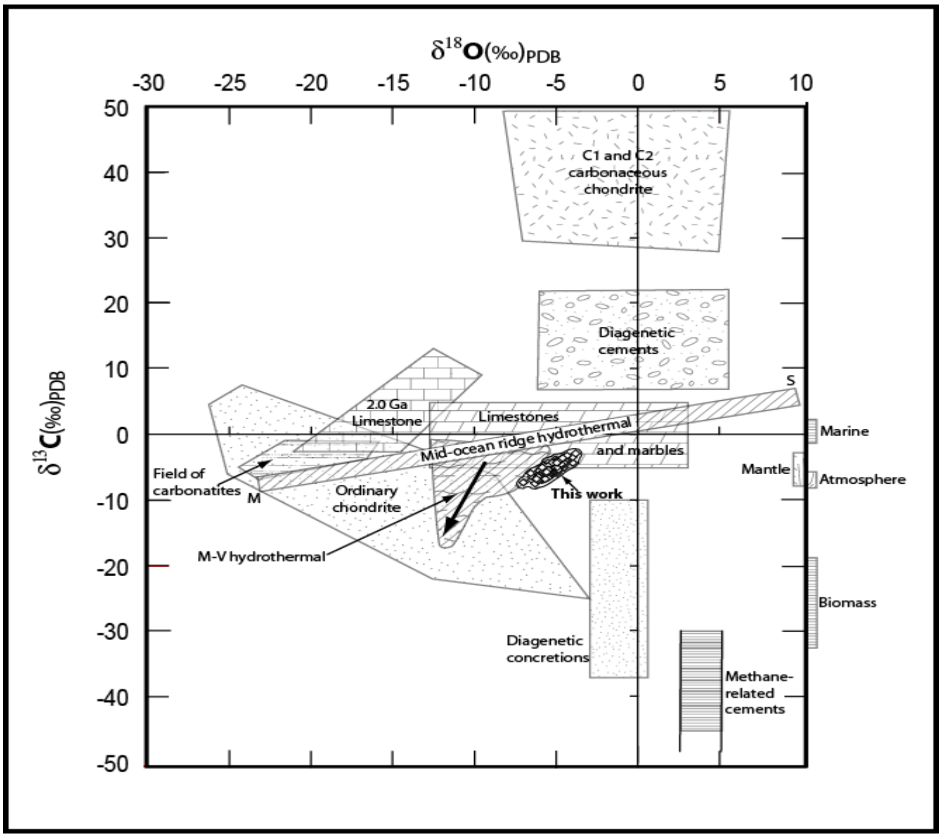

Figure 4-21 $\delta^{18}O$ and $\delta^{13}C$ plot showing the composition of carbonates from a variety of environments (Modified from Rollinson [72])

The isotopic composition of a number of different carbon reservoirs is plotted along the right-hand side of the diagram. The values for sedimentary carbonates (horizontal rule) are from Hudson in 1977 and Baker and Fallick in 1989; hydrothermal calcites (stippled ornament) from the mid-ocean ridges show mixing between mantle-derived carbon (M) and seawater carbon (S) by Stakes and O'Neil, in 1982; in the field of hydrothermal calcites from Mississippi Valley-type deposits (M-V hydrothermal) the arrow shows the direction of younging by Richardson *et al.* in 1988. Chondrite compositions (unornamented) are from Wright *et al.* in 1988. The field of carbonatites is from Deines and Gold in 1973 [72].

According to the isotope values of stalagmite NJ1 (this work) is located between limestones and marbles zone and M-V hydrothermal at atmosphere reservoir. This suggests that limestone is the parent rock of the speleothems of Namjang cave and the original speleothems could be influenced by hydrothermal process which affected to aragonite species in stalagmite NJ1. This diagram used to confirm the type of parent rock which was investigated by the petrography and XRD technique.

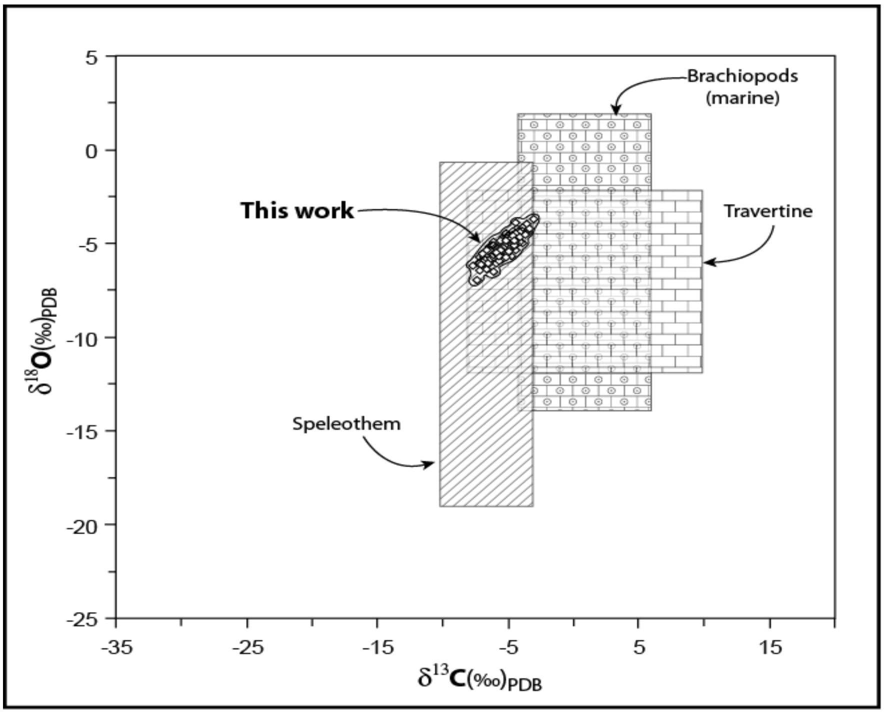

Figure 4-22 The δ^{18}O and δ^{13}C composition of marine carbonates and secondary "terrestrial" carbonates (Modified from Clark and Frize [41])

Sources of data: Limestone, Dolomite - various sources including Al Aasm (pers. comm.), Land in 1991, Azmy in 1997; Brachiopod aragonite (marine carbonate) - Veizer *et al.* in 1997; Speleothems - Schwarcz in 1986, Lauriol *et al.* in 1996; Diagenetic calcite - Irwin *et al.* in 1977, Dimitrakopoulos and Muehlenbachs in 1987, Hutcheon *et al.* in 1989, Al-Aasm in 1997; High pH waters (kinetic) - Barnes and O'Neil in 1969, Clark *et al.* in 1990; Cryogenic calcite - Clark and Lauriol in 1992; Hydrothermal calcite - Bottomley in 1992, Douglas in 1997, McDermott *et al.* in 1996, Shemesh *et al.* in 1992 [41].

Figure 4-22 shows that the isotope values of samples are plotted in the field of speleothems. This confirms the results of the analysis to be no doubt because the sample is stalagmite which is a subclass of speleothems.

4.2.4 Stalagmite chronology

The ages of the samples taken from 3 different parts of the stalagmite NJ1 are as follows; NJ1-8 (near the top) is 130 ±42 years BP, NJ-166 (in the middle) is 778 ±48 years BP and NJ1-388 (near the base) is 1,661 ± 39 years BP respectively (Table 4-3). The detail shows in Appendix C.

Table 4-3 Samples identification the ages and equipments used for ^{230}Th dating

Sample code	Distance from top (mm)	Sample weight (g)	Age Uncorrected (year,BP)	Age Corrected (year,BP)	Error (Year)	Equipment used
NJ1-8	8	1.98	214	130	±42	TIMS (Australia)
NJ1-166	166	2.0	874	778	±48	TIMS (Australia)
NJ1-388	388	0.086	1,710	1,661	±39	ICP-MS (USA)

Laminated stalagmites appear to be common in caves which correlating with seasonality in temperature and/or rainfall. In addition, it should be possible to develop cross-dating methods if it is possible to demonstrate that the thickness of the growth layers of different stalagmites from the same cave, or stalagmites from different caves (same region), show the same growth rate trends [39]. This study, there has data of dating only stalagmite NJ1 then the layer was counted for investigate the thickness of the growth layers which is data base and should be possible to develop cross-dating methods in the future. One method that has been widely reported is to compare the number of layer counts between well-dated layers [39].

The result from counting the layer of growth of this stalagmite NJ1 by Tree-ring width measurements (TSAP version 3.2) based on different positions that the ages were known by dating along the length of the stalagmite, is divided into 3 parts. The first part, there are 28 layers between top and NJ1-8 of stalagmite, with a resolution of about 130 years between the years 2006 and 1876. This part does not show a clear layer. The second part, there are 639 layers between NJ1-8 and NJ1-166, with a resolution of 648 years between the years 1875 and 1228. The third part, there are 825 layers between NJ1-166 and NJ1-388, with a resolution of 883 years between the years 1227 and 345. This part does not show a clear layer. Table 4-4 shows the growth rate of stalagmite NJ1. However, the detail from counting the layer of growth rate shows in Appendix B.

Table 4-4 Growth rate of the layers in stalagmite NJ1

Part of stalagmite	(1) Number of layer* (layer)	(2) Calculated ages ** (year)	(2)-(1) Difference value	(3) Growth rate (yr/layer)	(4) Growth rate (mm/yr)
Top to NJ1-8***	28	130	102	4.64	0.062
NJ1-8 to NJ1-166	639	648	9	1.01	0.244
NJ1-166 to NJ1-388***	825	883	58	1.07	0.251

* The number of layer were counted by Tree-ring width measurements (TSAP version 3.2)

** Calculated ages between dating points

*** Do not show a clear layer for the accurate counting

From Table 4-4 it is explained that the first part, difference value between counting from tree-ring width measurements and calculate from age is 102 years likewise the growth rate is 0.062 mm/year. This point demonstrates a very low growth rate which suggests low precipitation. In this period, one layer precipitated in 4.64 years. These data indicated that the stalagmite NJ1 does not have one growth layer to one year. Remarkably, the top most of stalagmite is a dark brown layer which could be due to a hiatus resulting in the difficulty to determine the layer. The second part, there is 9 years of difference value and the growth rate is 0.244 mm/year. Although, the values between counting by Tree-ring width measurements and calculation of the age are not the same. This could be because some layers of the sample are not clear in this part. One layer precipitated in 1.01 years. This could probably be assumed the growth rate is one year has one layer. According to the third part, many layers are not clear, so amount of layer by counting is uncertainly. There is 58 years of difference value and the growth rate is 0.251 mm/year. One layer precipitated in 1.07 years which is resemble to the second part. This demonstrates that similar factor such as geochemistry or environmental has an influence on both parts which is in contrast with the first part.

4.2.5 Past variations in $\delta^{18}O$ and $\delta^{13}C$

A plot of $\delta^{18}O$ and $\delta^{13}C$ against the age of stalagmite NJ1 is shown in Figure 4-23. If the aragonite is isotopic equilibrium deposition, this variation of $\delta^{18}O$ is considered to reflect fluctuations in the paleotemperature from the site in mid to high latitude regions, whereby higher temperature corresponds to higher $\delta^{18}O$ values [9]. From experiments with inorganically precipitated carbonates, the changes in $\delta^{18}O$ of calcite have been found to be -0.21‰/°C at 25°C, -0.22‰/°C at 20°C and 0.24‰ at 10°C [73]. However, a negative correlation between $\delta^{18}O$ of precipitation and amount of rainfall is observed in tropic and negligible temperature factor which is termed as the "amount effect" [74]. World wide modern precipitation data available from island stations in the equatorial belt (collected by IAEA) have shown a linear relationship between the mean monthly $\delta^{18}O$ of precipitation and the mean monthly rainfall which seasonal temperature variations are small. Average rate of depletion is found to be -1.5 ± 0.2 ‰ for a 100 mm increase in the mean monthly rainfall [75].

The $\delta^{13}C$ depends upon $p\text{CO}_2$ of the water, temperature of calcite precipitation, type of overhead vegetation (C_3 or C_4) and the dripping rate of water in a complex fashion. Broadly, the slow changes occurring in $\delta^{13}C$ at decadal scale or more are ascribed to variations in the abundance of C_3 or C_4 plants. At shorter time scales (e.g. yearly) the fast changes are due to varying dripping rate which finally depends upon the amount of rainfall in the cave region [8].

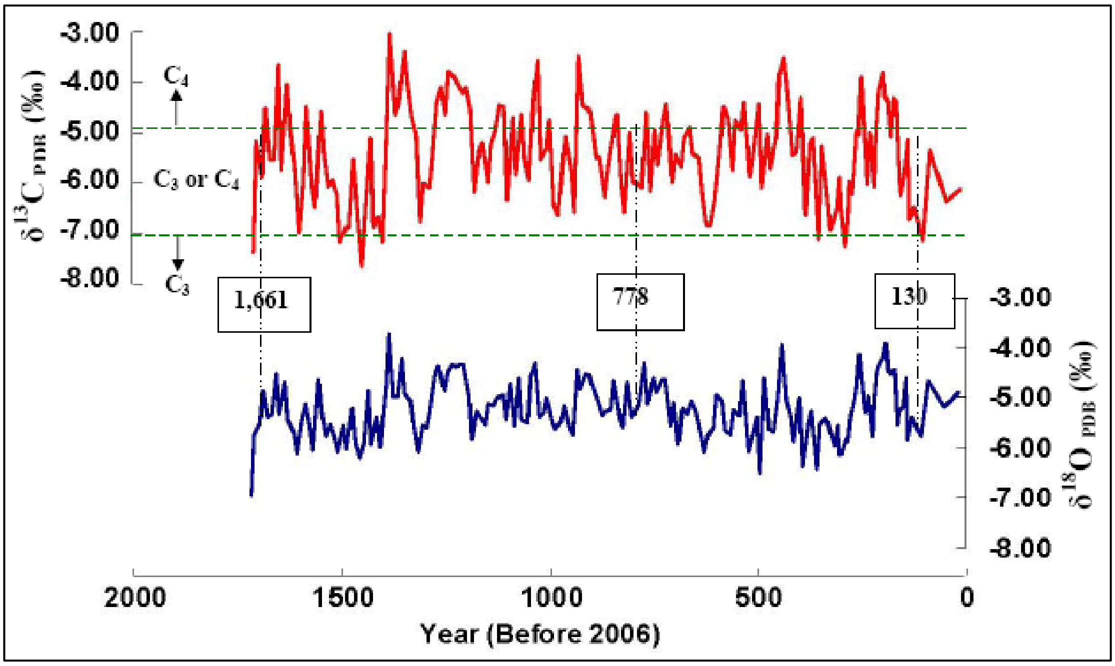

Figure 4-23 $\delta^{18}O$ and $\delta^{13}C$ *vs* age for measurements along the growth direction (from bottom to top) of the stalagmite NJ1.

* The numbers in the plot area represent the analyzed corrected ages and the green dash lines separate two types of plant (C_3 and C_4)

The fluctuation of $\delta^{13}C$ means that there were switching between C_3 and C_4 types or mixing both types in some periods. McDermott [71] suggested that a range of $\delta^{13}C$ in is typically -14‰ to -6‰ for secondary carbonates deposited in equilibrium with CO_2 respired from C_3 plants, and -6‰ to +2‰ for that from C_4 plants. Stalagmite NJ1, the value of $\delta^{13}C$ ranges from -7.69 to -3.08‰ (mean value is -5.42‰) with approximately by 4‰ variations which is very small rang. Base on McDermott, these data is difficult to demonstrate the type of plant. Therefore, this study separates the data into three condition base on the estimates standard deviation (SD) of the value of $\delta^{13}C$ which is 1.05‰. The value of $\delta^{13}C$ more than -4.95‰ represent C_4 plants, the value of $\delta^{13}C$ range from -4.95 to-7.05‰ represent C_3 or C_4 plants, and the value of $\delta^{13}C$ less than -7.05‰ represent C_3 plants.

The values of $\delta^{13}C$ more than -4.95‰ are deciphered to C_4 plant in the years of 1673, 1641, 1621, 1573, 1542, 1383-1323, 1263-1184, 1116-1104, 1084, 1064, 1037-1025, 997, 925-897, 838, 766, 725-716, 663, 581-573, 552, 532, 499, 450-

429, 397, 253, 212-192, and 179-171 years BP. These results are concordant with the enrichment of mean value of $\delta^{18}O$ (-4.68‰) in these periods. This mean value is greater than the mean value of $\delta^{18}O$ (-5.22‰) along the growth axis. This indicates that in these periods the rainfall decreased that caused dry climate and affect the dominant distribution of C_4 plant in these periods.

The values of $\delta^{13}C$ between -4.95‰ and -7.05‰ are deciphered to C_3 or C_4 plant in the years of 1693-1681, 1661-1653, 1633, 1613-1581, 1562-1554, 1534-1502, 1482-1454, 1434-1402, 1315-1275, 1176-1124, 1096, 1076, 1056-1044, 1017-1005, 985-937, 885-846, 826-778, 757-737, 704-675, 655-593, 561, 540, 520-511, 491-458, 417-409, 388-368, 347-302, 286-261, 245-220, 183, 163-130, and 81-16 years BP. These periods have mean value of $\delta^{18}O$ is-5.46‰ which is in the middle of decreasing and increasing values. These results are uncertainly implied that C_3 or C_4 plants could be available in these periods.

The values of $\delta^{13}C$ less than -7.05‰ are deciphered to C_3 plant in these years of 1701, 1494, 1442, 1395, 356, 294, and 98 years BP. These results are concordant with the depletion of mean value of $\delta^{18}O$ (-6.23‰) in these periods (less than mean value of $\delta^{18}O$ along the growth axis which is -5.22‰). This indicated that the increasing of rainfall which caused wet climate, affecting the dominant distribution of C_3 plant in these periods, however at the present day the plants is dominated by C_3 type.

However, the paleovegetation is reconstructed by $\delta^{13}C$ are switching between C_3 and C_4 plants. It can not be divided in the distinct periods because there are fluctuations along the growth axis. All data interpretation derived from every single analysis is shown in Appendix D.

Seasonality, amount of precipitation, altitude dependence, continentality, the role of local temperature, together with the source specific fractionation between oxygen-18 and deuterium: all these effects can contribute to the isotope content of a sample of precipitation [76]. A comparison of stalagmites from other locations influenced by the same monsoon as Namjang cave, Thailand is shows in Table 4-5.

Table 4-5 Characteristics of stalagmites of the present study (Namjang cave) and other locations which are affected by the Indian and Pacific monsoon climates

Cave/Location/ Elevation/ Roof thickness (soil layer+bed rock)/ Monsoon	Mineralogy/ Growth rate	$\delta^{18}O$ (‰ PDB) Min/Max Mean	$\delta^{13}C$ (‰ PDB) Min-Max Mean	Time interval covered
Namjang cave, Thailand 18º46'N, 98º49' E Elev: 902 above m.s.l. Roof thick: 5 m. Indian and Pacific monsoon	Aragonite 0.06-0.25 mm/yr	-6.95/ -3.75 -5.22	-7.69/ -3.08 -5.42	~1701 yr BP to 2006 AD
Dandak cave,India [8] 19º00' N, 82º00' E Elev: 604 above m.s.l. Roof thick: 6 m Indian monsoon	Pure calcite 0.18 mm/yr	-2.85/ -6.18 -3.99	-5.41/-11.04 -8.68	~3700 yr BP to 1996 AD
Dongge cave, China [62] 25º17'E, 108º5' N Elev: 680 above m.s.l. Indian and Pacific monsoon	-	-6.64/-9.14 -7.89		6930 yr BP to 2000AD

Three caves are located in low latitude which isotopic content is modulated by the seasonal variations in the volume of precipitation instead and surface temperature is negligible. During the rainy season, precipitation is isotopically depleted [9, 76]. The $\delta^{18}O$ mean values of Namjang cave and Dongge cave are less than that of the Dandak cave. This could be due to the bigger in size of roof thickness of Dandak cave affect to the residence time of the water should be long, responding to enrichment of the $\delta^{18}O$ values. It means that the average drip rate is low compared to other caves. Including to, the amount of rainfall from different local meteorology or different moisture source regions affect to $\delta^{18}O$. Namjang cave and Dongge cave are influenced by both Indian monsoon and Pacific monsoon, the mean values of $\delta^{18}O$ are depletion compared to Dandak cave which is influenced by only Indian monsoon. Moreover, an altitude and continental effect of the location may affect the $\delta^{18}O$ value. Although Namjang cave and Dongge cave are influenced by the same climate (monsoon) but they have different mean values of $\delta^{18}O$. There are different locations which are distinct altitude and distance from the coast. When the clouds move inland from the coast, they become isotopically depleted progressively, as a result of their loss of moisture. The isotopic signatures also reflect the topography of the continent. Mountain chains deplete the clouds too, because of orographically forced rainout [76]. This reason it could be different mean value of $\delta^{18}O$ between Namjang cave and Dongge cave.

The mean values of $\delta^{13}C$ at Namjang cave, Thailand are higher than all caves that implied for different plant or a soil layer above the cave. Namjang cave is covered with vegetation is switching between C_3 and C_4 plants which reflect the enrichment of $\delta^{13}C$ levels. The soil layer above Dandak cave is thicker in size. The rainwater resides in the soil layer is a longer period of time, together with dominantly by C_3 plant above the cave [8]. It could be a domain to depleted $\delta^{13}C$ compared to Namjang cave in Thailand.

There are many layers of stalagmite NJ1 are not clear. The unclear layers show a dark brown color (Figure 4-24). These regard with suspicion the $\delta^{18}O$ and $\delta^{13}C$ of these layers which bring to investigate these layers in finally.

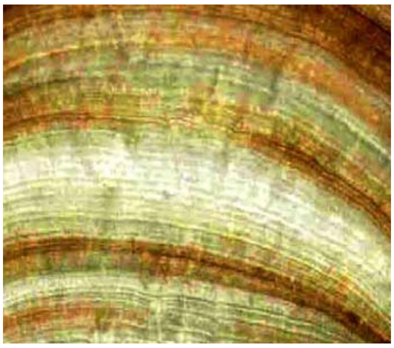

Figure 4-24 The layers of stalagmite NJ1 with dark brown color and white color

Along the growth axis of NJ1, there are approximately 11 layers with dark brown color. A possible explanation for the occurrence of dark brown layers is the seeping water with fine detrital particles which are either derived from soil zone or from bedrock fissures and carried to the dripping spot. These detrital particles fall on the tip of a stalagmite, and are trapped in the growing carbonate layers. This provides them to remain on the growing surface for a sufficient time [8]. Table 4-6 shows a correlation between layers of dark brown color and $\delta^{13}C$ and $\delta^{18}O$. Two layers are very strong dark brown color such as distance of layer is 246 mm from top has -5.45‰ of $\delta^{18}O$ and -6.38‰ of $\delta^{13}C$ (decreasing of these isotope), caused increasing of rainfall. This interpret that increasing of rainfall the drip rate is quite high most of the detrital particles are removed from the growing surface and hence the compact (dark brown layer) carbonate layer is formed

Table 4-6 The dark brown layer with $\delta\ ^{18}O$ and $\delta\ ^{13}C$ of stalagmite NJ1

Distance from top (mm)	$\delta^{18}O$ (‰)	$\delta^{13}C$ (‰)
48	-6.11	-7.29
93	-4.62	-5.07
113	-5.74	-5.77
138	-5.33	-4.94
158	-4.61	-4.98
*246	-5.45	-6.38
316	-3.75	-3.08
343	-5.58	-6.94
353	-5.76	-6.11
378	-4.70	-4.08
*381	-5.34	-5.77

* very strong dark brown color

However, not all the dark brown layers in the sample, NJ1 have the low values of $\delta^{13}C$ and $\delta^{18}O$. Generally, from Yadava [8] it should be low isotopic in these layers. For this study the drilling may cover the wide area on the surface, or the precise scale of measurement is different between Thai and China equipment.

4.2.6 Rainfall reconstruction

Before using the isotopic data of the stalagmite NJ1, the isotopic equilibrium should be checked and it is indicated by (i) $\delta^{18}O$ remains constant along a single growth layer while $\delta^{13}C$ varies irregularly, and (ii) there is no correlation between $\delta^{18}O$ and $\delta^{13}C$ along a growth layer [32]. In practice, consistent sampling along single growth layers is often difficult to achieve, not least because visible layers are often thinner. Likewise, this study lacks the data of $\delta^{18}O$ and $\delta^{13}C$ for the same layer but there are 170 values along the growth axis. Then the correlation between of $\delta^{18}O$ and $\delta^{13}C$ is checked and given as R=0.83 (Figure 4-25). This should be regarded with suspicion that was caused by kinetic isotopic fractionations and fast CO_2 degassing, thus the aragonite was not in ^{18}O equilibrium with the water from which it precipitated.

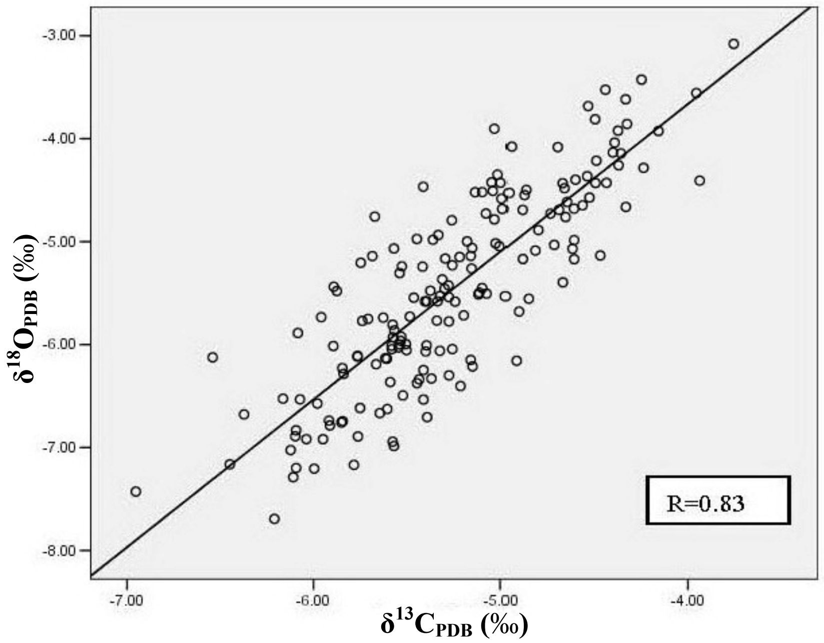

Figure 4-25 Plot of 170 coordinates for $\delta^{18}O$ and $\delta^{13}C$ of the stalagmite NJ1 measured along the growth axis

However, Yadava [8] presented a high correlation (R=0.6) between $\delta^{13}C$ and $\delta^{18}O$ of AKG cave, India. It is indirect evidence that Rayleigh type calcite precipitation plays an important role in deciding that the $\delta^{13}C$ of the tropical speleothems and the dripping rate of the seepage water are affecting the short (yearly) fluctuation in the $\delta^{13}C$. Long term (more than years) fluctuations are controlled by; 1) soil components having different residence times; 2) climate changes affecting C_3/C_4 ratios. A high correlation indicates that 1) it is the changes in the drip rate of the seepage water (proportional to the annual rainfall) which is responsible for the changes in both $\delta^{18}O$ and $\delta^{13}C$; 2) $\delta^{13}C$ of annual laminations can also be used as an indicator of past rainfall [8].

Contradiction between the result of Hendy [32] and Yadava [8], so the assumption is aragonite was isotopic equilibrium deposition or not is uncertainly for this work. Fortunately, this case can be proved by compare with another data such as isotopic composition of rainfall from GNIP; peleoprecipitation was constructed by index of tree ring which located near the study area and pelaeoclimate record in speleothems in similar region.

Based on the available data from GNIP, this database includes mean monthly $\delta^{18}Op$, δD, precipitation amount, surface temperature, and vapor pressure values for 5 sites around the study area as; New Delhi in India, Luang Prabang in Lao and Bangkok, Koh Sichang, Koh Samui in Thailand. However many of these records are discontinuous. To prevent inter-annual variability in stable isotope systematics from biasing on results, the Bangkok site was chosen and it has the continuous record of meteorological observations between 1968 and 2004 (Appendix E). According to Araguas [9] who illustrated that the climatic sensitivity of the isotopic signal in precipitation varies considerably: $\delta^{18}O$ and $\delta^{2}H$ of rainfall in the northern part of the region (above approximately $35^{o}N$) are mainly controlled by temperature; in the southern and southeastern parts they are dominated by the precipitation amount effect. Assuming that given site, surface temperature is negligible and the amount of precipitation is the main environmental variable correlated with $\delta^{18}O$, these data are ideally suited for a polynomial regression analysis (Figure 4-26).

Plots of δ^{18}O and precipitation have the significant relationship between them. Low R^2 value (R^2 = 0.42) illustrates that precipitation has an influence over the δ^{18}O equal to 42% and the rest of 58% is unexplained by precipitation but for elevation, latitude, source of moisture, topography, degree of water vapor recycling, and atmospheric transport pathways [77]. Moreover, many processes other than climate may be involved in producing the δ^{18}O signal odserved in speleothems [62]

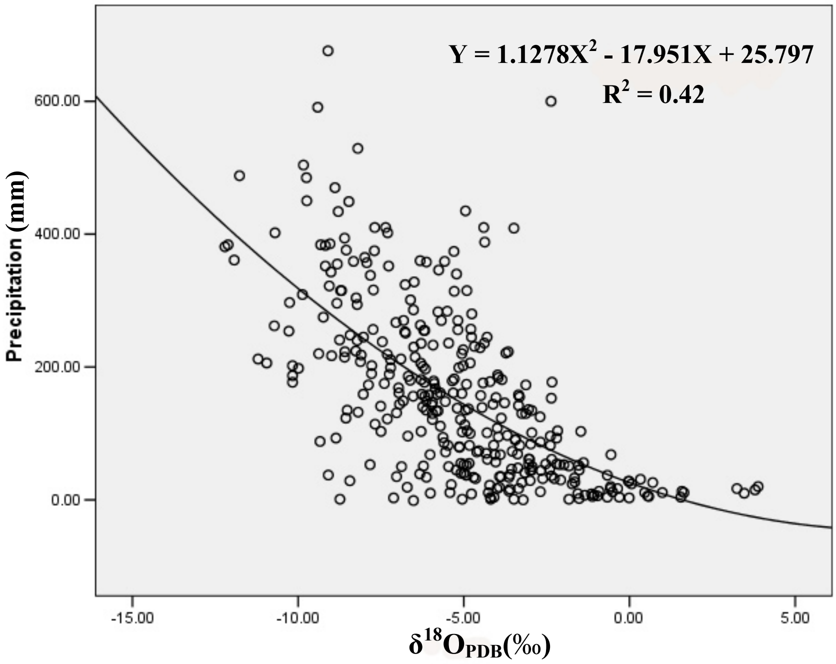

Figure 4-26 Negative correlation between monthly δ^{18}O of precipitation (independent variable) and monthly precipitation (dependent variable) at Bangkok during years 1968 to 2004 (the data taken from GNIP)

Figure 4-26 shows a non linear relationship (polynomial regression) between the mean monthly δ^{18}O (δ^{18}O of precipitation) and the mean monthly precipitation (this study means rainfall only because in Thailand there is rarely hail, and snow), with R^2 = 0.42 for observations between 1968 and 2004 (more than 280 monthly observations). As these stations are near the equator, seasonal temperature variations are small. The δ^{18}O and mean monthly rainfall is negative correlation, increasing of δ^{18}O with decreasing of mean monthly rainfall. However, there is a high correlation (R = 0.6) (Figure 4-27) between the mean monthly rainfall at Bangkok and

Mae Hong Son province which data are available for 37 years (1968 to 2004). Although the data only available for 19 years (1986 to 2004) are plotted between the precipitation of Pang Ma Pha and Bangkok, the graph still shows high correlation (R=0.52) in Figure 4-28. This assumes that the monthly rainfall of the cave area is nearly the same as Mae Hong Son province (R = 0.82) (Figure 4-29). Furthermore these results show in Table 4-7. Note that the rainfall data at Pang Ma Pha and Mae Hong Son station shows in Appendix F.

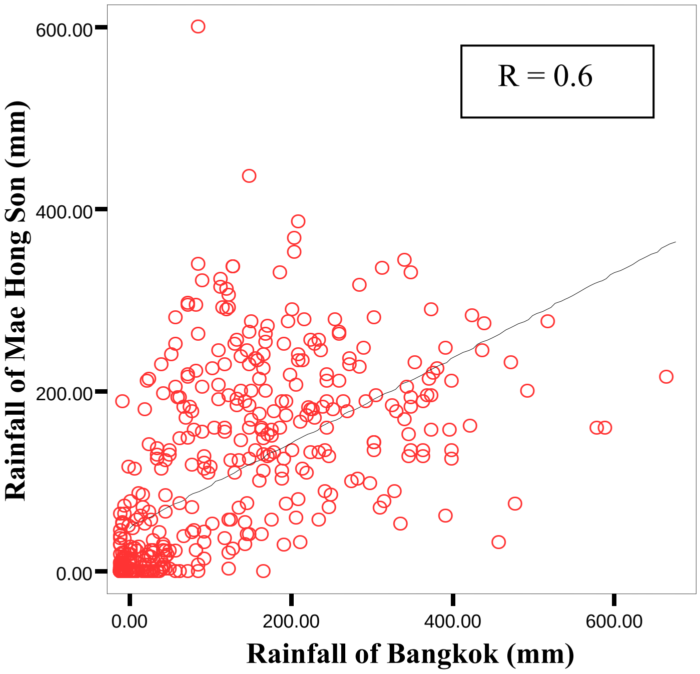

Figure 4-27 The correlation of mean monthly rainfall between Bangkok and Mae Hong Son during the year 1968 and 2004

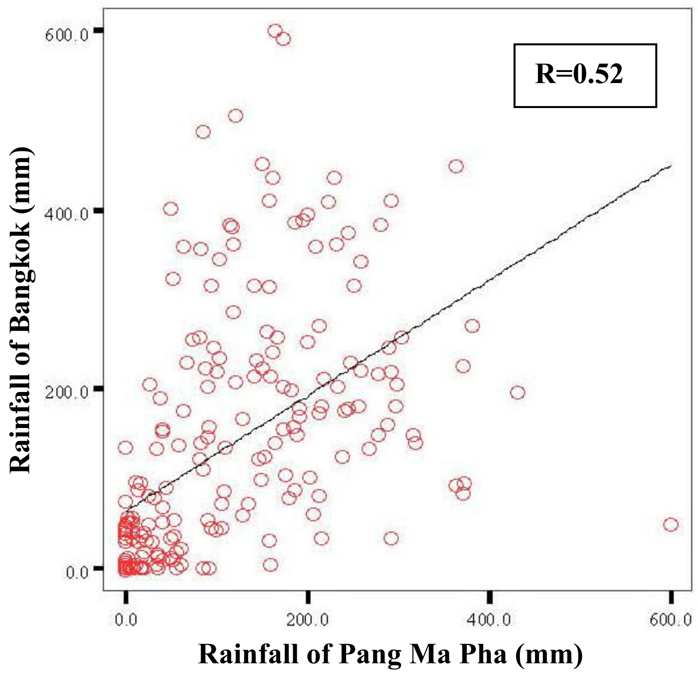

Figure 4-28 The correlation of mean monthly rainfall between Bangkok and Pang Ma Pha during the years 1986 and 2004

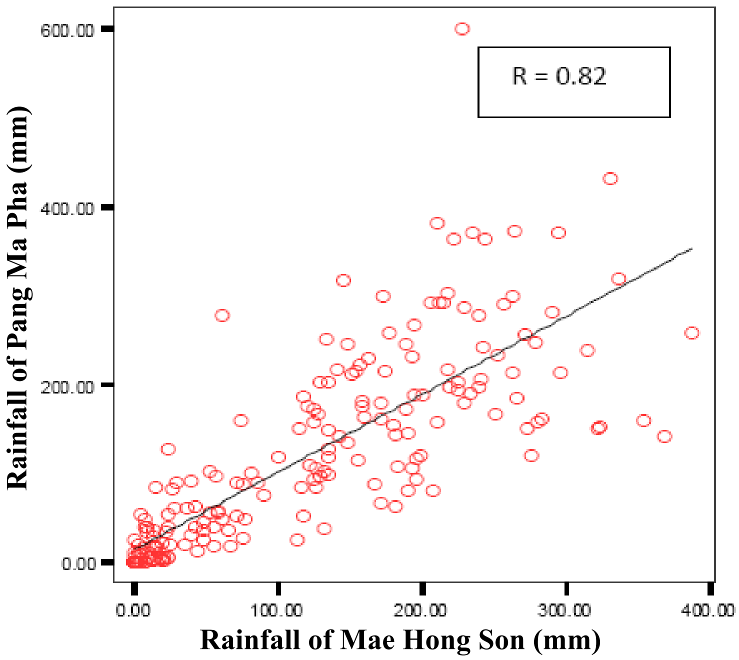

Figure 4-29 The correlation of mean monthly rainfall between Mae Hong Son and Pang Ma Pha during the year 1986 and 2005

Table 4-7 R values of correlation between the rainfall data of different pairs of site

Site	R value	Period (Year)
Bangkok-Mae Hong Son	0.60	36
Bangkok-Pang Ma Pha	0.52	18
Mae Hong Son-Pang Ma Pha	0.82	19

According to the R values for 3 pairs of correlation (Table 4-7), the equation (4-1) from polynomial regression model in Bangkok site (Figure 4-26) is a key for paleoprecipitation reconstruction of the study area.

$$\boxed{\textbf{Precipitation} = 1.1278(\delta^{18}O)^2 - 17.951\,\delta^{18}O + 25.797} \quad (4\text{-}1)$$

The data of $\delta^{18}O$ in Stalagmite NJ1 were used in the equation 4-1 to reconstruct the past precipitation in this area. Allan and Matthews [78] suggested that $\delta^{13}C$ values of secondary carbonate come from a combination of two carbonate reservoirs (soil-derived CO_2 and the original carbonate) whereas oxygen is dominated by a single reservoir, meteoric water then assuming that precipitation data from stalagmite NJ1 is similar to precipitation (rainfall) above the cave.

Namjang cave has a thick roof (soil layer+bed rock) about 5 m. This means that the residence time of the water should be long, probably more than a month that is affected to the low growth rate of stalagmite NJ1 (0.06-0.25 mm/yr). In such a case the mixing of older water is expected to be negligible and the original amount-dependent oxygen isotopic signature of the rain water will be recorded in the yearly laminations [8]. However, the winter season and summer season at the study area minimize amount of rainfall and the soil above the cave is unsaturated in these periods. The reconstructed rainfall is averaged monthly rainfall during wet season (rainy season) only (Figure 4-30).

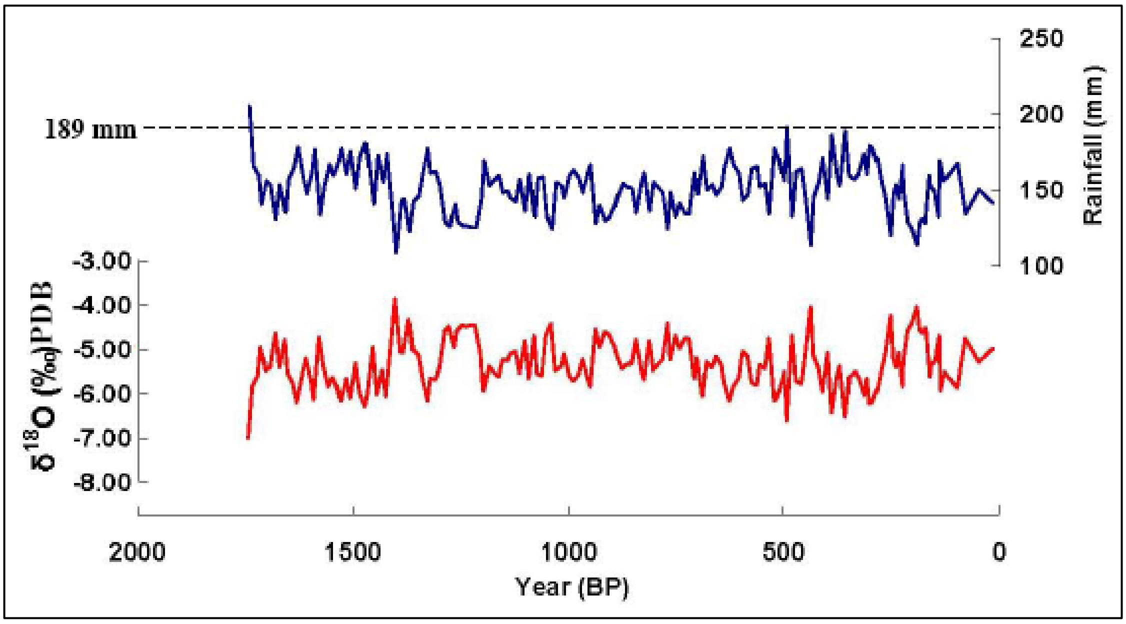

Figure 4-30 Comparison plot of $\delta^{18}O$ in stalagmite NJ1 (relative to PDB) and amount of reconstructed rainfall base on the same period, dash line shows the mean monthly rainfall in wet period during 1911-2002 years AD

Based on the mean monthly rainfall during years 1986 to 2004 at Pang Ma Pha is 189 mm in wet period. There are two years of the excess rainfall (more than 189 mm) as 1701 and 491 yr BP (305 and 1515 yr AD) are seen in the stalagmite NJ1 reconstruction. The rest of many years are the severely deficient rain fall events. All data interpretation derived from every single analysis is shown in Appendix D.

Moreover, this study represents the signal of stalagmite oxygen isotopes which is reconstructed to regional rainfall with other proxy records such as tree rings in the same province, it is possible to evaluate and calibrate the climatic differences and similarities between them.

Annually laminated stalagmites should be expected in caves which have an overlying climate that has a strong seasonality, similar climate zones to where trees grow with distinct annual rings [39]. A comparison between the data reconstruction of rainfall by stalagmite NJ1 and tree-ring of Teak at the same province agrees well with each other as shown in Appendix G and Figure 4-31. Note that the missing data of rainfall in the past were reconstructed by using the equation obtained from the correlation plot between the tree-ring index against the available rainfall data year by year [79]

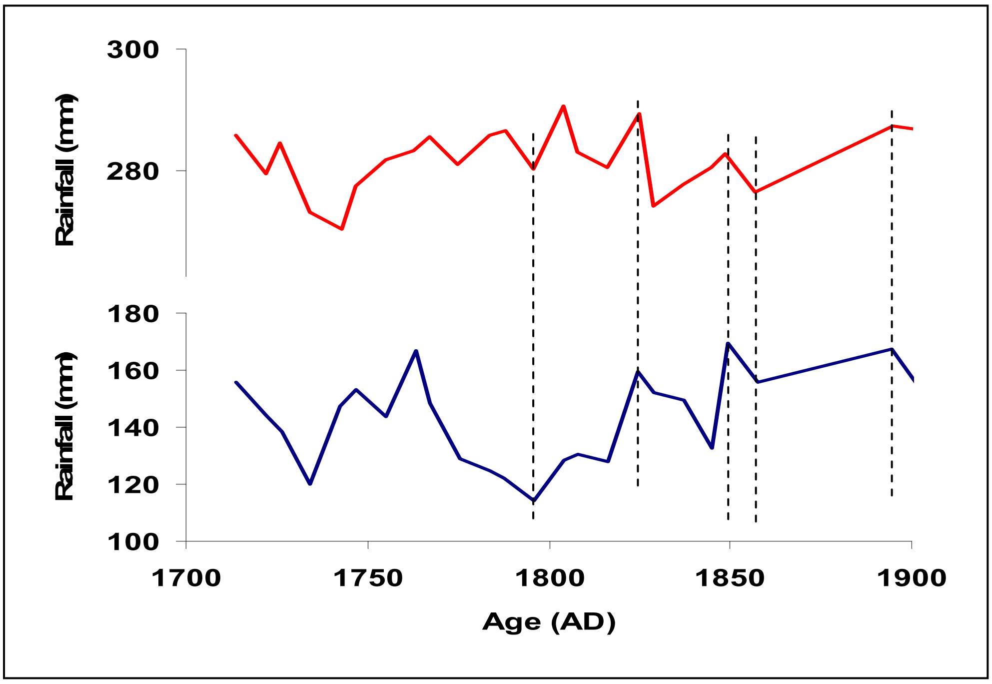

Figure 4-31 Rainfall reconstructed by Teak tree-ring (mean monthly from March to May) (upper line) compared to the rainfall from stalagmite NJ1 reconstruction (during wet period) (lower line) as during year 1714-1913

Figure 4-31 shows that the patterns of both data are agree well during 1796-1825 year and 1849-1895 year. The amounts of rainfall from both methods are different. This could be the reason of the stalagmite is more complex and the distance between two sites (Stalagmite is located at 98°49'E, 18°46'N whereas Teak is located at 98 39'E, 19 40'N) and elevation etc. Esper *et al.* [63] suggested that the most notable is the possibility of obtaining long (10^2-10^3 years) continuous stalagmite lamina records are capable of preserving low frequency climate information at annual resolution. Whereas, tree ring records which there are many more samples that are better at preserving high frequency climate variability but which are limited in their ability to retain climate variations on a multi-centennial time scale. Then laminated stalagmites and tree rings should therefore to some degree provide complementary climate information [39]. However, not all the deficient or excess rainfall events shown by all Thailand rainfall time series are registered in the stalagmite NJ1. The reasons could be due to large spatial variability in the rainfall. There are occasions when some parts of the country receive excess rain whereas other part has serious deficient conditions [8].

The values of $\delta^{18}O$, $\delta^{13}C$ and rainfall are plotted against the time series can be used for anticipation roughly of the trend of those three parameters in the future as shown in Figures 4-32 to 4-34.

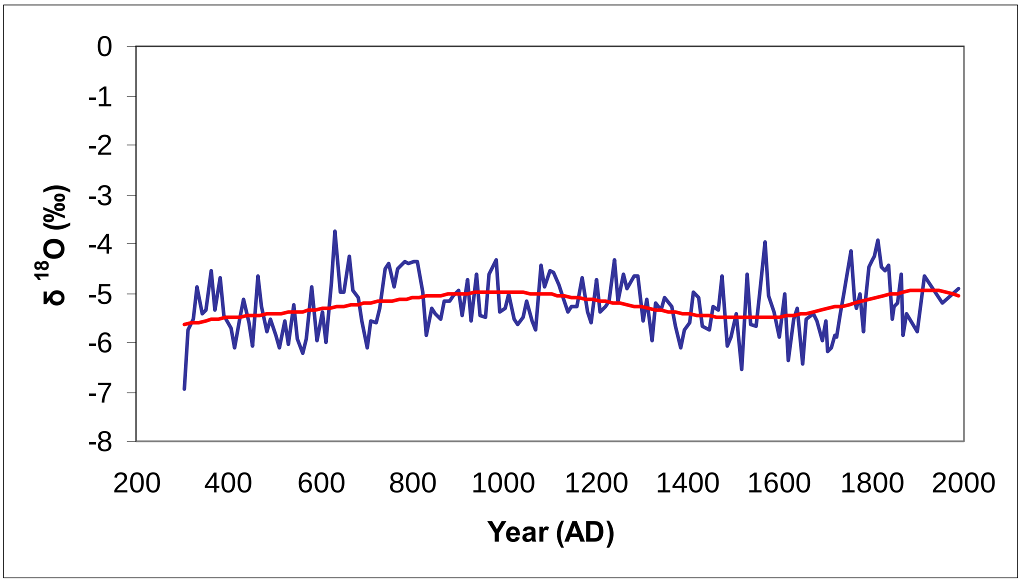

Figure 4-32 The $\delta^{18}O$ observed in Namjang cave from 305 to 1990 AD. The red line is the 6 th-order polynomial fit

Figure 4-32 shows $\delta^{18}O$ having a fluctuation. The trend increases in the periods of the years 305-981, 1515-1915 AD. There are the decreased periods during the years 982-1514 and 1516-1990 AD. The trend of $\delta^{18}O$ will switch between decreasing and increasing and have 600 year period. This trend can forecast that the values $\delta^{18}O$ in the next 600 year will decrease (the year 2116- 2716 AD).

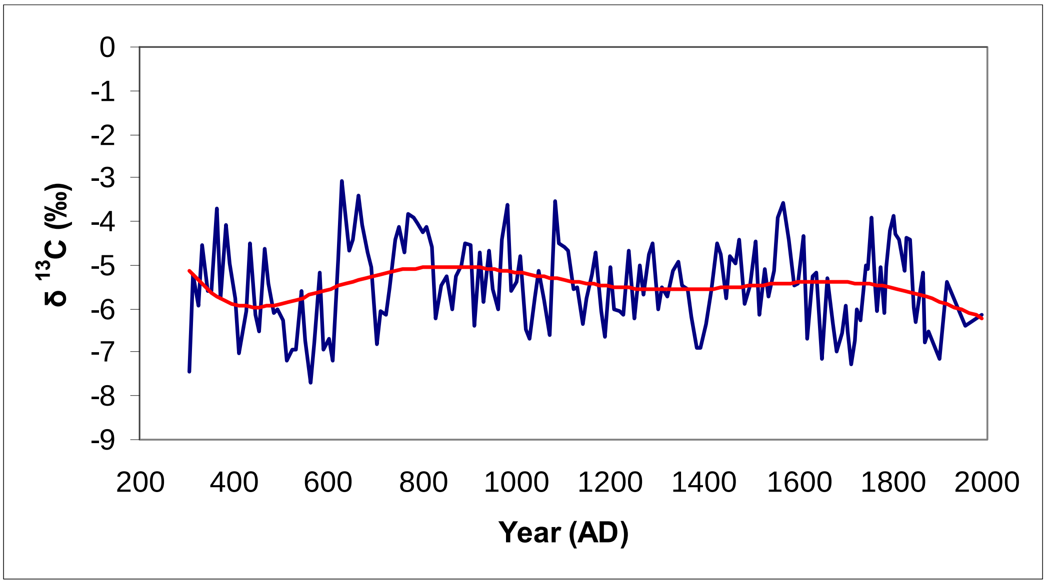

Figure 4-33 The $\delta^{13}C$ observed in Namjang cave from 305 to 1990 AD. The red line is the 6 th-order polynomial fit

Figure 4-33 shows $\delta^{13}C$ having a fluctuation. The trend increases in periods of the years 453-801, 1385-1753 AD and decreases in periods of the years 305-452, 802-1384 and 1754-1990 AD. For over all, the trend of $\delta^{13}C$ will switch between decreasing and increasing and have 350-400 year period. The next 350-400 years in the future the trend of the $\delta^{13}C$ will be increase (the year 2154- 2524 AD).

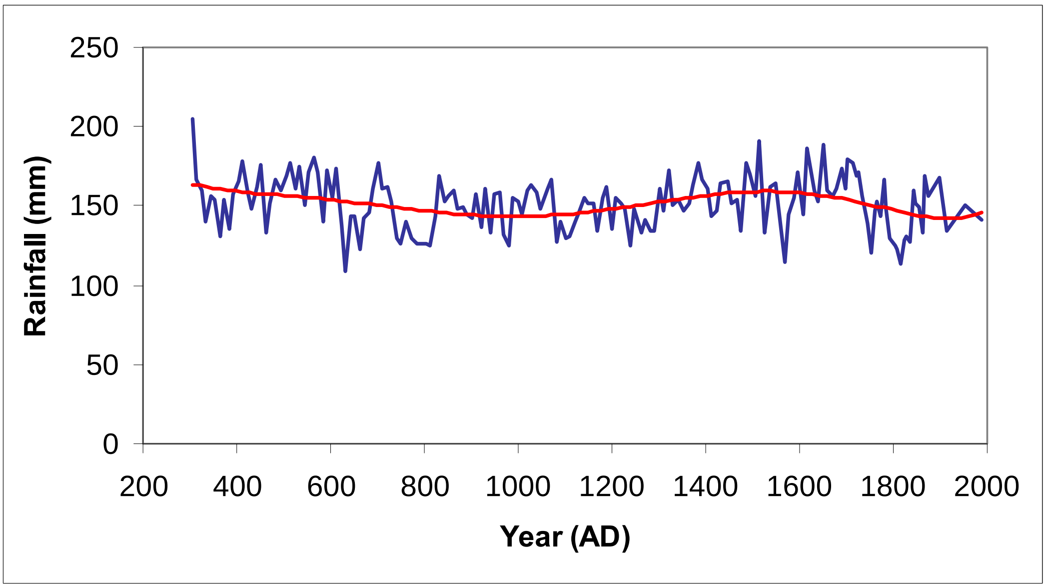

Figure 4-34 The rainfall observed in Namjang cave from 305 to 1990 AD. The red line is the 6 th-order polynomial fit

Figure 4-34 shows the rainfall having a fluctuation. The trend increases in periods of the years 982-1536 and 1915-1990 AD. There are decreasing periods of the year 305-981, 1537-1914 AD. The trend of rainfall will switch between decreasing and increasing and have 600 year period. This trend can forecast that the rainfall in the next 600 year will increase (the year 2137- 2736 AD).

CHAPTER V

CONCLUSIONS AND RECOMMENDATIONS

5.1 Conclusions

5.1.1 Mineral species, petrography and morphology

The parent rock of the stalagmite in Namjang cave is limestone with skeletal grain composition or biosparite. This result is implied to the origin of this limestone that deposited in Permian from the shallow seawater in tropical climate.

Under the microscope, stalagmite NJ1 and NJ2 show a brown to dark brown layers separated from each other by a dark brown layer. The observation by the SEM, each layer contains many groups of fan-like polycrystalline fibrous crystals diverging from the bottom to the top. They contain the aragonite crystals analyzed by the XRD of tabular and blade habits.

5.1.2 Relationship between δ^{18}O and δ ^{13}C variations of stalagmite NJ1

For stable isotope measurement 170 subsamples were prepared from the stalagmite NJ1. δ^{18}O is ranging from -6.95 to -3.75 ‰ and δ^{13}C is ranging from -7.69 to -3.08 ‰ with approximate 3 ‰ variations in δ^{18}O and up to 4 ‰ in δ^{13}C. The values of both isotopes agree well with each other with the high correlation (R = 0.83) this is implied that the geochemical or environment factors should have affected the δ^{18}O and δ^{13}C values in a similar way. Furthermore, the isotopic composition can be used to interpret their origin.

5.1.3 Stalagmite chronology

The stalagmite NJ1 was dated by the used of TIMS and ICP-MS at USA and Australia respectively for 3 dating points. The age of NJ1-8 which is near the top (8 mm from top) is 130 ±42 years BP and the age of NJ1-166 which is in the middle is

778 ±48 years BP. These two points were investigated by TIMS. The age of NJ1-388 which is near the base is 1,661 ± 39 BP was investigated by ICP-MS. Counting layer under the microscope with Tree-ring width measurements (TSAP.version 3.2) with the assumption that one year has one layer. The first part (between the top and NJ1-8) has the growth rate of 0.062 mm/year. This point demonstrates a very low growth rate which suggests low precipitation. One layer in this period is not for one year but it is for 4.64 years. Remarkably, the top most of stalagmite is a dark brown layer which could be due to a hiatus resulting in the difficulty for the determination of the layer. The second part between NJ1-8 and NJ1-166 has the growth rate of 0.244 mm/year. It has one layer for 1.01 year. This can be interpreted that one year have one layer. According to the third part between NJ1-166 and NJ1-388, many layers are not clear, so the amount of layer by counting is uncertainly. The growth rate of this point is 0.251 mm/year or one layer is for 1.07 year which is resemble to the second part. This demonstrates that similar factors such as geochemistry or environment have an influence on both parts which contrast from the first part.

5.1.4 Past variations in $\delta^{18}O$ and $\delta^{13}C$

A negative polynomial correlation between $\delta^{18}O$ of precipitation and amount of rainfall is observed in tropical zone. The value of $\delta^{13}C$ more than -4.95‰ in the year of 1673, 1641, 1621, 1573, 1542, 1383-1323, 1263-1184, 1116-1104, 1084, 1064, 1037-1025, 997, 925-897, 838, 766, 725-716, 663, 581-573, 552, 532, 499, 450-429, 397, 253, 212-192, and 179-171 years BP which is deciphered to C_4 plant in these years. These results are concordant with the enrichment of mean value of $\delta^{18}O$ (-4.68‰) in these periods (more than mean value of $\delta^{18}O$ along the growth axis which is -5.22‰). This indicated that the decreasing of rainfall which caused dry climate, affecting the dominant distribution of C_4 plant in these periods. The value of $\delta^{13}C$ less than -7.05‰ in the year of 1701, 1494, 1442, 1395, 356, 294, and 98 years BP which is deciphered to C_3 plant in these years. These results are concordant with the depletion of mean value of $\delta^{18}O$ (-6.23‰) in these periods (less than mean value of $\delta^{18}O$ along the growth axis which is -5.22‰). This indicated that the increasing of rainfall which caused wet climate, affecting the dominant distribution of C_3 plant in these periods. However, in the present day, vegetation is dominant C_3 type at the study area.

Along the growth layer have approximately 11 layers are dark brown color. The layer is absolute dark brown color such as distance of layer is 246 mm from top has -5.45‰ of $\delta^{18}O$ and -6.38‰ of $\delta^{13}C$ (decreasing of these isotope), caused increasing of rainfall. This interpret that increasing of rainfall the drip rate is quite high most of the detrital particles are removed from the growing surface and hence the compact (dark brown layer) carbonate layer is formed. However, not all the dark brown layers have the low value of $\delta\ ^{13}C$ and $\delta\ ^{18}O$. It should be drilling cover the wide area on the surface, or the precise scale of measurement is different between Thai and China equipment.

5.1.5 Rainfall reconstruction

Based on the available data from GNIP, Bangkok site has continuous record meteorological observations between 1968 and 2004. Assuming that given site, surface temperature is negligible and amount of precipitation is the main environmental variable correlated with $\delta^{18}O$. These data are ideally suited for polynomial regression analysis.

A plot of $\delta^{18}O$ and precipitation data of the Bangkok site gives a significant relationship between these data with low of R^2 value ($R^2 = 0.42$). This illustrates that precipitation has an influence to $\delta^{18}Op$ of 42% and the rest 58% are unexplained and these may be the factors of e.g. elevation, latitude, source of moisture, topography, degree of water vapor recycling, and atmospheric transport pathways. However, there is a high correlation ($R= 0.52$) between the mean monthly rainfall at Bangkok and study area. Therefore the equation from polynomial regression model in Bangkok site is a key to apply for paleoprecipitation reconstruction of the study area.

There are two years of the excess rainfall ((more than 189 mm in wet period)) as 1701 and 491 yr BP (305 and 1515 yr AD) are seen in the stalagmite NJ1 reconstruction. The rest of many years are the severely deficient rain fall events when compared to the mean monthly rainfall in wet period during 1986-2004 year AD at study area.

The values of $\delta^{18}O$, $\delta^{13}C$ and rainfall are plotted against the time series can be used for anticipation roughly of the trend of those three parameters in the future. The trend can forecast that the values $\delta^{18}O$ in the next 600 year will decrease (the year 2116- 2716 AD). The next 350-400 years in the future the trend of the $\delta^{13}C$ will be increase (the year 2154- 2524 AD). Finally, the trend can forecast that the rainfall in the next 600 year will increase (the year 2137- 2736 AD).

5.2 Recommendations

1 Future studies should carefully choose the suitable cave that has high humidity because if low humidity in the cave, the precipitation of mineral in stalagmite will not be in equilibrium with the stable isotopes.

2 The type of parent rock, the result from XRD technique was confirmed by XRF technique hence future study should only one technique to investigate for reduce budget.

3 The study of the variation in $\delta^{18}O$ and $\delta^{13}C$ in the same layer in stalagmite should be considered in order to indicated the isotopic equilibrium.

4 The similar equipment for dating technique should be used on the individual stalagmite in order to increase the precision.

5 Multi-proxy studies should be undertaken on individual speleothems (e.g. combining stable isotopes with trace elements, petrographic information and growth-rate information). These approaches help narrow the uncertainties associated with the interpretation of stable isotope data from individual speleothems.

6 Finally, studies should include more systematic seasonal monitoring of present-day precipitation and cave drip-waters. It is essential to provide constraints on the O isotopic composition of cave drip-waters to assess seasonal biases in speleothems deposition rates, to investigate the extent to which drip-waters reflect the weighted mean $\delta^{18}O$ value of precipitation and to understand better the factors that control the $\delta^{13}C$ of the DIC.

REFERENCES

[1] Bradley RS. Paleoclimatology: Reconstructing Climates of the Quaternary. 2nd ed. San Diego: Academic Press; 1999.

[2] Bradley RS and Eddy JA. Records of past global changes. In: Bradley RS, editor. Global Changes of the Past. University Corporation for Atmospheric Research; 1991. p. 5-9.

[3] Mickler PJ, Ketcham RA, Colbert MW and Banner JL. Application of high-resolution X-ray computed tomography in determining the suitability of speleothems for use in paleoclimatic, paleohydrologic reconstructions. Journal of Cave and Karst Studies. 2004; 66(1): 4-8.

[4] Hendy CH and Wilson AT. Palaeoclimatic data from speleothems. Nature. 1968; 219(5147): 48–51.

[5] Leng MJ and Marshall JD. Palaeoclimate interpretation of stable isotope data from lake sediment archives. Quaternary Science Reviews. 2004; 23: 811–831.

[6] Johnson KR, Ingram BL, Sharp WD and Zhang P. East Asian summer monsoon variability during Marine Isotope Stage 5 based on speleothem $\delta^{18}O$ records from Wanxiang Cave, central China. Palaeo. 2006; 236: 5-19.

[7] Cruz FW, Burns SJ, Karmann I, Sharp WD, Vuille M and Ferrari JA. A stalagmite record of changes in atmospheric circulation and soil processes in the Brazilian subtropics during the Late Pleistocene. Quaternary Science Reviews. 2006; 25: 2749–2761.

[8] Yadava MG. Stable isotope systematics in cave calcites: Implications to past climatic changes in tropical India (Dissertation). Physical research laboratory, Navrangpura; 2002. 208p.

[9] Araguas AL, Froehlich K and Rozanski K. Stable isotope composition of precipitation over Southeast Asia. Geophysical Research. 1998; 102 (D22): 28721–28742.

[10] Alpha TR, Galloway JP and Tinsley III JC. Karst Topography: Computer animations and paper model. U.S. Geological survey; 1997.

[11] Jennings JN. Karst Geomorphology. Oxford: Basil Blackwell; 1985.

[12] Yuan D, Cheng H, Edwards RL, Dykoski CA, Kelly MJ, Zhang M, Qing J, Lin Y, Wang Y, Wu J, Dorale JA, An Z and Cai Y. Timing, duration, and transitions of the last interglacial Asian monsoon. Science. 2004; 304: 575-578.

[13] Bakalowicz M. Epikarst. In: Culver D and White W, editors. Encyclopedia of cave. Amsterdam, Netherlands: Academic Press; 2004. p. 220-222.

[14] Tooth AF. Controls on the geochemistry of speleothem-forming karstic drip waters (Dissertation). School of Earth Sciences and Geography, Keele University; 2000.

[15] Tucker ME. Sedimentary Petrology: An Introduction to the origin of Sedimentary Rocks. 3rd ed. Department of Geology science, University of Durham: Blackwell science; 2001.

[16] Gilluly J, Water AC and Woodford AO. Principles of Geology. 2nd ed. San Francisco: W.H. Freeman and company; 1959.

[17] Ford D and Williams P. Karst Hydrogeology and Geomorphology. England: John &Sons, Ltd ; 2007.

[18] Onac BP. Minerals. In: Culver D and White W, editors. Encyclopedia of cave. Amsterdam, Netherlands: Academic Press; 2004. p. 371-374.

[19] Klein C and Hurlbut CS. Manual of Mineralogy. 21st ed. USA: Ward's Natural Science; 1993.

[20] Carlson WD. The polymorphs of $CaCO_3$ and the Aragonite - Calcite Transformation. In: Reeder RJ, editor. Carbonates: Mineralogy and Chemistry. Mineralogical Society of America; 1983. p. 191–226.

[21] Hill CA. and Forti P. Cave Minerals of the World. 2nd ed. USA: National Speleological Society, Huntsville Alabama; 1997.

[22] Gilluly J, Water AC and Woodford AO. Principles of Geology. 4th ed. San Francisco: W.H. Freeman and company; 1975.

[23] Mcdermott F, Schwarcz H and Rowe PJ. Isotopes in Speleothems. In: Leng MJ. Editor. Isotopes in Palaeoenvironmental Research. Netherlands: Springer; 2005. p. 185-218.

[24] Dreybrodt W. Speleothem Doposition. In: Culver D and White W, editors. Encyclopedia of cave. Amsterdam, Netherlands: Academic Press; 2004. p. 543-548.

[25] Klimchouk AB, Ford DC, Palmer AN and Dreybrodt W. Speleogenesis: Evolution of Karst Aquifers. Huntsville, Alabama: National Speleological Society; 2000.

[26] Spötl C, Fairchild IJ and Tooth AF. Speleothem deposition in a dynamically ventilated cave, Obir Caves (Austrian Alps): Evidence from cave air and drip water monitoring. GCA. 2005; 69: 2451-2468.

[27] ไพศาล ศรีพิเศษ. ประติมากรรมธรรมชาติใต้พิภพ. ใน: สิทธิพงษ์ ดิลกวณิช, บรรณาธิการ. การประชุมวิชาการ เรื่อง ทรัพยากรถ้ำ; 4-5 สิงหาคา 2542; กรุงเทพ : สำนักงานกองทุนสนับสนุนการวิจัย; 2543. หน้า 20-26.

[28] White WB and Culver DC. Cave: Definition of. In: Culver D and White W, editors. Encyclopedia of cave. Amsterdam, Netherlands: Academic Press; 2004. p. 81-85.

[29] Holland HD, Kirsipu TV, Huebner JS and Oxburgh UM. On some aspects of the chemical evolution of cave water. Journal of Geology. 1964; 72: 36-67.

[30] Bögli A. Lakosung unde Karrenbilding. Zeitschrift fur Geomorphologie. In: Sweeting MM, editor. Karst geomorphology. Stroudsbrug PA: Hutchinson Ross; 1981. p. 64-89.

[31] Fairchild IJ, Frisia S, Borsato A and Tooth AF. Speleothems. In: Nash DJ and McLaren SJ, editors. Geochemical Sediments and Landscapes. Oxford: Blackwells; 2006. p. 1-21.

[32] Hendy CH. The isotopic geochemistry of speleothems: I. The calculation of the effects of different modes of formation on the isotopic composition of speleothems and their applicability as palaeoclimatic indicators. Geochimica et Cosmochimica Acta. 1971; 35: 801-824.

[33] Baldini J. Morphological and dimensional linkage between recently deposited speleothems and drip water from Browns Folly Mine, Wiltshire, England. Journal of Cave and Karst Studies. 2001; 63: 83-90.

[34] Moore GW. The growth of stalactites. National Speleological Society Bulletin. 1962; 24: 95-105.

[35] Huang Y, Fairchild IJ, Borsato A, Frisia S, Cassidy NJ, McDermott F and Hawkesworth CJ. Seasonal variations in Sr, Mg and P in modern speleothems (Grotta di Ernesto, Italy). Chemical Geology. 2001; 175: 429-448.

[36] Fairchild IJ, Baker A, Borsato A, Frisia S, Hinton RW, McDermott F. and Tooth AF. High-resolution, multiple-trace-element variation in speleothems. Journal of the Geological Society. 2001; 158: 831-841.

[37] Frisia S. Stalactites and Stalagmites. In: Culver D and White W, editors. Encyclopedia of cave. Amsterdam, Netherlands: Academic Press; 2004. p. 570-573.

[38] Folk RL. Some aspects of recrystallization in ancient limestones. In Pray LC and Murray RC, editors. Dolomitization and Limestone Diagenesis: SEPM Special Publication 13. 1965. p. 14-48.

[39] Tan M, Baker A, Genty D, Smith C, Esper J and Cai B. Applications of stalagmite laminae to paleoclimate reconstructions: comparison with dendrochronology/climatology. Quaternary Science Reviews. 2006; 1791: 1-15.

[40] Wang YJ, Cheng H, Edwards RL, An ZS, Wu JY, Shen CC and Shen JA. A High-resolution absolute-dated late Pleistocene monsoon record from Hulu Cave, China. Science. 2001; 294: 2345-2348.

[41] Clark ID and Frize P. Environmental Isotopes in Hydrogeology. New York: Lewis publishers; 1954.

[42] Wikipedia.org. [database on the Internet]. Environmental isotope. [cited 2007 Sep 20]. Available from: http://www.wikipedia.org

[43] Attendorn HG and Bowen RNC. Radioactive and Stable Isotope Geology. London: Chapman & Hall; 1997.

[44] McDermott F. Palaeo-climate reconstruction from stable isotope variations in speleothems: a review. Quaternary Science Reviews. 2004; 23: 901–918.

[45] Dreybrodt W. Processes in Karst Systems. Berlin: Springer-Verlag; 1988.

[46] Gentya D, Blamarta D, Ghalebb B, Plagnesc V, Caussed Ch, Bakalowicze M, Zouari K, Chkir N, Hellstrom J, Wainer K and Bourges F. Timing and dynamics of the last deglaciation from European and North African $\delta^{13}C$ stalagmite profiles-comparison with Chinese and South Hemisphere stalagmites. Quaternary Science Reviews. 2006: 1-25.

[47] Baldini JUL, McDermott F, Baker A, Baldini LM, Mattey DP and Railsback LB. Biomass effects on stalagmite growth and isotope ratios: A 20th century analogue from Wiltshire, England. Earth and Planetary Science Letters. 2005; 240: 486–494.

[48] Cruz JrFW, Burns SJ, Karmann I, Sharp WD, Vuille M and Ferrari JA. A stalagmite record of changes in atmospheric circulation and soil processes in the Brazilian subtropics during the Late Pleistocene. Quaternary Science Reviews. 2006; 25: 2749–2761.

[49] Richards DA and Dorale JA. Uranium-series chronology and environmental applications of speleothems, in Uranium-series Geochemistry (eds B. Bourdon, G.M. Henderson, C.C. Lundstrom and S.P. Turner). Review in Mineralogy and Geochemistry, 52, 407-61. 2003.

[50] Zhou J, Lundstrom CC, Fouke B, Panno S, Hackley K and Curry B. Geochemistry of speleothem records from southern Illinois: Development of (^{234}U)/(^{238}U) as a proxy for paleoprecipitation. Chemical Geology. 2005; 221: 1-20.

[51] Department of Mineral Resources. Limestone Resources Map of Thailand (1: 2,000,000). 1998.

[52] Natural Park, Wildlife and Plant Conservation Department. [database on the Internet]. Tham Pla - Namtok Pha Suea National Park. [cited 2007 Sep 20]. Available from: http://www.dnp.go.th/parkreserve/asp/style1/default.asp

[53] Thai Meteorological Department. [database on the Internet]. Average temperature and rainfall amount 30 year. [cited 2007 Sep 20]. Available from: http://www.tmd.go.th/province_stat.php

[54] Tan M, Liu TS, Hou J, Qin X, Zhang H and Li T. Cyclic rapid warming on centennial-scale revealed by a 2650-year stalagmite record of warm season temperature. Geophysical Research Letters. 2003; 30(12): 19-1-19-4.

[55] Phillips WmR. Mineral optics principles and techniques. San Francisco: W.H. freeman and company; 1971.

[56] Reed SJB. Electron microprobe analysis and scanning electron microscopy in geology. USA: University of Cambridge; 1996.

[57] Heywood VH. Scanning electron microscopy: Systematic and evolutionary applications. 4th ed. England: Department of Botany, University of Reading; 1970.

[58] Burgess J, Marten M and Taylor R. [database on the Internet]. Microcosmos. [cited 2007 Sep 20]. Available from: http://acept.la.asu.edu/PiN/rdg/elmicr/elmicr-sem.html

[59] Scintag Inc. [database on the Internet]. Basics of X-ray Diffraction. [cited 2007 Aug 20]. Available from: http://epswww.unm.edu/xrd/xrdbasics.pdf

[60] Palmiter J. [database on the Internet]. X-ray Diffraction (XRD). [cited 2007 Aug 20]. Available from: http://physics.pdx.edu/~pmoeck/phy381/Topic5a-XRD.pdf

[61] Cai B, Edwards RL, Cheng H, Tan M, Wang X and Liu T. A dry episode during the Younger Dryas and Centennial-scale weak monsoon events during the early Holocene: A High-Resolution Stalagmite Record from Southeast of the Loess Plateau, China. Geophysical Research Letters. 2008; 35, L02705.

[62] Dykoski CA, Edward RL, Cheng H, Yuan D, Cai Y, Zhang M, Lin Y, Qing J, An Z and Revenaugh. A high-resolution, absolute-date Holocene and deglacial Asian monsoon record from Dongge Cave, China. Earth and Planetary Science Letter. 2005; 233: 71-86.

[63] Esper J, Frank DC and Wilson RJS. Climate reconstructions-low frequency ambition and high frequency ratification. EOS. 2004; 85: 113-120.

[64] Chessin H and Hamilton WC. ACCRA9 (vol 18); 1965. p 689.

[65] Dickens B and Bowen JS. JNBAAR (vol 75); 1971. p 27.

[66] Allis-Chalmes Mfg. Co. Atomic Structure of Minerals.

[67] Rowling J. Cave Aragonites of New South Wales (Master degree Thesis). Faculty of Science, the University of Sydney; 2004. 303p.

[68] Siegel FR. and Reams MW. Temperature effect on precipitation of calcium carbonate from calcium bicarbonate solutions and its application to cavern environments. Journal of Sedimentology. 1966; 7:241–248.

[69] Frisia S, Borsato A, Fairchild IJ. and Longinelli A. Aragonite precipitation at Grotte de Clamouse (Herault, France): role of magnesium and drip rate. In Jeannin P-Y, editor. Physical Speleology: Proceedings of the 12th International Congress of Speleology (vol. 7). International Union of Speleology and Swiss Speleological Society; 1997. p. 247–250.

[70] Niggeman S, Habermann D, Oelze R. and Richter DK. Aragonitic / calcitic coralloids in carbonate caves: evidence for solutions of different Mg influence.In Jeannin P-Y, editor. Physical Speleology: Proceedings of the 12th International Congress of Speleology (vol. 7). International Union of Speleology and Swiss Speleological Society; 1997. p. 251–256.

[71] McDermott F. Palaeo-climate reconstruction from stable isotope variations in speleothems: a review. Quaternary Science Reviews. 2003; 23: 901-918.

[72] Rollinson H. Using geochemical data: evaluation, presentation, interpretation. Singapore: Longmar Singapore Publishers (Pte) Ltd. 1993.

[73] O’Neil JR, Clayton RN and Mayeda TK. Oxygen isotope fractionation of divalent metal carbonates. Journal of Chemical Physics. 1969; 30: 5547-5558.

[74] Dansgaard W. Stable isotopes in precipitation. Tellus. 1964; 16: 436-468.

[75] Yurtsever Y and Gat JR. Atmospheric waters. In Gat JR and Gonfiantini, editors. Stable Isotope Hydrology: Deuterium and Oxygen-18 in the Water Cycle, IAEA, Vienna. Techreport. 1981; 210: 103-142.

[76] International Atomic Energy Agency. [database on the Internet]. The global water cycle. [cited 2007 Oct 2]. Available from: www.iaea.or.at/Publications/Magazines/Bulletin/Bull432/article1.pdf

[77] Johnson KR and Ingram BL. Spatial and temporal variability in the stable isotope systematics of modern precipitation in China. Earth and Planetary Science Letters. 2004; 220: 365-377.

[78] Allan and Matthews RK. Isotopes signatures associated with early meteoric diagenesis. Sedimentology. 1982; 29: 797-817.

[79] นาฏสุดา ภูมิจำนงค์. รายงานฉบับสมบูรณ์โครงการบ่งบอกสภาพภูมิอากาศอย่างชัดเจนโดยใช้วงปีไม้ในประเทศไทย. สำนักงานกองทุนสนับสนุนการวิจัย.2548.

APPENDIX

APPENDIX A

Methodology of CaO convert to $CaCO_3$

Atomic mass; Ca = 40.078

Mg = 24.3050

O = 15.9994

C = 12.0107

Molecular mass; $MgO = 24.3050 + 15.9994$

$= 40.3044$

$CaMg(CO_3)_2 = 40.078 + 24.3050 + [12.0107 + (15.9994 \text{ x } 3)]_2$

$= 184.4008$

This study contains 3.93%MgO which is converted to $CaMg(CO_3)_2$ by;

$$CaMg(CO_3)_2 = \frac{3.93 \text{ x } 184.4008}{40.3044}$$

$$= 17.98\%$$

APPENDIX B

The result from counting the layers of growth of stalagmite NJ1 by Tree-ring width measurements (TSAP. version 3.2)

Period	Range	Distance (mm)	Left	Middle	Right	Average
1	Top to NJ1-8	8	20	28	36	28
2	NJ1-8 to NJ1-166	158	633	647	636	639
3	NJ1-166 to NJ1-388	222	855	795	825	825

APPENDIX C

Uranium and thorium isotopic compositions and ^{230}Th ages by TIMS (Australia)

Sample Name	**U (ppm)**	**±2σ**	**^{232}Th (ppb)**	**±2σ**	**^{230}Th/^{232}Th**	**^{230}Th/^{238}U**	**±2σ**	**^{234}U/ ^{238}U**	**±2σ**	**uncorr. ^{230}Th Age (ka)**	**±2σ**	**corr. ^{230}Th Age (ka)**	**±2σ**	**corr. Initial (^{234}U/ ^{238}U)**	**±2σ**
NJ1-8	1.4514	0.0022	10.929	0.087	2.111	0.0052	0.0001	2.6667	0.0030	0.214	0.004	0.130	0.042	2.6708	0.0034
NJ1-66	1.1651	0.0016	10.065	0.057	7.471	0.0213	0.0002	2.6543	0.0023	0.874	0.007	0.778	0.048	2.6618	0.0031

Note: As this sample contains a lot of non-radiogenic ^{230}Th (as reflected by ^{230}Th of 10 ppb), 70-90% of the age errors in the corrected ^{230}Th ages are related to the uncertainty in the assumption of non-radiogenic component for correction. Nevertheless, the 2-sigma errors of 42 and 48 years for samples of 130 and 780 years old are still quite acceptable. We use bulk-earth U/Th ratios for non-radiogenic ^{230}Th correction.

Uranium and thorium isotopic compositions and ^{230}Th ages by ICP-MS (USA)

Sample Name	**from top (mm)**	**Weight (g)**	**Spike (g)**	**^{238}U (ppb)**	**^{232}Th (ppt)**	**d^{234}U (measured)^{a}**	**d^{234}U (corr. initial)^{b}**	**[^{230}Th/^{238}U] (activity)^{c}**	**[^{230}Th/^{232}Th] (ppm)^{d}**	**Age (uncorrected)**	**Error**	**Age (corrected)$^{c, e}$**	**Error**	**Error %**
NJ1-388	388	0.0835	0.1021	1402.7	402.1	1384.5	1408.4	0.1298	7475.1	6,081	64	**6,075**	**±65**	1.1

APPENDIX D

The values of $\delta^{18}O$, $\delta^{13}C$ and data interpretation from stalagmite NJ1

From top (mm)	Age (BP)	Year (AD)	$\delta^{18}O$ (‰)	$\delta^{13}C$ (‰)	Rainfall (mm)	Vegetation
0	0	2006	0	0	0	C_3
1	16	1990	-4.92	-6.16	141.3682	C_3 or C_4
3	49	1953	-5.21	-6.40	149.9942	C_3 or C_4
5	81	1915	-4.67	-5.40	134.2625	C_3 or C_4
6	98	1897	-5.78	-7.17	167.3513	C_3
8*	130	1876	-5.41	-6.53	155.9446	C_3 or C_4
10	138	1868	-5.85	-6.76	169.439	C_3 or C_4
11	142	1864	-4.61	-5.17	132.5237	C_3 or C_4
13	151	1855	-5.19	-5.72	149.4777	C_3 or C_4
15	159	1847	-5.27	-6.30	151.8477	C_3 or C_4
16	163	1843	-5.53	-5.96	159.6299	C_3 or C_4
18	171	1835	-4.44	-4.43	127.6513	C_4
20	179	1827	-4.54	-4.37	130.5331	C_4
21	183	1823	-4.47	-5.13	128.5712	C_3 or C_4
23	192	1814	-3.94	-4.41	113.9563	C_4
25	200	1806	-4.24	-4.28	122.1195	C_4
26	204	1802	-4.33	-3.86	124.5827	C_4
28	212	1794	-4.49	-4.21	129.1532	C_4
30	220	1786	-5.15	-5.06	148.158	C_3 or C_4
31	224	1782	-5.76	-6.12	166.7628	C_3 or C_4
33	233	1773	-5.00	-5.04	143.8756	C_3 or C_4
35	241	1765	-5.32	-6.06	153.3099	C_3 or C_4
36	245	1761	-5.12	-5.51	147.1544	C_3 or C_4
38	253	1753	-4.16	-3.93	119.933	C_4
40	261	1745	-4.82	-5.09	138.4602	C_3 or C_4
41	265	1741	-5.02	-5.02	144.4567	C_3 or C_4
43	274	1732	-5.41	-6.25	155.9386	C_3 or C_4
45	282	1724	-5.89	-6.01	170.7679	C_3 or C_4
46	286	1720	-5.84	-6.74	169.2027	C_3 or C_4
48	294	1712	-6.11	-7.29	177.5554	C_3

The values of $\delta^{18}O$, $\delta^{13}C$ and data interpretation from stalagmite NJ1 (Continued)

From top (mm)	Age (BP)	Year (AD)	$\delta^{18}O$ (‰)	$\delta^{13}C$ (‰)	Rainfall (mm)	Vegetation
50	302	1704	-6.16	-6.53	179.299	C_3 or C_4
51	306	1700	-5.57	-5.93	160.913	C_3 or C_4
53	315	1691	-5.98	-6.57	173.4588	C_3 or C_4
56	327	1679	-5.57	-6.99	160.7421	C_3 or C_4
58	335	1671	-5.43	-6.34	156.6509	C_3 or C_4
61	347	1659	-5.54	-5.31	159.8217	C_3 or C_4
63	356	1650	-6.45	-7.16	188.4808	C_3
66	368	1638	-5.29	-5.16	152.4485	C_3 or C_4
68	376	1630	-5.53	-5.24	159.4669	C_3 or C_4
71	388	1618	-6.37	-6.68	186.0063	C_3 or C_4
73	397	1609	-5.01	-4.35	144.1535	C_4
76	409	1597	-5.89	-5.44	170.7184	C_3 or C_4
78	417	1589	-5.37	-5.48	154.8304	C_3 or C_4
81	429	1577	-5.05	-4.43	145.0897	C_4
83	438	1568	-3.95	-3.56	114.4208	C_4
86	450	1556	-5.03	-3.90	144.6617	C_4
88	458	1548	-5.69	-5.14	164.3042	C_3 or C_4
91	470	1536	-5.63	-5.74	162.5003	C_3 or C_4
93	479	1527	-4.62	-5.07	132.7631	C_3 or C_4
96	491	1515	-6.54	-6.12	191.4624	C_3 or C_4
98	499	1507	-5.41	-4.47	155.9657	C_4
101	511	1495	-5.87	-5.48	170.1845	C_3 or C_4
103	520	1486	-6.08	-5.89	176.7628	C_3 or C_4
106	532	1474	-4.67	-4.43	134.2743	C_4
108	540	1466	-5.36	-4.98	154.4276	C_3 or C_4
111	552	1454	-5.26	-4.79	151.3917	C_4
113	561	1445	-5.74	-5.77	165.9539	C_3 or C_4
116	573	1433	-5.67	-4.76	163.8907	C_4
118	581	1425	-5.10	-4.52	146.5752	C_4
121	593	1413	-4.97	-5.53	143.0128	C_3 or C_4

The values of $\delta^{18}O$, $\delta^{13}C$ and data interpretation from stalagmite NJ1 (Continued)

From top (mm)	Age (BP)	Year (AD)	$\delta^{18}O$ (‰)	$\delta^{13}C$ (‰)	Rainfall (mm)	Vegetation
123	602	1404	-5.59	-6.36	161.3389	C_3 or C_4
126	614	1392	-5.76	-6.89	166.6761	C_3 or C_4
128	622	1384	-6.10	-6.89	177.2065	C_3 or C_4
131	634	1372	-5.66	-6.19	163.6663	C_3 or C_4
133	643	1363	-5.27	-5.54	151.8583	C_3 or C_4
136	655	1351	-5.10	-5.45	146.5709	C_3 or C_4
138	663	1343	-5.33	-4.94	153.5454	C_4
141	675	1331	-5.22	-5.15	150.1534	C_3 or C_4
143	684	1322	-5.96	-5.73	172.8023	C_3 or C_4
146	696	1310	-5.11	-5.50	147.0225	C_3 or C_4
148	704	1302	-5.58	-6.01	161.125	C_3 or C_4
151	716	1290	-4.66	-4.48	134.0045	C_4
153	725	1281	-4.66	-4.76	133.82	C_4
156	737	1269	-4.91	-5.68	140.9857	C_3 or C_4
158	745	1261	-4.61	-4.98	132.5265	C_3 or C_4
161	757	1249	-5.15	-6.21	148.0853	C_3 or C_4
163	766	1240	-4.33	-4.66	124.7518	C_4
166*	778	1228	-5.16	-6.15	148.381	C_3 or C_4
168	786	1220	-5.26	-6.04	151.3052	C_3 or C_4
171	798	1208	-5.39	-6.01	155.4498	C_3 or C_4
173	806	1200	-4.72	-5.03	135.5672	C_3 or C_4
176	818	1188	-5.60	-6.63	161.8398	C_3 or C_4
178	826	1180	-5.40	-6.07	155.5876	C_3 or C_4
181	838	1168	-4.69	-4.69	134.8367	C_4
183	846	1160	-5.26	-5.23	151.3112	C_3 or C_4
186	858	1148	-5.27	-5.78	151.8519	C_3 or C_4
188	866	1140	-5.37	-6.33	154.6457	C_3 or C_4
191	877	1129	-5.07	-5.51	145.8745	C_3 or C_4
193	885	1121	-4.85	-5.56	139.4821	C_3 or C_4
196	897	1109	-4.57	-4.65	131.2538	C_4

The values of $\delta^{18}O$, $\delta^{13}C$ and data interpretation from stalagmite NJ1 (Continued)

From top (mm)	Age (BP)	Year (AD)	$\delta^{18}O$ (‰)	$\delta^{13}C$ (‰)	Rainfall (mm)	Vegetation
198	905	1101	-4.53	-4.57	130.1897	C_4
201	917	1089	-4.87	-4.50	139.8617	C_4
203	925	1081	-4.44	-3.52	127.8291	C_4
206	937	1069	-5.75	-6.62	166.3212	C_3 or C_4
208	945	1061	-5.58	-5.81	160.9649	C_3 or C_4
211	957	1049	-5.16	-5.14	148.3751	C_3 or C_4
213	965	1041	-5.48	-5.73	158.1446	C_3 or C_4
216	977	1029	-5.65	-6.67	163.0715	C_3 or C_4
218	985	1021	-5.52	-6.49	159.271	C_3 or C_4
221	997	1009	-5.03	-4.78	144.6478	C_4
223	1005	1001	-5.31	-5.37	152.9241	C_3 or C_4
226	1017	989	-5.39	-5.58	155.4017	C_3 or C_4
228	1025	981	-4.33	-3.62	124.7684	C_4
231	1037	969	-4.60	-4.40	132.3204	C_4
233	1044	962	-5.50	-6.00	158.7849	C_3 or C_4
236	1056	950	-5.46	-5.54	157.5152	C_3 or C_4
238	1064	942	-4.61	-4.68	132.552	C_4
241	1076	930	-5.57	-5.86	160.6819	C_3 or C_4
243	1084	922	-4.74	-4.73	136.1509	C_4
246	1096	910	-5.45	-6.38	156.9949	C_3 or C_4
248	1104	902	-4.96	-4.53	142.4764	C_4
251	1116	890	-5.04	-4.51	144.8911	C_4
253	1124	882	-5.18	-5.00	148.9487	C_3 or C_4
256	1136	870	-5.15	-5.26	148.2509	C_3 or C_4
258	1144	862	-5.54	-6.03	159.9739	C_3 or C_4
261	1156	850	-5.42	-5.24	156.0919	C_3 or C_4
263	1164	842	-5.30	-5.46	152.5471	C_3 or C_4
266	1176	830	-5.85	-6.23	169.2721	C_3 or C_4
268	1184	822	-4.99	-4.58	143.5354	C_4
271	1196	810	-4.36	-4.14	125.4853	C_4

The values of $\delta^{18}O$, $\delta^{13}C$ and data interpretation from stalagmite NJ1 (Continued)

From top (mm)	Age (BP)	Year (AD)	$\delta^{18}O$ (‰)	$\delta^{13}C$ (‰)	Rainfall (mm)	Vegetation
273	1204	802	-4.37	-4.26	125.8376	C_4
276	1216	790	-4.39	-4.04	126.4229	C_4
278	1223	783	-4.37	-3.92	125.9154	C_4
281	1235	771	-4.50	-3.81	129.355	C_4
283	1243	763	-4.89	-4.69	140.4225	C_4
286	1255	751	-4.40	-4.13	126.6904	C_4
288	1263	743	-4.50	-4.43	129.3121	C_4
291	1275	731	-5.32	-5.53	153.2842	C_3 or C_4
293	1283	723	-5.61	-6.13	162.148085	C_3 or C_4
296	1295	711	-5.58	-6.04	161.1062	C_3 or C_4
298	1303	703	-6.09	-6.83	177.0656	C_3 or C_4
301	1315	691	-5.57	-5.07	160.7429	C_3 or C_4
303	1323	683	-5.08	-4.73	145.9619	C_4
306	1335	671	-4.94	-4.08	142.1074	C_4
308	1343	663	-4.25	-3.43	122.4227	C_4
311	1355	651	-5.00	-4.43	143.6939	C_4
313	1363	643	-4.99	-4.68	143.4185	C_4
316	1375	631	-3.75	-3.08	109.1046	C_4
318	1383	623	-4.80	-4.89	137.9911	C_4
321	1395	611	-6.00	-7.21	174.0025	C_3
323	1402	604	-5.39	-6.70	155.3398	C_3 or C_4
326	1414	592	-5.95	-6.92	172.513	C_3 or C_4
328	1422	584	-4.88	-5.17	140.3927	C_3 or C_4
331	1434	572	-5.91	-6.79	171.3633	C_3 or C_4
333	1442	564	-6.21	-7.69	180.7534	C_3
336	1454	552	-5.92	-6.74	171.5197	C_3 or C_4
338	1462	544	-5.24	-5.58	150.8427	C_3 or C_4
341	1474	532	-6.04	-6.92	175.3171	C_3 or C_4
343	1482	524	-5.58	-6.94	160.9457	C_3 or C_4
346	1494	512	-6.09	-7.20	177.0538	C_3

The values of $\delta^{18}O$, $\delta^{13}C$ and data interpretation from stalagmite NJ1 (Continued)

From top (mm)	Age (BP)	Year (AD)	$\delta^{18}O$ (‰)	$\delta^{13}C$ (‰)	Rainfall (mm)	Vegetation
348	1502	504	-5.84	-6.29	169.0556	C_3 or C_4
351	1514	492	-5.54	-6.00	159.8042	C_3 or C_4
353	1522	484	-5.76	-6.11	166.734	C_3 or C_4
356	1534	472	-5.28	-5.43	151.9205	C_3 or C_4
358	1542	464	-4.65	-4.62	133.6103	C_4
361	1554	452	-6.07	-6.53	176.4045	C_3 or C_4
363	1562	444	-5.61	-6.14	161.9085	C_3 or C_4
366	1573	433	-5.13	-4.52	147.6864	C_4
368	1581	425	-5.50	-6.05	158.702	C_3 or C_4
371	1593	413	-6.12	-7.02	177.9898	C_3 or C_4
373	1601	405	-5.71	-5.75	165.0012	C_3 or C_4
376	1613	393	-5.45	-4.97	157.013	C_3 or C_4
378	1621	385	-4.70	-4.08	135.0092	C_4
381	1633	373	-5.34	-5.77	153.7937	C_3 or C_4
383	1641	365	-4.53	-3.68	130.3917	C_4
386	1653	353	-5.34	-5.58	153.6768	C_3 or C_4
388*	1661	345	-5.40	-5.58	155.7224	C_3 or C_4
391	1673	333	-4.88	-4.55	140.1395	C_4
393	1681	325	-5.53	-5.92	159.556	C_3 or C_4
396	1693	313	-5.75	-5.21	166.213	C_3 or C_4
398	1701	305	-6.95	-7.43	205.1372	C_3

* The point is dating

Note The range of $\delta^{13}C$ more than-4.95‰ means C_4, the range between -4.95 and -7.05‰ means C_4 or C_3 and less than-7.05‰ means C_3

APPENDIX E

Statistical treatment of GNIP data at Bangkok (Copyright IAEA)

(Lat: 13.73, Long :100.5, Altitude: 2)

period		H_2	^{18}O	precipitation	air-temp	vapor pressure
from	to					
1/1/1968	1/31/1968			9	26.1	25.2
2/1/1968	2/29/1968			29	27.6	28.4
3/1/1968	3/31/1968			34	29.2	31
4/1/1968	4/30/1968			89	30.3	33.2
5/1/1968	5/31/1968			166	29.8	34.4
6/1/1968	6/30/1968			171	28.9	32.2
7/1/1968	7/31/1968		-6.02	68	29.4	31.1
8/1/1968	8/31/1968	-47.4	-6.82	270	29.3	30.9
9/1/1968	9/30/1968	-60.7	-8.22	294	28.9	32.2
10/1/1968	10/31/1968	-49.7	-7.88	173	28.4	22.9
11/1/1968	11/30/1968	-9.3	-1.73	24	28.7	21.9
12/1/1968	12/31/1968			0	28.6	21.2
1/1/1969	1/31/1969	-46.3	-6.33	39	28.3	21.9
2/1/1969	2/28/1969			0	28.6	21.5
3/1/1969	3/31/1969	21.7	3.79	15	30.2	24.9
4/1/1969	4/30/1969			0	31	33.6
5/1/1969	5/31/1969	-20.8	-3.38	69	30.6	35.3
6/1/1969	6/30/1969	-28.7	-4.76	280	29.5	34.2
7/1/1969	7/31/1969	-24.4		78	28.7	32.3
8/1/1969	8/31/1969	-54	-6.69	96	28.6	33
9/1/1969	9/30/1969	-54	-8.25	304	28.2	33.5
10/1/1969	10/31/1969	-35.9	-6.27	159	28.6	32.8
11/1/1969	11/30/1969	-32.9	-5.63	94	26.6	27.7
12/1/1969	12/31/1969			2	25.1	23
1/1/1970	1/31/1970			1	27.2	27.3
2/1/1970	2/28/1970	1.4	-0.56	68	27.7	30.2
3/1/1970	3/31/1970	-9.9	-1.52	45	29.4	34.5
4/1/1970	4/30/1970	-17.3	-3.35	158	29.7	34.2
5/1/1970	5/31/1970	-36.8	-5.78	283	30.7	37.5
6/1/1970	6/30/1970	-46.9	-6.61	301	29.2	33
7/1/1970	7/31/1970	-48	-7.25	189	28.6	31.4
8/1/1970	8/31/1970	-46.3	-6.94	144	28.4	32.1
9/1/1970	9/30/1970	-58.2	-8.82	355	28.7	33.4
10/1/1970	10/31/1970	-66.6	-10.17	187	27.9	30.9
11/1/1970	11/30/1970	-29.4	-5.46	50	27.2	28.2
12/1/1970	12/31/1970	-46.7	-6.29	103	26.5	28.7
1/1/1971	1/31/1971			0	24.8	24.6
2/1/1971	2/28/1971		-0.02	28	26.8	28.4
3/1/1971	3/31/1971		1.64	11	28.6	31.1
4/1/1971	4/30/1971		0.33	31	29.7	33.5
5/1/1971	5/31/1971		-4.38	236	29.3	33.4

Statistical treatment of GNIP data at Bangkok (Continued)

---

period		H_2	^{18}O	precipi tation	air- temp	vapor pressure
from	to					
6/1/1971	6/30/1971		-2.39	82	28.8	31.7
7/1/1971	7/31/1971		-5.91	179	28.3	30.9
8/1/1971	8/31/1971		-9.18	352	28.2	31.1
9/1/1971	9/30/1971		-9.18	383	28.6	31.9
10/1/1971	10/31/1971		-10.17	177	27.7	29.9
11/1/1971	11/30/1971			3	25.5	23.5
12/1/1971	12/31/1971			1	26.1	25.6
1/1/1972	1/31/1972			0	25.3	22.5
2/1/1972	2/29/1972		3.88	20	27.9	29.2
3/1/1972	3/31/1972		-0.36	17	28.1	29.2
4/1/1972	4/30/1972		-5.95	147	29.1	32.6
5/1/1972	5/31/1972		-4.84	55	30.8	32.7
6/1/1972	6/30/1972			128	29.2	32.4
7/1/1972	7/31/1972		-4.33	70	29.2	32.3
8/1/1972	8/31/1972		-4.49	157	28.7	30.9
9/1/1972	9/30/1972		-9.1	676	28.4	32.4
10/1/1972	10/31/1972		-7.46	238	28.8	32.5
11/1/1972	11/30/1972			88	28.1	31.6
12/1/1972	12/31/1972	-29.9	-5.09	55	26.7	27.5
1/1/1973	1/31/1973			0	26.9	26.2
2/1/1973	2/28/1973			0	29.1	30.1
3/1/1973	3/31/1973	-4	-1.47	103	29.5	32.4
4/1/1973	4/30/1973	12	0.55	6	31.2	34.6
5/1/1973	5/31/1973	-36.5	-6.06	158	29.8	33.4
6/1/1973	6/30/1973	-54.8	-8.19	132	29.5	32.5
7/1/1973	7/31/1973	-28.6	-4.06	68	29.4	31.6
8/1/1973	8/31/1973	-25.3	-3.69	97	29	31.6
9/1/1973	9/30/1973	-57.7	-7.99	365	28.3	32.3
10/1/1973	10/31/1973	-51.6	-7.68	114	28.1	30.7
11/1/1973	11/30/1973	-34.5	-4.93	37	26.2	25.9
12/1/1973	12/31/1973	7.9	0.46	11	24.2	21.1
1/1/1974	1/31/1974			1	25.2	24
2/1/1974	2/28/1974			0	26.9	26.1
3/1/1974	3/31/1974		3.46	10	28.6	29.6
4/1/1974	4/30/1974	-16.6	-3.25	130	28.5	31
5/1/1974	5/31/1974	-35	-5.35	179	28.4	31.3
6/1/1974	6/30/1974	-27.6	-4.83	82	28.3	30.1
7/1/1974	7/31/1974	-41.7	-5.95	130	28.1	29.7
8/1/1974	8/31/1974	-47.9	-6.96	161	27.9	30.4
9/1/1974	9/30/1974	-67.3	-9.38	220	28.1	30.8
10/1/1974	10/31/1974	-58.3	-8.89	470	27.3	31.3
11/1/1974	11/30/1974	-57	-8.52	135	26.2	27.6
12/1/1974	12/31/1974			0	26.2	25.5
1/1/1975	1/31/1975	-20.9	-3.61	38	25.7	26.1
2/1/1975	2/28/1975			1	27.6	28.4

Statistical treatment of GNIP data at Bangkok (Continued)

period		H_2	^{18}O	precipitation	air-temp	vapor pressure
from	to					
3/1/1975	3/31/1975	-9.1	-2.62	32	29.1	32.7
4/1/1975	4/30/1975			4	30.1	33
5/1/1975	5/31/1975	-42.6	-6.68	186	28.7	31.7
6/1/1975	6/30/1975	-27.4	-4.3	101	28.3	30.5
7/1/1975	7/31/1975	-37.6	-5.89	175	28.1	30.1
8/1/1975	8/31/1975	-43.3	-6.77	324	27.8	30.1
9/1/1975	9/30/1975	-76.8	-11.21	212	27.6	32
10/1/1975	10/31/1975	-75.4	-10.72	262	28.1	31.7
11/1/1975	11/30/1975	-23.6	-3.88	35	26.9	27.1
12/1/1975	12/31/1975	-5.1	-1.15	9	23.7	20.1
1/1/1976	1/31/1976			0	23.8	19.6
2/1/1976	2/29/1976	2.1	-1.54	52	26.6	27.6
3/1/1976	3/31/1976			2	28.2	29.1
4/1/1976	4/30/1976	-32.5	-5	53	30	30.9
5/1/1976	5/31/1976	-30.3	-4.4	410	28.2	30.5
6/1/1976	6/30/1976	-17	-3.54	73	29	29.3
7/1/1976	7/31/1976	-37.4	-5.5	284	28.1	29.7
8/1/1976	8/31/1976	-66.1	-8.43	248	27.7	30.1
9/1/1976	9/30/1976	-76.1	-10.26	297	27.9	30
10/1/1976	10/31/1976	-46.1	-7.21	199	27.8	30.6
11/1/1976	11/30/1976	1.7	-0.58	17	25.9	25.5
12/1/1976	12/31/1976			0	26.1	24.1
1/1/1977	1/31/1977		-1.65	27	26.6	25.3
2/1/1977	2/28/1977		0.7	26	26.6	23.7
3/1/1977	3/31/1977		-0.67	4	27.6	27.6
4/1/1977	4/30/1977		-0.03	28	29.6	31.5
5/1/1977	5/31/1977		-2.95	101	29.3	30.8
6/1/1977	6/30/1977		-4.29	61	29.8	30.7
7/1/1977	7/31/1977		-4.97	113	28.8	29.9
8/1/1977	8/31/1977		-5.1	121	28.5	29.1
9/1/1977	9/30/1977		-5.58	359	27.9	29.8
10/1/1977	10/31/1977		-5.2	138	28.4	30.6
11/1/1977	11/30/1977		-3.02	61	26.6	25.1
12/1/1977	12/31/1977		1.55	4	26.4	24.2
1/1/1978	1/31/1978	10.3	0.06	24	27	26.4
2/1/1978	2/28/1978	-2.9	-2.17	104	26.9	27.5
3/1/1978	3/31/1978			1	29.5	31.1
4/1/1978	4/30/1978	9.1	-0.92	13	30.4	31.9
5/1/1978	5/31/1978	-24.9	-4.77	245	29	31.7
6/1/1978	6/30/1978	-35.3	-6.21	255	28.8	31.7
7/1/1978	7/31/1978	-36.4	-6.14	135	28.4	30.7
8/1/1978	8/31/1978	-35.3	-5.48	82	28.3	29.4
9/1/1978	9/30/1978	-61.3	-9.24	275	27.6	30.4
10/1/1978	10/31/1978		-7.5	103	28	29.3
11/1/1978	11/30/1978			1	27.4	26.7
12/1/1978	12/31/1978			0	26.4	23

Statistical treatment of GNIP data at Bangkok (Continued)

period		H_2	^{18}O	precipi tation	air- temp	vapor pressure
from	to					
1/1/1979	1/31/1979	2.1	-0.67	37	27.7	27.9
2/1/1979	2/28/1979	-1.8	-1.35	7	28.5	29.4
3/1/1979	3/31/1979			0	29.8	31.2
4/1/1979	4/30/1979	-40.7	-5.42	11	30.3	31
5/1/1979	5/31/1979	-21.1	-3.35	142	30	30.6
6/1/1979	6/30/1979	-33.7	-5.3	374	28.7	30.3
7/1/1979	7/31/1979	-30	-3.99	108	28.9	30.5
8/1/1979	8/31/1979	-18.7	-3.13	130	28.6	30.3
9/1/1979	9/30/1979	-60.2	-8.83	296	28.5	31.6
10/1/1979	10/31/1979	-26.5	-4.22	22	28.1	27.9
11/1/1979	11/30/1979	10.2	1.58	13	26.7	24
12/1/1979	12/31/1979			0	26	23.2
1/1/1980	1/31/1980			0	26.8	24.8
2/1/1980	2/29/1980			0	28.1	26.9
3/1/1980	3/31/1980			4	30.5	32.6
4/1/1980	4/30/1980	-9.5	-2.11	53	30.8	32.7
5/1/1980	5/31/1980	-11.2	-2.08	30	31	32.5
6/1/1980	6/30/1980	-47	-6.76	251	28.5	30.9
7/1/1980	7/31/1980	-34.1	-4.81	206	28.8	30.5
8/1/1980	8/31/1980	-43.7	-6.24	201	28.4	29.5
9/1/1980	9/30/1980	-47.8	-7.27	352	28	30.2
10/1/1980	10/31/1980	-42.6	-6.5	328	27.8	30.6
11/1/1980	11/30/1980	-30.7	-5	40	27.4	27.4
12/1/1980	12/31/1980			0	26.7	24.3
1/1/1981	1/31/1981			0	25.5	22.2
2/1/1981	2/28/1981	8.7	0.99	11	27.5	27.2
3/1/1981	3/31/1981	27.7	3.24	17	29.2	30.4
4/1/1981	4/30/1981	-22.8	-4.03	154	29.6	31.1
5/1/1981	5/31/1981	-42.8	-7.3	402	28.9	31.9
6/1/1981	6/30/1981	-13.5		115	28.7	30.8
7/1/1981	7/31/1981	-34.3		158	28.5	30.3
8/1/1981	8/31/1981	-26.8	-4.12	144	28.2	29.8
9/1/1981	9/30/1981	-57.8		178	28.1	30.4
10/1/1981	10/31/1981	-51.5		258	27.9	29.8
11/1/1981	11/30/1981	-39.8	-6.18	156	26.7	28
12/1/1981	12/31/1981			0	24.4	20.7
1/1/1982	1/31/1982			0	25.5	22.2
2/1/1982	2/28/1982	0.2	-0.57	20	28	28.9
3/1/1982	3/31/1982	-27	-4.42	176	28.9	30.4
4/1/1982	4/30/1982	-21.1	-3.66	223	29.2	30.3
5/1/1982	5/31/1982	-30.7	-5.46	236	29.8	32.1
6/1/1982	6/30/1982	-27.1	-3.98	188	28.6	30.6
7/1/1982	7/31/1982	-34.4	-5.15	199	28.3	29.9
8/1/1982	8/31/1982	-29.4	-3.73	221	27.8	29.6
9/1/1982	9/30/1982	-43.4	-6.18	255	27.7	30.2
10/1/1982	10/31/1982	-31.5	-5.55			

Statistical treatment of GNIP data at Bangkok (Continued)

period		H_2	^{18}O	precipi tation	air-temp	vapor pressure
from	to					
11/1/1982	11/30/1982	-20.6	-3.95			
12/1/1982	12/31/1982	-12.8	-3.11			
1/1/1983	1/31/1983					
12/1/1982	12/31/1982	-12.8	-3.11			
1/1/1983	1/31/1983					
2/1/1983	2/28/1983					
3/1/1983	3/31/1983	16.8	0.97			
4/1/1983	4/30/1983			0	30.8	32.7
5/1/1983	5/31/1983	-15.6	-3.37	48	30.7	31.8
6/1/1983	6/30/1983	-30.9	-5.32	161	29.5	31.3
7/1/1983	7/31/1983	-43.9	-6.51	230	29.6	31.9
8/1/1983	8/31/1983	-59.5	-8.2	529	28.1	31.1
9/1/1983	9/30/1983	-69.3	-9.75	485	27.8	31.1
10/1/1983	10/31/1983	-70.5	-9.7			
11/1/1983	11/30/1983	-56.5	-8.42			
12/1/1983	12/31/1983	-7.6	-2.13			
1/1/1984	1/31/1984			1	25.5	23.4
2/1/1984	2/29/1984	-19.1	-3.64	13	28.2	28
3/1/1984	3/31/1984		-6.13	34	28.9	29
4/1/1984	4/30/1984	-53.3	-7.83	53	30.2	31.7
5/1/1984	5/31/1984	-18.8	-3.96	184	29.8	31.1
6/1/1984	6/30/1984	-46.3	-7.03	131	28.6	29.7
7/1/1984	7/31/1984	-56.3	-8.22	240	28.4	29.6
8/1/1984	8/31/1984	-10.3	-2.2	93	28.6	28.6
9/1/1984	9/30/1984	-59.5	-8.69	315	27.7	29.9
10/1/1984	10/31/1984	-67.6	-9.87	309	27.3	28.5
11/1/1984	11/30/1984	-19.7	-3.25	26	27.4	26.4
12/1/1984	12/31/1984			0	26.3	23.5
1/1/1985	1/31/1985	-21.4	-3.93	19	27	25.7
2/1/1985	2/28/1985	-5.3	-1.83	1	28.7	29
3/1/1985	3/31/1985	-15.4	-3.35	17	29.5	29
4/1/1985	4/30/1985	-6.6	-2.35	61	29.9	30.5
5/1/1985	5/31/1985	-19	-4.92	174	29	30.9
6/1/1985	6/30/1985	-19.4	-3.45	90	28.7	29.2
7/1/1985	7/31/1985	-39.4	-5.97	143	27.8	28.2
8/1/1985	8/31/1985	-31.8	-4.95	135	28.3	28.7
9/1/1985	9/30/1985	-53.5	-7.82	338	27.6	29.3
10/1/1985	10/31/1985	-63.4	-8.55	376	27.3	29.3
11/1/1985	11/30/1985	-24	-4	17	28.6	29.4
12/1/1985	12/31/1985			0	25.7	21.1
1/1/1986	1/31/1986			0	25	20.1
2/1/1986	2/28/1986	2.8	-0.97	6	27.2	26.1
3/1/1986	3/31/1986			0	28	25.3
4/1/1986	4/30/1986	-12.5	-2.36	36	29.8	29.7
5/1/1986	5/31/1986	-67.2	-9.84	504	29.1	29.6
6/1/1986	6/30/1986	-39.5	-5.55	72	29.3	29.5

Statistical treatment of GNIP data at Bangkok (Continued)

period		H_2	^{18}O	precipi tation	air- temp	vapor pressure
from	to					
7/1/1986	7/31/1986	-23.5	-3.32	155	28.1	28.8
8/1/1986	8/31/1986	-39.6	-5.02	202	28.4	28.4
9/1/1986	9/30/1986	-44	-6.13	358	28.2	28.9
10/1/1986	10/31/1986	-63	-9.06	322	27.7	30.1
9/1/1986	9/30/1986	-44	-6.13	358	28.2	28.9
10/1/1986	10/31/1986	-63	-9.06	322	27.7	30.1
11/1/1986	11/30/1986	-43.2	-5.83	134	27.1	25.4
12/1/1986	12/31/1986	-41	-6.01	10	25.9	23.4
1/1/1987	1/31/1987			1	26.4	21.8
2/1/1987	2/28/1987			0	27.6	25.7
3/1/1987	3/31/1987	-15.5	-3.16	41	28.9	27.4
4/1/1987	4/30/1987	-6.3	-2.2	54	30.2	29.8
5/1/1987	5/31/1987	-18.8	-3.77	146	30	31.1
6/1/1987	6/30/1987	-44.2	-6.52	286	29.5	31.1
7/1/1987	7/31/1987	-10.9	-2.27	32	29.7	28.5
8/1/1987	8/31/1987	-45.2	-6.88	50	29.4	29.2
9/1/1987	9/30/1987	-59.5	-8.79	434	28.2	30.3
10/1/1987	10/31/1987	-59.7	-8.99	217	28.6	31.2
11/1/1987	11/30/1987	-32.9	-5.71	111	28.5	30.5
12/1/1987	12/31/1987			0	24.5	19
1/1/1988	1/31/1988			0	27.1	23.2
2/1/1988	2/29/1988	-8.8	-2.39	96	28.1	28.1
3/1/1988	3/31/1988	-47.2	-7.12	3	30.1	29.9
4/1/1988	4/30/1988	-17.8	-4.45	139	29.9	31.2
5/1/1988	5/31/1988	-57.8	-8.6	394	28.8	31.2
6/1/1988	6/30/1988	-28.8	-4.81	100	29.1	29.2
7/1/1988	7/31/1988	-42	-6.62	180	22.8	29.5
8/1/1988	8/31/1988	-54.4	-8.72	315	28.2	30.3
9/1/1988	9/30/1988	-82.6	-11.77	488	28.3	30.9
10/1/1988	10/31/1988	-85.5	-12.21	381	27.4	28.9
11/1/1988	11/30/1988			4	26	22
12/1/1988	12/31/1988			0	25.3	20.6
1/1/1989	1/31/1989	-15.1	-3	29	27.6	27.6
2/1/1989	2/28/1989	-60.4	-8.74	1	27.6	27.7
3/1/1989	3/31/1989	-15.1	-3.31	82	28.4	28.5
4/1/1989	4/30/1989	1.1	-1.52	2	30.9	29.8
5/1/1989	5/31/1989	-20.5	-4.21	178	29.7	29.6
6/1/1989	6/30/1989	-34	-5.14	80	28.9	28.1
7/1/1989	7/31/1989	-42.5	-6.19	177	28.8	28.7
8/1/1989	8/31/1989	-45.8	-6.29	181	28.5	28
9/1/1989	9/30/1989	-51.1	-7.36	410	28	29.3
10/1/1989	10/31/1989	-55.2	-7.73	316	27.7	29.6
11/1/1989	11/30/1989	-26.3	-3.64	34	27.3	24.9
12/1/1989	12/31/1989			0	20.7	15.5
1/1/1990	1/31/1990	-37.4	-4.19	1	27.7	25.9
2/1/1990	2/28/1990	-30.8	-3.49	1	28.5	27.6

Statistical treatment of GNIP data at Bangkok (Continued)

period		H_2	^{18}O	precipi tation	air- temp	vapor pressure
from	to					
3/1/1990	3/31/1990	-3	-1.83	51	29.1	28.4
4/1/1990	4/30/1990	-20.6	-3.61	16	30.7	28.6
5/1/1990	5/31/1990	-33.1	-5.06	220	29.6	30.4
6/1/1990	6/30/1990			59	29.5	28.8
7/1/1990	7/31/1990	-32.3	-5.06	160	28.5	28.1
8/1/1990	8/31/1990	-15	-3.13	173	28.8	28.2
9/1/1990	9/30/1990	-27.2	-4.79	257	28.1	29.2
10/1/1990	10/31/1990	-75.4	-10.7	402	27.7	29.1
11/1/1990	11/30/1990	-30.6	-5.38	23	27.2	25.9
12/1/1990	12/31/1990			0	26.5	22.4
1/1/1991	1/31/1991	3.5	-0.01	3	28.4	23.4
2/1/1991	2/28/1991	4.9	-1.07	7	28.5	21.7
3/1/1991	3/31/1991	4.8	-0.51	12	30.5	26.6
4/1/1991	4/30/1991	-12	-2.53	54	30.2	30.4
5/1/1991	5/31/1991	-43.3	-6.9	212	30.1	30.8
6/1/1991	6/30/1991	-13.7	-2.7	125	29.2	29.4
7/1/1991	7/31/1991	-35	-5.29	182	29	28.8
8/1/1991	8/31/1991	-35.9	-5.71	161	28.2	28.8
9/1/1991	9/30/1991	-45.5	-7.05	267	28.2	29.6
10/1/1991	10/31/1991	-32.3	-5.22	340	28.1	26.4
11/1/1991	11/30/1991	-32.4	-5.05	1	27.5	22.1
12/1/1991	12/31/1991			0	27.6	18
1/1/1992	1/31/1992			8	25.3	22.3
2/1/1992	2/29/1992			13	27.6	26.6
3/1/1992	3/31/1992				29.3	28.8
4/1/1992	4/30/1992			0	31.1	24.7
5/1/1992	5/31/1992	-29.6	-3.9	68	31.2	31.3
6/1/1992	6/30/1992	-57.7	-7.51	141	29.6	30.5
7/1/1992	7/31/1992	-56	-8.1	218	28.9	29.9
8/1/1992	8/31/1992	-30	-4.3	245	28.4	29.5
9/1/1992	9/30/1992	-30.1	-4.37	388	28.4	29.5
10/1/1992	10/31/1992	-52.4	-7.93	357	26.7	27.7
11/1/1992	11/30/1992			2	26.2	21.8
12/1/1992	12/31/1992			1	26.4	22.3
1/1/1993	1/31/1993			0	26.4	23.8
2/1/1993	2/28/1993			0	27	24.5
3/1/1993	3/31/1993	-33.8	-5.13	79	28.8	29.4
4/1/1993	4/30/1993	-33.2	-5.23	45	30	30.8
5/1/1993	5/31/1993	-37.2	-5.56	148	30.1	31.5
6/1/1993	6/30/1993	-42	-6.13	149	29.8	30.4
7/1/1993	7/31/1993	-40.4	-5.95	121	29.6	29.4
8/1/1993	8/31/1993	-30.9	-4.95	435	28	29.8
9/1/1993	9/30/1993	-34.9	-5.29	314	27.8	30
10/1/1993	10/31/1993	-53.2	-8.03	245	27.6	29
11/1/1993	11/30/1993			4	27.5	25
12/1/1993	12/31/1993			1	25.4	20

Statistical treatment of GNIP data at Bangkok (Continued)

period		H_2	^{18}O	precipi tation	air- temp	vapor pressure
from	to					
1/1/1994	1/31/1994			0	26.9	24.5
2/1/1994	2/28/1994			0	28.9	28.8
3/1/1994	3/31/1994	-45.5	-7.03	35	28.7	28.7
4/1/1994	4/30/1994	-7.2	-2.36	153	30.7	30.9
5/1/1994	5/31/1994	-16.5	-3.49	409	29.5	31.5
6/1/1994	6/30/1994	-38.3	-5.93	233	28.7	30.6
7/1/1994	7/31/1994	-21.5	-2.98	84	28.5	30
8/1/1994	8/31/1994	-42.5	-6.24	140	28	29.7
9/1/1994	9/30/1994	-51.1	-7.7	375	28.1	30.2
10/1/1994	10/31/1994	-40.7	-6.53	156	27.1	26.6
11/1/1994	11/30/1994	-3	-0.31	4	27.8	24.2
12/1/1994	12/31/1994	1.3	0.58	5	26.9	23.2
1/1/1995	1/31/1995			0	26.2	23.3
2/1/1995	2/28/1995			1	27.1	25.2
3/1/1995	3/31/1995	-23	-4.04	57	29.5	29.8
4/1/1995	4/30/1995	-21.4	-4.09	4	30.8	32.1
5/1/1995	5/31/1995	-23.4	-3.85	181	30.1	31.8
6/1/1995	6/30/1995	-33.8	-5.18	256	29.5	31.8
7/1/1995	7/31/1995	-42	-6.16	197	29.1	30.1
8/1/1995	8/31/1995	-66.7	-9.32	384	28.7	30.8
9/1/1995	9/30/1995	-66.5	-9.01	343	28.2	30.8
10/1/1995	10/31/1995	-72.7	-10.28	254	28.3	29.7
11/1/1995	11/30/1995			19	28.2	25.2
12/1/1995	12/31/1995			1	26.4	20.3
1/1/1996	1/31/1996			0	27.3	23.5
2/1/1996	2/29/1996			14	27.4	22.6
3/1/1996	3/31/1996			2	29.7	29.3
4/1/1996	4/30/1996	-55.6	-7.78	202	30.6	31
5/1/1996	5/31/1996	-9.2	-2.37	600	29.6	31
6/1/1996	6/30/1996	-34.8	-5.78	134	29.7	30.4
7/1/1996	7/31/1996	-34.1	-5.68	270	28.7	30
8/1/1996	8/31/1996	-61.2	-8.86	93	29.2	29.9
9/1/1996	9/30/1996	-82.6	-11.93	361	28	30.4
10/1/1996	10/31/1996	-76.4	-10.95	206	28.7	29.2
11/1/1996	11/30/1996	-26.1	-4.86	137	28.2	26.9
12/1/1996	12/31/1996			0	26.3	20.6
1/1/1997	1/31/1997			0	26.7	22.8
2/1/1997	2/28/1997			39	28.9	26.4
3/1/1997	3/31/1997			29	29.7	29.2
4/1/1997	4/30/1997			95	30.2	28.9
5/1/1997	5/31/1997	-12	-2.69	87	31.1	30
6/1/1997	6/30/1997	-11.5	-2.41	46	30.8	28.5
7/1/1997	7/31/1997	-32.8	-4.71	34	29.7	28.6
8/1/1997	8/31/1997	-24.7	-3.87	123	29.5	28.8
9/1/1997	9/30/1997	-39.2	-6.32	360	28.7	29.9
10/1/1997	10/31/1997	-46.3	-7.31	219	28.9	30

Statistical treatment of GNIP data at Bangkok (Continued)

period		H_2	^{18}O	precipitation	air-temp	vapor pressure
from	to					
11/1/1997	11/30/1997	-26.9	-4.65	32	29.1	27.7
12/1/1997	12/31/1997			0	29.1	25.9
1/1/1998	1/31/1998	-12.8	-2.95	45	29.1	28.1
2/1/1998	2/28/1998	-4.1	-1.66	33	30	32.3
3/1/1998	3/31/1998			1	30.8	31.9
4/1/1998	4/30/1998	0	-1.39	56	31.6	33.9
5/1/1998	5/31/1998	-26.8	-4.68	231	31.4	33.9
6/1/1998	6/30/1998	-54.9	-8.26	224	30.4	31.7
7/1/1998	7/31/1998	-58	-8.59	223	29.4	32.2
8/1/1998	8/31/1998	-57.9	-8.47	449	29.2	31.3
9/1/1998	9/30/1998	-64.5	-9.41	591	28.4	32.1
10/1/1998	10/31/1998	-69.1	-10.17	202	29	31.4
11/1/1998	11/30/1998	-46.6	-6.71	19	28.1	27.9
12/1/1998	12/31/1998			0	27.2	24.8
1/1/1999	1/31/1999	-23.9	-3.92	35	27.8	26.1
2/1/1999	2/28/1999	-28	-4.915	52	28.4	29.4
3/1/1999	3/31/1999	-37.1	-6.22	51	30.3	30.2
4/1/1999	4/30/1999	-49.6	-7.785	190	28.6	32.1
5/1/1999	5/31/1999	-48.9	-7.69	410	28.6	31.7
6/1/1999	6/30/1999	-30.8	-4.9	104	29.1	31
7/1/1999	7/31/1999	-30.1	-4.61	72	29.6	29.9
8/1/1999	8/31/1999	-54.8	-8.035	159	28.9	29.9
9/1/1999	9/30/1999	-46.6	-7.21	211	28.6	30.5
10/1/1999	10/31/1999	-83.7	-12.12	384	28	30
11/1/1999	11/30/1999	-63.5	-9.34	88	27.7	26.8
12/1/1999	12/31/1999	-50.2	-6.52	-1	24.5	17.9
1/1/2000	1/31/2000			0	28	25.1
2/1/2000	2/29/2000	-33.5	-5.09	40	28.1	25.4
3/1/2000	3/31/2000	-9.3	-3	44	29.7	28.8
4/1/2000	4/30/2000	-67.8	-9.99	198	29.5	32.2
5/1/2000	5/31/2000	-32	-5.18	270	29.9	31.4
6/1/2000	6/30/2000	-41.7	-6.31	263	28.9	30.8
7/1/2000	7/31/2000	-30.7	-5.02	226	28.8	29.9
8/1/2000	8/31/2000	-45.2	-6.78	253	28.9	29.8
9/1/2000	9/30/2000	-41.4	-6.47	215	28.5	30
10/1/2000	10/31/2000	-55.5	-8.33	359	28.4	31.1
11/1/2000	11/30/2000			0	27.9	23.9
12/1/2000	12/31/2000			4	28.5	24.3
1/1/2001	1/31/2001	-23.5	-4.26	10.8	27.3	28.7
2/1/2001	2/28/2001	-2.8	-1.56	9.4	28.1	29.2
3/1/2001	3/31/2001	-48.4	-7.4	175.1	30.7	29
4/1/2001	4/30/2001	-53.4	-8.44	28.7	33.5	31.6
5/1/2001	5/31/2001	-50.5	-7.74	256.6	31.4	29.4
6/1/2001	6/30/2001	-31.8	-5.05	102.2	30.1	29.5
7/1/2001	7/31/2001	-15	-3.04	61.6	30.2	29.8
8/1/2001	8/31/2001	-46	-6.83	148.9	29.3	29.2

Statistical treatment of GNIP data at Bangkok (Continued)

period		H_2	^{18}O	precipi tation	air- temp	vapor pressure
from	to					
9/1/2001	9/30/2001	-67.4	-9.74	450.2	31.6	29
10/1/2001	10/31/2001	-60.3	-9.04	385.5	31.4	28.1
11/1/2001	11/30/2001	-60.6	-9.09	37.3	23	26.9
12/1/2001	12/31/2001			4.3	23.5	27.4
1/1/2002	1/31/2002	-12.6	-3.21	0	27.4	23.8
2/1/2002	2/28/2002	-0.3	-1.98	53	29.1	30.6
3/1/2002	3/31/2002	-12.5	-2.67	44	29.6	30.6
4/1/2002	4/30/2002	-26.4	-4.77	9	31.2	32.1
5/1/2002	5/31/2002	-25.7	-4.51	229	29.8	32.3
6/1/2002	6/30/2002	-23.1	-4.1	82.2	29.8	32.6
7/1/2002	7/31/2002	-37.6	-5.6	86	29.9	32.8
8/1/2002	8/31/2002	-58.6	-8.56	123	28.9	29.5
9/1/2002	9/30/2002	-54.1	-8.12	208	28.6	29.4
10/1/2002	10/31/2002	-12.1	-5.76	346	28.6	29.7
11/1/2002	11/30/2002	-14.2	-3.05	136	28.3	28
12/1/2002	12/31/2002	-14.2	-3.04	54.1	28.7	27.6
1/1/2003	1/31/2003			0	27.4	24.7
2/1/2003	2/28/2003			0.7	29.1	28.1
3/1/2003	3/31/2003	-11.3	-2.95	134.6	29.4	30.6
4/1/2003	4/30/2003	-8.4	-2.69	12.3	31.4	32.1
5/1/2003	5/31/2003	-34.8	-5.81	158.8	30.6	30.8
6/1/2003	6/30/2003	-43.2	-6.97	168.6	29.9	30.1
7/1/2003	7/31/2003	-57.9	-8.75	240.7	29	31.3
8/1/2003	8/31/2003	-29.9	-4.91	315	29.4	30.7
9/1/2003	9/30/2003	-39.6	-6.3	205.8	28.2	30.1
10/1/2003	10/31/2003	-45.7	-7.31	121.8	29.1	29.7
11/1/2003	11/30/2003			0	29.8	26.3
12/1/2003	12/31/2003			0	27	20.6
1/1/2004	1/31/2004	-17.8	-3.56	46.4	27.8	25.5
2/1/2004	2/29/2004	-21.7	-4.55	73.9	27.9	27.1
3/1/2004	3/31/2004	-20.8	-4.2	3.5	30.2	30.9
4/1/2004	4/30/2004	-14.9	-3.44	91.1	31.9	32.4
5/1/2004	5/31/2004	-20.1	-3.96	94.9	30	31.6
6/1/2004	6/30/2004	-37.8	-5.86	167.4	29.4	30.7
7/1/2004	7/31/2004	-33.5	-2.34	177.2	29.7	29.8
8/1/2004	8/31/2004	-37.5	-6.29	235.5	29.1	29.7
9/1/2004	9/30/2004	-54.9	-8.6	214.7	28.9	30.4
10/1/2004	10/31/2004	-16.8	-2.94	50.1	29.8	27.3
11/1/2004	11/30/2004	-8.3	-1.12	5	29.9	25.2
12/1/2004	11/30/2004			0	27.3	20.1

APPENDIX F

Rainfall at Mae Hong Son and Pang Ma Pha station

Mae Hong Son station

Year / Month	JAN	FEB	MAR	APR	MAY	JUN	JUL	AUG	SEP	OCT	NOV	DEC
1911	72	0	0	33	78	243	234	209	110	174	0	0
1912	0	0	11	0	219	179	218	340	169	126	55	0
1913	0	0	0	0	103	196	206	208	185	100	92	15
1914	0	0	0	27	155	122	219	267	145	86	22	5
1915	0	0	0	48	136	211	242	315	85	89	0	71
1916	2	6	57	14	160	186	303	293	212	67	17	26
1917	19	0	0	0	118	155	201	297	218	149	0	23
1918	0	6	0	4	270	212	292	321	173	63	13	10
1919	0	14	0	0	224	176	247	320	131	16	188	0
1920	1	4	4	11	143	134	164	293	182	104	23	13
1921	0	0	18	80	155	68	301	291	183	92	98	0
1922	0	0	14	54	175	108	220	131	225	95	98	0
1923	4	0	0	238	127	130	146	322	70	104	31	0
1924	0	0	0	36	138	130	169	239	42	106	18	8
1925	12	0	0	29	92	149	242	90	238	40	3	0
1926	0	0	0	12	81	130	306	236	136	160	38	38
1927	0	39	0	7	267	138	269	122	133	141	20	0
1928	0	0	43	192	82	185	198	187	132	30	79	0
1929	0	21	0	129	139	149	194	305	268	98	8	2
1930	22	0	0	45	270	163	194	189	143	23	11	0
1931	0	26	0	0	66	76	154	333	279	15	0	26
1932	0	0	0	4	31	85	246	206	166	172	8	0
1933	20	0	0	30	222	137	337	240	101	175	4	0
1934	0	0	0	121	135	302	382	264	251	121	37	0
1935	0	0	0	0	230	211	242	214	322	138	0	51
1936	0	21	10	13	151	220	280	57	185	94	25	0
1937	5	24	16	51	260	199	316	293	251	173	22	119
1938	0	0	32	47	212	193	419	247	189	47	17	0
1939	0	0	0	0	160	101	370	332	305	83	0	0
1940	0	0	0	0	114	296	170	346	222	196	25	0
1941	0	13	0	27	104	313	273	201	214	63	15	0
1942	0	0	3	155	164	321	229	285	244	90	75	13
1943	0	9	7	78	227	209	235	263	330	1	45	0
1944	50	43	6	28	61	248	264	203	136	102	33	12
1945	9	4	7	47	165	182	231	252	203	9	0	6
1946	1	12	1	78	166	125	159	191	118	167	9	0
1947	26	5	4	107	124	263	176	303	348	91	0	0
1948	2	0	28	87	211	142	199	264	312	251	0	5
1949	0	0	0	138	100	135	241	280	329	190	45	0
1950	0	0	0	32	233	252	260	221	302	163	3	22

Mae Hong Son station (Continued)

Year / Month	JAN	FEB	MAR	APR	MAY	JUN	JUL	AUG	SEP	OCT	NOV	DEC
1951	69	0	1	5	115	190	172	239	248	209	21	3
1952	0	1	48	0	107	111	242	274	241	52	47	0
1953	57	0	0	76	157	230	177	263	292	88	33	12
1954	0	1	4	7	157	84	170	231	142	156	46	1
1955	0	0	19	111	157	257	183	185	304	11	42	0
1956	0	26	0	97	106	213	117	231	452	104	22	0
1957	0	2	0	102	150	220	261	338	196	45	7	0
1958	38	0	47	29	164	206	181	161	105	176	3	0
1959	24	2	0	50	167	127	454	467	315	30	1	0
1960	44	0	6	0	200	170	223	262	166	58	21	10
1961	1	1	8	95	224	186	220	279	327	71	3	42
1962	0	0	0	33	205	128	189	104	115	62	0	0
1963	0	0	1	64	110	219	193	310	113	148	48	7
1964	0	0	4	80	133	214	250	226	241	179	29	10
1965	0	17	5	28	160	216	241	190	170	287	5	16
1966	0	0	0	1	247	139	191	344	184	49	32	0
1967	8	0	2	57	149	198	186	314	304	75	95	1
1968	19	0	0	71	235	214	205	265	102	100	6	0
1969	0	0	0	38	252	176	181	340	187	158	22	10
1970	4	0	0	41	235	246	177	255	204	57	5	43
1971	0	0	22	52	255	216	200	343	213	111	20	7
1972	6	0	0	122	121	154	193	243	215	179	178	17
1973	0	0	33	6	184	312	281	601	231	53	18	0
1974	0	0	18	37	252	146	229	198	239	32	58	0
1975	57	0	0	0	150	204	156	334	289	84	0	49
1976	0	4	0	28	133	75	228	245	317	102	26	10
1977	70	0	14	83	154	135	223	244	329	337	3	63
1978	62	13	3	3	132	159	304	216	187	112	0	9
1979	0	0	0	27	110	133	109	158	226	87	0	0
1980	0	0	22	31	179	181	187	188	167	78	24	46
1981	3	2	1	30	246	158	436	190	129	71	76	1
1982	2	0	0	31	179	156	111	233	210	81	23	0
1983	0	0	0	31	44	167	110	275	232	157	74	9
1984	0	10	0	197	128	289	250	293	143	97	1	0
1985	0	0	0	130	159	157	183	291	184	127	113	0
1986	0	1	1	66	198	192	188	251	151	70	21	117
1987	14	0	20	85	71	100	210	227	161	60	116	0
1988	0	4	0	26	223	322	262	142	75	195	73	0
1989	4	0	0	12	147	171	241	153	124	195	17	0
1990	0	14	3	12	386	224	229	173	127	61	28	0
1991	4	0	0	67	134	291	126	275	277	89	188	31
1992	0	13	0	64	23	250	205	256	218	126	54	52
1993	0	0	38	129	145	238	190	282	279	56	7	0
1994	0	0	140	54	157	181	294	336	188	41	36	9
1995	0	0	20	10	270	189	330	290	176	89	57	0

Mae Hong Son station (Continued)

Year / Month	JAN	FEB	MAR	APR	MAY	JUN	JUL	AUG	SEP	OCT	NOV	DEC
1996	0	47	1	124	159	194	261	221	135	74	58	0
1997	0	0	13	7	117	125	214	314	193	80	19	0
1998	0	0	4	23	171	114	166	244	158	29	24	3
1999	7	7	12	131	211	120	147	264	217	155	43	6
2000	1	34	135	156	210	179	234	134	353	180	3	0
2001	18	3	41	7	216	128	240	199	272	194	23	17
2002	0	23	0	9	278	295	181	322	275	52	121	4

Pang Ma Pha station

Year / Month	JAN	FEB	MAR	APR	MAY	JUN	JUL	AUG	SEP	OCT	NOV	DEC
1986	0	0	0	16.8	120.1	105.2	172.8	233.9	209.5	50.6	33.4	52.1
1987	85	0	5.9	89.7	89.3	119.3	157.5	598.9	229.1	277.6	85.9	0
1988	0	11.2	0	83.5	200.6	148.9	297.3	141	86	117.2	159.3	7.2
1989	12.3	0	25	4.2	245	179.1	241	215.9	156.6	94.8	7.2	0
1990	0	16.2	3.3	36.1	257.7	127.4	286.7	214.1	165.5	49.6	61.2	0
1992	0	17.6	0	36.1	39.4	164.7	291.5	289.3	196.2	83.8	18.2	56.3
1993	0	0	30.4	95.1	317	277.6	145.9	161.6	155.9	96.2	0	0
1994	0	0	216.4	40.9	222.9	142.6	369.2	317.7	243.8	39.9	60.3	32.6
1995	0	0	1.6	10.9	255.5	81.4	430.2	281.3	258.3	74.8	56.4	0
1996	0	35.9	0	172.1	164.2	266	212.3	363.4	118.4	26.1	58.5	0
1997	0	0	29	15.6	186.8	106.1	291.8	238.3	230.6	100	22.9	0
1998	0	0	7.6	5.9	67.3	149.2	87	363.6	173.6	89.2	19.8	19.3
1999	49.8	40.9	2.4	36.9	292.2	175	135	184.4	217	113.9	12.8	0
2000	0	20.6	99.2	180.9	381.8	154	370.1	200.6	159.5	62.5	0	0
2001	1.4	0	61.8	0	303.2	201.2	205.8	188.9	149.5	187.2	53.4	11.1
2002	0	6	0	40	247.4	213.1	106.8	152.3	120.7	103.8	109.2	53.7
2003	90.7	17.7	0	48.5	92.9	189.9	161.8	252.1	297.8	80.1	4.1	0
2004	0	0	0	44.1	372.5	128.2	191.5	103.6	141.2	24.9	11.6	0
2005	0	0	6.9	24.4	147.1	197	180.1					
2006	0	0	44	141.4	140.7	169.2	294.1	279.9	305	208.7	24.6	0
2007		0	3.5	31.6	314.1	222.7	161.3	265.3	165.5	96.6	61	

APPENDIX G

Rainfall reconstruction from stalagmite is compared with that of Teak tree-ring

Year (AD)	Stalagmite (mm)	Tree-ring (mm)
1712	177.5554	282
1720	169.2027	291
1724	170.7679	287
1732	155.9386	280
1741	144.4567	276
1745	138.4602	272
1753	119.933	282
1761	147.1544	284
1765	153.3099	283
1773	143.8756	284
1782	166.7628	280
1786	148.158	284
1794	129.1532	282
1802	124.5827	282
1806	122.1195	283
1814	113.9563	286
1823	128.5712	280
1827	130.5331	284
1835	127.6513	278
1843	159.6299	288
1847	151.8477	279
1855	149.4777	280
1864	132.5237	286
1868	169.439	277
1876	155.9446	285
1913	167.3513	286
1932	134.2625	290
1969	149.9942	289

BIOGRAPHY

NAME	Miss Panisara Phutong
DATE OF BIRTH	November 9th 1982
PLACE OF BIRTH	Kalasin, Thailand
INSTITUTIONS ATTENDED	Kasetsart University Bachelor of Science (Forestry), 2001-2004 Mahidol University Master of Science, 2005-2008 (Technology of Environmental Management)
CONTACT ADDRESS	88 Moo 9, Tambon Kam Yai, Amphoe Huay Mex, Kalasin 46170